NASA Technical Memorandum 85817

NASA-TM-85817 19840020678

CALCULATION OF UNSTEADY AERODYNAMICS FOR FOUR AGARD STANDARD AEROELASTIC CONFIGURATIONS

Samuel R. Bland and David A. Seidel

May 1984

National Aeronautics and
Space Administration

Langley Research Center
Hampton, Virginia 23665

CALCULATION OF UNSTEADY AERODYNAMICS FOR FOUR AGARD STANDARD AEROELASTIC CONFIGURATIONS

Samuel R. Bland and David A. Seidel
NASA Langley Research Center
Hampton, VA 23665

INTRODUCTION

Methods for calculating transonic flow over oscillating airfoils have come into routine use in the recent past. These methods typically employ finite-difference methods to solve the nonlinear, mixed flow equations and require extensive computer resources. In order to conserve the resources needed to evaluate and compare competing methods, the AGARD Structures and Materials Panel established a Working Group on "Standard Configurations for Aeroelastic Applications of Transonic Unsteady Aerodynamics" at its Fall 1977 meeting. The Working Group published test cases for seven two-dimensional airfoils (ref. 1) in 1979 and for five three-dimensional wings (ref. 2) in 1982. This paper presents calculations for four of these airfoils and for one of the wings. A limited discussion of these results is included.

The analytic results reported herein employ the time-marching solution of the finite-difference equations for transonic small disturbance potential flow. The two-dimensional code used is called XTRAN2L (ref. 3) and the three-dimensional code is XTRAN3S (ref. 4). The alternating-direction-implicit solution algorithms used in these codes are derivatives of the algorithm introduced in the LTRAN2 code (ref. 5). All of the AGARD cases for the NACA 64A006, NACA 64A010, and NLR 7301 airfoils are included. Comparisons with experimental data from reference 6 are made for all cases for which data were available. In addition, calculations for six of the MBB-A3 airfoil cases and for three of the three-dimensional rectangular wing cases are reported. All calculations were made with the inviscid versions of the codes.

SYMBOLS

C	abbreviation for case, as in C3
C_p	pressure coefficient
C_p^*	critical pressure coefficient
$\tilde{C}_p$	normalized unsteady pressure coefficient; first harmonic of C_p divided by oscillation amplitude
$\Delta\tilde{C}_p$	normalized unsteady lifting pressure coefficient
c	airfoil chord, m
c_ℓ	steady lift coefficient
c_{ℓ_α}	first harmonic lift coefficient due to pitch, per radian
c_{ℓ_h}	first harmonic lift coefficient due to plunge
c_{ℓ_δ}	first harmonic lift coefficient due to flap rotation, per radian
c_{m_α}	first harmonic pitching moment coefficient due to pitch, per radian
c_{m_h}	first harmonic pitching moment coefficient due to plunge
c_{m_δ}	first harmonic pitching moment coefficient due to flap rotation, per radian
c_{h_α}	first harmonic hinge moment coefficient due to pitch, per radian
c_{h_δ}	first harmonic hinge moment coefficient due to flap rotation, per radian
f	oscillation frequency, Hz
h	plunge displacement in z-direction, m
h_o	plunge amplitude, m
k	reduced frequency, $\omega c/2V$
M	free stream Mach number
Re	Reynolds number, Vc/ν
t	time, s

V	free stream velocity, m/s
x	streamwise coordinate relative to leading edge, m
x_α	pitch axis location relative to leading edge, m
x_δ	flap axis location relative to leading edge, m
y	coordinate normal to x and z, positive to right, m
z	coordinate normal to free stream, positive up, m
α	angle of attack, deg
α_m	mean α, deg
α_o	dynamic pitch angle, deg
δ	flap angle, deg
δ_m	mean δ, deg
δ_o	dynamic flap angle, deg
η	fraction of semi-span
ν	kinematic viscosity, m^2/s
ω	angular frequency, $2\pi f$, rad/s

All angles are positive for trailing edge down. Moments are positive nose up. Pitching moments are taken about the quarter chord in all cases except for the NLR 7301 airfoil, for which they are about the pitch axis which is located at 40 percent chord. Hinge moments are taken about the hinge axis which is located at three-quarters chord in all cases.

ANALYTICAL METHODS

The analytical methods used herein involve solution of the transonic small disturbance (TSD) potential equation. The equation is solved on a rectangular spatial grid by marching the solution in time. The complete small disturbance equation, including all time derivative terms, is employed.

The two-dimensional solutions reported employ the XTRAN2L code as described in reference 3. This code is a modification of the LTRAN2-NLR code (ref. 7). The XTRAN2L code uses the alternating-direction-implicit (ADI)

method of Rizzetta and Chin (ref. 8) to advance the solution in time. Engquist-Osher monotone spatial differencing (ref. 9) is used to provide a robust solution that avoids expansion shocks. The nonreflecting boundary conditions of Kwak (ref. 10) have been extended to the full frequency equation by Whitlow (ref. 3) and are used in the code. The code may be used to obtain solutions for transient or harmonic motions. For the cases shown herein, the harmonic option was used with the solution being marched in time for several cycles of harmonic motion until the unwanted transients had decayed. Typically, between 1000 and 2000 time steps were employed. An 80 x 61 grid in the x-z space was used. The grid used was carefully chosen as described in reference 11.

The calculations for the rectangular wing were made with the XTRAN3S code of reference 4. This code employs a time-accurate ADI algorithm to solve the three-dimensional TSD equation. Nonlinear cross derivative terms are retained to capture swept shocks. Five cycles of oscillation with a total of 2500 time steps were used for each of the two cases reported. A 60 x 20 x 40 grid in x-y-z was used (see ref. 11).

For all calculations the NLR scaling as described in reference 12 was used. Although both codes employed in the present study have some capability for including quasi-steady boundary layer effects, this capability was not used, and only inviscid results are given.

RESULTS AND DISCUSSION

Results are given for 42 of the 81 two-dimensional AGARD standard cases described in reference 1. Note that the NACA 64A010 airfoil has the coordinates of the section as tested at NASA Ames Research Center (given in

ref. 1) and has a small amount of camber and is thicker than the symmetric design section. In addition, six of the cases for the MBB-A3 airfoil are reported. Tables 1-4 give the analytical test conditions for each of these cases with the priority cases indicated by an asterisk. The reduced frequency k is based on semichord. Finally, two results are shown for the rectangular wing of reference 2. These two results actually cover three of the standard cases, since cases 3 and 4 (table 5) differ only in Reynolds number, which could not be varied in the present inviscid analysis. The AGARD conditions for this wing specify oscillation about two pitch axes; only pitching about the quarter-chord axis is analyzed herein.

The modes of motion are described as follows. For pitch about a mean angle of attack α_m, the total angle of attack is expressed as

$$\alpha(t) = \alpha_m + \alpha_o \sin \omega t$$

where $\omega = 2kV/c$. For plunge,

$$h(t) = h_o \sin \omega t$$

For control rotation,

$$\delta(t) = \delta_m + \delta_o \sin \omega t$$

For each of the configurations analyzed, the steady flow pressure distribution is plotted. In addition, for each two-dimensional unsteady case, four figures are grouped together on one page. These figures show: (a) the mean pressure distribution over the airfoil chord during the last cycle of harmonic motion, (b) the lifting pressure (lower minus upper), (c) the upper surface pressure, and (d) lower surface pressure. The unsteady pressures (b-d) are given as the real (in-phase) and imaginary (in-quadrature) parts of the first harmonic component of the pressure computed from the last cycle of the imposed simple harmonic motion using a fast Fourier transform analysis.

These first harmonic components are normalized by the nondimensional amplitude of motion, i.e., angle of attack and flap rotation in radians or plunge displacement in chords, as appropriate. Although the harmonic pressures plotted on each page are shown to the same scale, there is some variation in the scales between figures. In addition to the plotted pressure distributions, the first harmonic force coefficients for the two-dimensional cases are given in tables 6-9.

The AGARD rectangular wing has a full-span aspect ratio of four. The analysis treats only the half span and imposes symmetry. The airfoil section is a symmetric version of the NACA 64A010 two-dimensional AGARD section and is defined in reference 2.

For the rectangular wing the steady, mean, and first harmonic pressure distributions are shown for each of the computational chords used in the analysis. Since this is a symmetric case, only upper surface pressures are shown. The first harmonic force coefficients are given in table 10.

NACA 64A006 Airfoil

The analytic test cases for the NACA 64A006 airfoil all involve oscillation of a flap with hinge axis located at three-quarter-chord about zero mean angle and were chosen to match the experimental conditions of reference 13. The variations include five Mach numbers, two frequencies, and two oscillation amplitudes (table 1). The steady flow pressure distributions for each Mach number are shown in figure 1. The unsteady results are shown in figures 2-13. In general, the agreement between experiment and theory improves with decreasing Mach number and increasing frequency. The calculated lift, moment, and hinge moment coefficients are given in table 6. There are

no experimental data for the two-degree flap oscillation amplitude; the "experimental" data shown for these cases is actually the data for one-degree amplitude.

The steady flow comparisons (fig. 1) are excellent at subcritical Mach numbers, but deteriorate as the shock wave develops. This discrepancy is at least partially attributable to wind tunnel interference (ref. 6, p. 1-1). The mean pressure distributions for one cycle of flap oscillation are given in part (a) of figures 2-13. In general the mean pressures are very similar to the steady pressures. The effect of variations in frequency and amplitude of oscillation may be illustrated by comparing figures 9(a), 10(a), and 11(a), all at M = 0.875. These are the priority cases (C8-10) for this airfoil. Figures 9(a) and 10(a) show the effect of increasing the flap oscillation amplitude from one to two degrees at the lower frequency (k = 0.059). As expected the shock oscillates over a larger distance at the larger amplitude. (The experimental data are both for $\alpha_0 = 1^0$). The effect of frequency is illustrated by comparing figure 9(a) (k = 0.059) to figure 11(a) (k = 0.235). At the higher frequency the calculated shock motion is less, as indicated by the steeper pressure rise; however, the experimental pressure rises for these two cases are similar.

Results for the first harmonics of the unsteady pressure distributions are shown in parts (b)-(d) of figures 2-13. Figures 2 and 3 illustrate the better agreement between theory and experiment that occurs at higher frequency. For this subcritical case (M = 0.8), a single pressure peak occurs at the flap axis location (x/c = 0.75). At M = 0.825, a bulge develops in the calculated pressure distribution (figs. 4-6) near the airfoil midchord due to

the development of a very weak shock wave during the unsteady motion. As expected, this effect is more pronounced at lower frequency (see figs. 4 and 6) and at larger oscillation amplitude (see figs. 4 and 5). As the Mach number increases, the shock pulse moves aft and interacts with the pressure pulse at the hinge location. The agreement with experiment deteriorates because of the discrepancy in shock location mentioned earlier. A comparison of figures 9 and 11 (M = 0.875) illustrates the effect. In the experiment, the shock peak (near x/c = 0.55) and hinge peak (x/c = 0.75) are easily distinguished. In the calculation the two peaks have merged into one at the lower frequency (fig. 9) but can be identified at the higher frequency (fig. 11). This result is not surprising since the shock excursion is expected to decrease as frequency increases.

The calculated results at M = 0.96 (figures 12-13) are qualitatively different from the experimental data. The potential flow code has placed the shock wave at the trailing edge in contrast to the experimental value of about x/c = 0.88 (see fig. 1(e)). The shock and hinge peaks can be distinguished in the experimental results in figure 12. Both theory and experiment show very small unsteady pressures ahead of the flap.

NACA 64A010 Airfoil

The AGARD cases for the NACA 64A010 airfoil are listed in table 2. The cases are for the model tested at the NASA Ames Research Center for which experimental data are reported in reference 14. The test cases are at essentially two Mach numbers, M = 0.5 and 0.8, two Reynolds numbers, and several frequencies and amplitudes of pitch oscillation about the

quarter-chord. This airfoil possesses a very small amount of camber and surface waviness, as is evident in the steady pressure distributions shown in figure 14. Figures 14(a)-(b) are for the low Mach number cases (C1-2) at two Reynolds numbers and agreement is excellent. Figures 14(c)-(e) are for the higher Mach number with part (d) giving a low Reynolds number result (for the experiment). The agreement in shock location and strength for these cases is quite good with the experiment for the lower Reynolds number case, figure 14(e), showing a slightly weaker and more forward located shock.

The unsteady results are shown in figures 15-24 and table 7. At M = 0.5 (figs. 15-16) the agreement is excellent with perhaps better agreement obtained at the higher Reynolds number (fig. 16). The remaining results are at M = 0.8. The priority cases 6 and 10 (figs. 20 and 24) were chosen to illustrate Reynolds number effects. However, the slight differences in Mach number, amplitude, and frequency may mask this comparison.

The oscillation amplitude effect is illustrated by comparing figures 19, 22, 23 for approximately α_0 = 1.0, 0.5, and 2.0 degrees, respectively, and at k = 0.101. In each case, the agreement with experiment is good. The amplitude effect is well illustrated by the theory. Away from the shock, the plotted normalized pressures (i.e., divided by oscillation amplitude) are essentially the same. (Note the different scale in figure 22). However, for small amplitude, the shock pulse is narrower (less shock motion) and higher (because of the amplitude normalization).

Cases 3-7 (figs. 17-21) illustrate the frequency effect, with k varying from about 0.025 to 0.3. The systematic decrease in calculated shock pulse width with increasing frequency is evident, with agreement of the theory and experiment perhaps being somewhat better at the intermediate frequencies.

MBB-A3 Airfoil

Analytical results only are presented for six of the cases for the MBB-A3 airfoil in figures 25-31. These six cases (see table 3) are all at M = 0.765 and α_m = 1.5 degrees. There are cases for airfoil pitch oscillation about the quarter chord and for plunge oscillation, each at three frequencies, k = 0.1, 0.3, and 0.9. The unsteady lift and moment coefficients are tabulated in table 8.

The steady pressure distribution is shown in figure 25. In choosing the cases for this airfoil, the conditions were specified to be the supercritical design point (M = 0.765, α_m = 1.5°, c_ℓ = 0.519) given in reference 1. This choice was based on the experimental data shown for this design condition (taken from fig. 8.2 of ref. 15) which show a typical supercritical flow without a discernible shock wave. In the experiment the region of supercritical flow terminates at about x/c = 0.53. In contrast, the present calculation for this point shows a strong shock located at about x/c = 0.66 with c_ℓ = 0.700. Transonic small disturbance theory typically predicts a shock that is too strong and located too far aft on the airfoil and is sensitive to the transonic scaling (ref. 12) used.

It may be noted that potential theory is now known to predict nonunique results in certain cases with moderately strong shocks (ref. 16). For conditions near the region of nonuniqueness, the potential theory can also be seriously in error. Calculations for this airfoil with the TSD code used herein were sensitive to time step and initial conditions.

The unsteady pressure distributions for the MBB-A3 airfoil are given in figures 26-31. The effect of varying frequency from k = 0.1 to 0.9 may be seen by comparing figures 26-28 for pitch and figures 29-31 for plunge. For

pitch increasing frequency leads to a decreasing magnitude of the shock pulse. For plunge, the most obvious effect is the increasing overall pressure level with frequency. This increase is consistent with piston theory which predicts forces proportional to frequency.

NLR 7301 Airfoil

The test cases for the thick supercritical NLR 7301 airfoil are listed in table 4. Three mean flow conditions were analyzed: a subcritical condition at M = 0.5 (cases 1-2 and 10); a supercritical case with shock at M = 0.7, $\alpha_m = 2.0^o$ (cases 3-5 and 11); and the design point at M = 0.721, $\alpha_m = -0.19^o$ (cases 6-9 and 12-14). Cases 1-9 are for pitch oscillation about an axis located at 40 percent chord and include variations in frequency and amplitude of motion. Cases 10-14 are for oscillation of a flap located at three-quarter chord with variation in frequency included at the design point. The experimental data are taken from chapter 4 of reference 6. These data are from tests at NLR (ref. 17) and were chosen for comparison instead of those from the NASA Ames Research Center (chapter 5 of reference 6) because the model matched the design airfoil more closely, and data were available for both upper and lower surfaces. The calculated harmonic forces are given in table 9.

The experimental data for the pitch cases and the flap cases were obtained on two different models (ref. 6). The steady flow pressure distributions for the three mean flow conditions are shown in figure 32. At the subcritical condition (fig. 32(a)-(b)) the upper surface pressures are in good agreement, but the pressures on the lower surface show a discrepancy in level. It would not be surprising if small disturbance theory were inadequate for this 16.5 percent thick, blunt-nosed airfoil. The comparison for the case

with a strong shock (fig. 32(c)-(d)) is poor, with the calculation giving too strong a shock, located too far aft. This discrepancy may be attributed, at least in part, to a breakdown of potential theory (as discussed in the preceding section of this report). In any case, it is certain that this comparison could be "improved" by performing the calculation at a lower steady angle of attack. The comparison of the steady pressure distributions at the design point (fig. 32(e)-(f)) is also poor. There are two weak shocks at about $x/c = 0.25$ and 0.60. In addition, there is a sharp pressure rise near the leading edge. One may anticipate that these features will lead to several shock pressure pulses in the unsteady results described below.

The unsteady results for all of the AGARD cases for this airfoil are shown in figures 33-46. Because of the differences between the calculated and measured steady flow fields, the unsteady comparison is poor. Several observations on the calculated results may be made, however.

The unsteady results at $M = 0.5$ are shown for pitch at two frequencies in figures 33-34 and for flap oscillation at the lower frequency in figure 42. The mean pressure comparison for the pitch cases (figs. 33(a) and 34(a)) is very similar to that for the steady flow (fig. 32(a)). The calculated mean pressure for the flap case (fig. 42(a)) is very similar to the calculated mean pressure for the pitch cases (figs. 33(a) and 34(a)). In contrast, the experimental mean pressure for the flap case is significantly different from the corresponding pressure for the pitch cases. In each of these three cases, however, the calculated first harmonic pressure distributions agree well with the experimental data.

Figures 38, 40, and 41 illustrate the effect of pitch frequency at the design point. Several shock peaks occur. At the lowest frequency (fig. 38)

three peaks are present at x/c = 0.20, 0.45, and 0.60, whereas at the highest frequency (fig. 41) only two peaks are discernable at x/c = 0.25 and 0.65. As usual, the peaks are narrowest at the highest frequency. The same comparison for flap oscillation frequency is given in figures 44-46 with the additional complication of the hinge peak at x/c = 0.75. The effect of oscillation mode can be examined by comparing these six figures (figs. 38, 40-41, and 44-46) in pairs. In each case, the calculated mean pressures (figure part (a)) appear the same for both modes at the same frequency whereas the experimental values can be significantly different for the two modes of oscillation (see figs. 38 and 44, for example). This difference in the experimental mean values is a reflection of the difference in the steady flow pressures (fig. 32(e)-(f)) for the two models.

Rectangular Wing

The conditions for which the AGARD rectangular wing was analyzed are given in table 5. The symmetric airfoil section (given in ref. 2) is constant over the span and was defined to be an average of the upper and lower surface coordinates for the 64A010 airfoil (given in ref. 1). The two distinct cases are for wing pitch about the quarter chord at M = 0.8 with two frequencies of oscillation, k = 0.20 and 0.45. The steady flow pressure distributions at the span locations used in the analysis are shown in figure 47 for this flow at α_m = 0. There is a shock near midchord at the root which weakens outboard. The pressures at the root may be compared with those for similar conditions on the NACA 64A010 airfoil shown in figure 14(c).

The unsteady pressure distributions are shown in figures 48-49 for the two frequencies. Since this is a symmetric case, only the upper surface values are given. The results for k = 0.2 may be compared with the two-dimensional airfoil results for similar conditions. The mean pressure

distribution (fig. 48(a)) at the root chord is quite similar to that for the airfoil (fig. 20(a)). The real parts of the harmonic upper surface pressures (figs. 20(c) and 48(b)) are also similar. The imaginary parts, however, are somewhat different. For the airfoil, the real and imaginary parts have similar shape, but differ in sign. For the wing, the imaginary part of the pressure (fig. 48(c)) shows only a single, very broad peak and not the double-peak "doublet" shape of the two-dimensional result (fig. 20(c)). The frequency effect for the rectangular wing is illustrated by comparing figures 48 and 49. In contrast with the two-dimensional airfoil results, the calculated shock pulse appears wider at the higher frequency. The overall lift and moment coefficients for the wing are given in table 10.

CONCLUSIONS

Calculations using the XTRAN2L all-frequency, transonic small disturbance potential flow code have been made for about half of the AGARD two-dimensional standard configurations. All of the cases for the NACA 64A006, NACA 64A010, and NLR 7301 airfoils are included with comparison with experiment in most cases. Six of the cases for the MBB-A3 airfoil are included. Calculations using the XTRAN3S code were made for the AGARD rectangular wing at two frequencies. The following general conclusions may be drawn from the two-dimensional airfoil results:

1. For the conventional NACA 64A006 and 64A010 airfoils, agreement between calculated and experimental pressure distributions is reasonable except at the highest Mach number (0.96) analyzed. Agreement between the unsteady pressures is excellent at subcritical conditions and deteriorates with increasing Mach number as the shock develops and moves aft.

2. For the thick, blunt supercritical NLR 7301 airfoil the agreement is poor for flows with shocks. For subcritical flow, however, even though the agreement between calculated and measured steady pressure distributions is poor, the unsteady pressures agree quite well.

3. For cases in which the steady flow agreement is good, the unsteady flow results are also good, with better agreement at higher frequency.

4. The effect of increasing oscillation amplitude is to increase the unsteady shock motion and to broaden the shock pulse in the harmonic pressure distributions.

5. The effect of increasing oscillation frequency is to narrow the shock pulse.

Results for the rectangular wing show a somewhat broader shock pulse at the higher frequency, is contrast with the two-dimensional airfoil predictions.

REFERENCES

1. Bland, Samuel R.: AGARD Two-Dimensional Aeroelastic Configurations. AGARD AR-156, Aug. 1979.

2. Bland, Samuel R.: AGARD Three-Dimensional Aeroelastic Configurations. AGARD AR-167, Mar. 1982.

3. Whitlow, Woodrow, Jr.: XTRAN2L: A Program for Solving the General-Frequency Unsteady Transonic Small Disturbance Equation. NASA TM 85723, Nov. 1983.

4. Borland, C. J.; and Rizzetta, D. P.: Nonlinear Transonic Flutter Analysis. AIAA Journal, Vol. 20, No. 11, Nov. 1982, pp. 1606-1615.

5. Ballhaus, W. F.; and Goorjian, P. M.: Implicit Finite-Difference Computations of Unsteady Transonic Flows About Airfoils. AIAA Journal, Vol. 15, No. 12, Dec. 1977, pp. 1728-1735.

6. Anon: Compendium of Unsteady Aerodynamic Measurements. AGARD R-702, August 1982.

7. Houwink, R.; and van der Vooren, J.: Improved Version of LTRAN2 for Unsteady Transonic Flow Computations. AIAA Journal, Vol. 18, No. 8, August 1980, pp 1008-1010.

8. Rizzetta, D. P.; and Chin, W. C.: Effect of Frequency in Unsteady Transonic Flow. AIAA Journal, Vol. 17, No. 7, July 1979, pp. 779-781.

9. Engquist, B. E.; and Osher, S. J.: Stable and Entropy Satisfying Approximations for Transonic Flow Calculations. Mathematics of Computation, Vol. 34, No. 149, January 1980, pp. 45-75.

10. Kwak, D.: Nonreflecting Far-Field Boundary Conditions for Unsteady Transonic Flow Computation. AIAA Journal, Vol. 19, No. 11, November 1981, pp. 1401-1407.

11. Seidel, David A.; Bennett, Robert M.; and Whitlow, Woodrow, Jr.: An Exploratory Study of Finite Difference Grids for Transonic Unsteady Aerodynamics. NASA TM 84583, December 1982.

12. van der Vooren, J.; Sloof, J. W.; Huizing, G. H.; and Van Essen, A.: Remarks on the Suitability of Various Transonic Small Perturbation Equations to Describe Three-Dimensional Transonic Flow; Examples of Computations Using a Fully-Conservative Rotated Difference Scheme. Symposium Transsonicum II, Gottingen, West Germany, September 1975, proceedings, Springer-Verlag, Berlin, 1976, pp. 557-566.

13. Tijdeman, H.; and Schippers, P.: Results of Pressure Measurements on an Airfoil with Oscillating Flap in Two-Dimensional High Subsonic and Transonic Flow (Zero Incidence and Zero Mean Flap Position). NLR TR 73078 U, 1973.

14. Davis, S.; and Malcolm G.: Experimental Unsteady Aerodynamics of Conventional and Supercritical Airfoils. NASA TM 81221, August 1980.

15. Anon: Experimental Data Base for Computer Program Assessment. AGARD AR-138, May 1979.

16. Salas, M. D.; Jameson, A.; and Melnik, R. E.: A Comparative Study of the Nonuniqueness Problem of the Potential Equation. AIAA Paper 83-1888-CP, presented at the 6th AIAA Computational Fluid Dynamics Conference, Danvers, Massachusetts, July 13-15, 1983.

17. Tijdeman, H.: Investigations of the Transonic Flow around Oscillating Airfoils. NLR TR 77090 U, 1977.

Table 1. - NACA 64A006 Airfoil, test cases

Case	M	δ_o	f	k
1	0.800	1	30	0.064
2	0.800	1	120	0.254
3	0.825	1	30	0.062
4	0.825	2	30	0.062
5	0.825	1	120	0.248
6	0.850	1	30	0.060
7	0.850	1	120	0.242
8*	0.875	1	30	0.059
9*	0.875	2	30	0.059
10*	0.875	1	120	0.235
11	0.960	1	30	0.054
12	0.960	1	120	0.217

Note: $\alpha_m = \alpha_o = \delta_m = 0$, $x_\delta/c = 0.75$

Table 2. - NACA 64A010 Airfoil, test cases

Case	M	ReX10^{-6}	α_o	f	k
1	0.490	2.5	0.96	10.4	0.100
2	0.502	10.0	1.02	10.8	0.100
3	0.796	12.5	1.03	4.2	0.025
4	0.796	12.5	1.02	8.6	0.051
5	0.796	12.5	1.02	17.2	0.101
6*	0.796	12.5	1.01	34.4	0.202
7	0.796	12.5	0.99	51.5	0.303
8	0.796	12.5	0.51	17.1	0.101
9	0.797	12.5	2.00	17.2	0.101
10*	0.802	3.4	0.94	33.2	0.200

Note: $\alpha_m = 0$, $x_\alpha/c = 0.25$

Table 3. - MBB-A3 Airfoil, test cases

Case	M	α_m	α_o	h_o/c	k
3*	0.765	1.5	0.5	0	0.1
4	0.765	1.5	0.5	0	0.3
5	0.765	1.5	0.5	0	0.9
11	0.765	1.5	0	0.01	0.1
12	0.765	1.5	0	0.01	0.3
13	0.765	1.5	0	0.01	0.9

Note: $x_\alpha/c = 0.25$

Table 4. - NLR 7301 Airfoil, test cases

Case	M	α_m	α_o	δ_o	f	k
1	0.500	0.40	0.5	0	30	0.098
2	0.500	0.40	0.5	0	80	0.263
3	0.700	2.00	0.5	0	30	0.072
4	0.700	2.00	1.0	0	30	0.072
5	0.700	2.00	0.5	0	80	0.192
6	0.721	-0.19	0.5	0	30	0.068
7	0.721	-0.19	1.0	0	30	0.068
8*	0.721	-0.19	0.5	0	80	0.181
9	0.721	-0.19	0.5	0	200	0.453
10	0.500	0.40	0	1	30	0.098
11	0.700	2.00	0	1	30	0.072
12	0.721	-0.19	0	1	30	0.068
13*	0.721	-0.19	0	1	80	0.181
14	0.721	-0.19	0	1	200	0.453

Note: $x_\alpha/c = 0.4$, $x_\delta/c = 0.75$, $\delta_m = 0$

Table 5. - Rectangular Wing, test cases

Case	M	$ReX10^{-6}$	α_o	k
3*	0.8	3.4	1	0.20
4*	0.8	12.5	1	0.20
6*	0.8	3.4	1	0.45

Note: $\alpha_m = 0$, $x_\alpha/c = 0.25$

Table 6. - NACA 64A006 Airfoil, harmonic forces

	c_{ℓ_δ}		c_{m_δ}		c_{h_δ}	
Case	Real	Imag	Real	Imag	Real	Imag
1	4.793	-2.053	-1.248	-0.052	-0.082	-0.003
2	2.546	-1.744	-1.368	0.024	-0.082	-0.024
3	4.986	-2.459	-1.383	-0.043	-0.083	-0.005
4	5.006	-2.520	-1.405	-0.036	-0.082	-0.005
5	2.336	-1.968	-1.526	0.172	-0.087	-0.026
6	5.148	-3.434	-1.703	0.103	-0.080	-0.013
7	1.672	-1.891	-1.460	0.685	-0.100	-0.030
8*	3.568	-5.687	-2.079	1.655	-0.072	-0.071
9*	3.493	-5.726	-2.062	1.835	-0.111	0.010
10*	1.699	-1.372	-0.902	0.644	-0.111	-0.024
11	1.555	0.025	-0.963	-0.013	-0.190	-0.002
12	1.537	-0.004	-0.956	0.004	-0.188	0.001

Table 7. - NACA 64A010 Airfoil, harmonic forces

	c_{ℓ_α}		c_{m_α}	
Case	Real	Imag	Real	Imag
1	5.767	-0.561	-0.052	-0.186
2	5.802	-0.581	-0.054	-0.189
3	12.552	-4.202	-0.903	0.169
4	9.836	-4.092	-0.709	0.039
5	7.342	-3.446	-0.600	-0.160
6*	5.635	-2.157	-0.648	-0.472
7	4.942	-1.341	-0.793	-0.631
8	7.370	-3.384	-0.583	-0.195
9	7.247	-3.713	-0.674	-0.014
10*	5.496	-2.421	-0.744	-0.310

Table 8. - MBB-A3 Airfoil, harmonic forces

	c_{ℓ_α}		c_{m_α}	
Case	Real	Imag	Real	Imag
3*	6.460	-5.352	-0.835	0.909
4	4.362	-0.954	-0.346	-0.233
5	4.791	2.136	-0.847	-1.686

	c_{ℓ_h}		c_{m_h}	
Case	Real	Imag	Real	Imag
11	-1.173	-1.147	0.228	0.144
12	-1.135	-2.203	0.092	0.108
13	0.131	-6.690	-1.011	1.156

Table 9. - NLR 7301 Airfoil, harmonic forces

	c_{ℓ_α}		c_{m_α}		c_{h_α}	
Case	Real	Imag	Real	Imag	Real	Imag
1	5.860	-0.792	0.842	-0.311	-0.030	-0.009
2	4.771	0.045	0.684	-0.504	-0.024	-0.032
3	8.280	-8.584	-0.320	0.751	0.028	-0.121
4	8.067	-8.867	-0.343	0.935	0.025	-0.124
5	4.697	-3.547	0.152	0.232	-0.025	-0.087
6	8.535	-2.839	1.364	-0.860	-0.022	-0.011
7	8.604	-3.048	1.272	-0.842	-0.020	-0.013
8*	6.104	-1.948	0.758	-1.122	-0.021	-0.030
9	4.808	-0.555	-0.112	-1.078	-0.021	-0.079

	c_{ℓ_δ}		c_{m_δ}		c_{h_δ}	
Case	Real	Imag	Real	Imag	Real	Imag
10	3.537	-0.787	-0.238	-0.190	-0.061	-0.005
11	4.022	-4.348	-0.873	0.399	-0.046	-0.059
12	4.989	-2.164	-0.412	-0.478	-0.057	-0.009
13*	3.139	-2.038	-0.867	-0.382	-0.059	-0.022
14	1.830	-1.056	-0.747	0.068	-0.072	-0.043

Table 10. - Rectangular Wing, harmonic forces

	C_{ℓ_α}		C_{m_α}	
Case	Real	Imag	Real	Imag
3/4*	4.578	0.119	-0.105	-0.648
6*	4.224	0.266	-0.709	-0.967

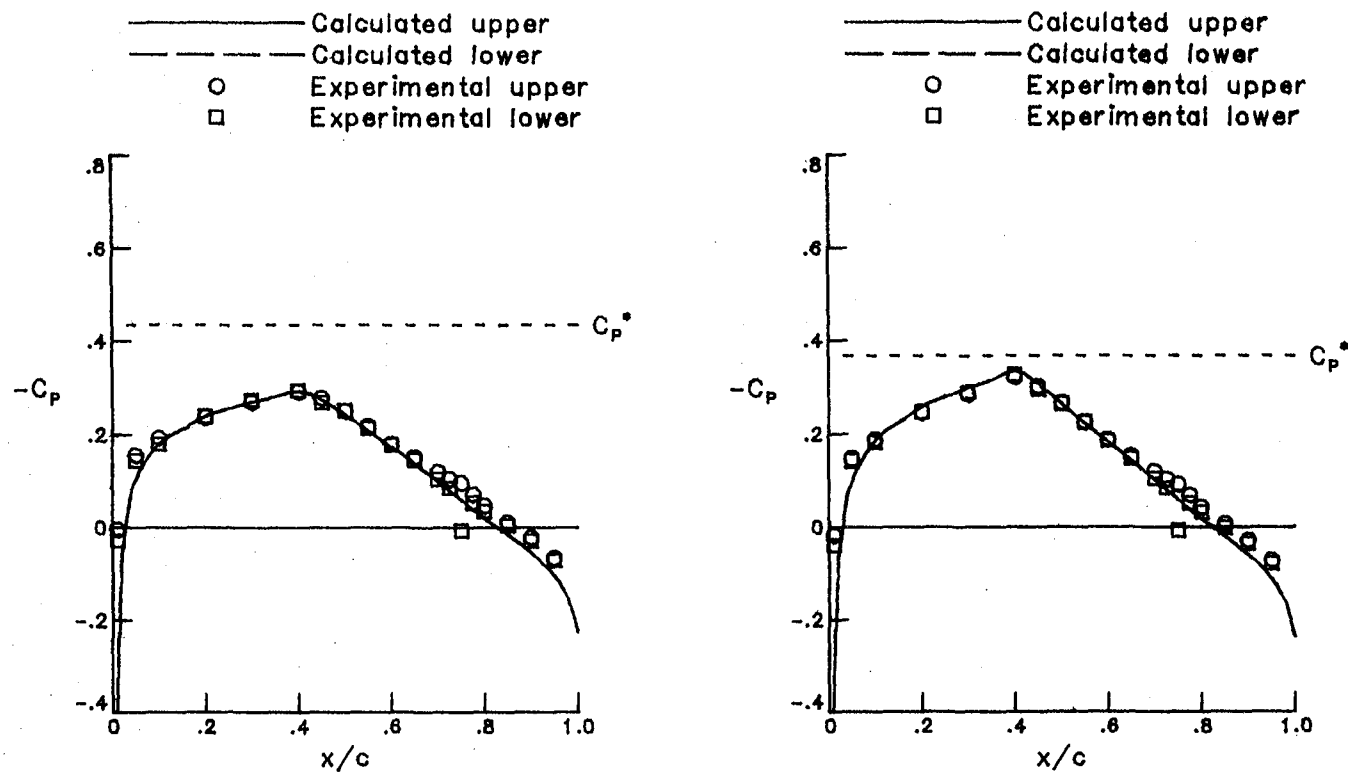

(a) M = 0,800, α_m = 0, C1-2.

(b) M = 0.825, α_m = 0, C3-5.

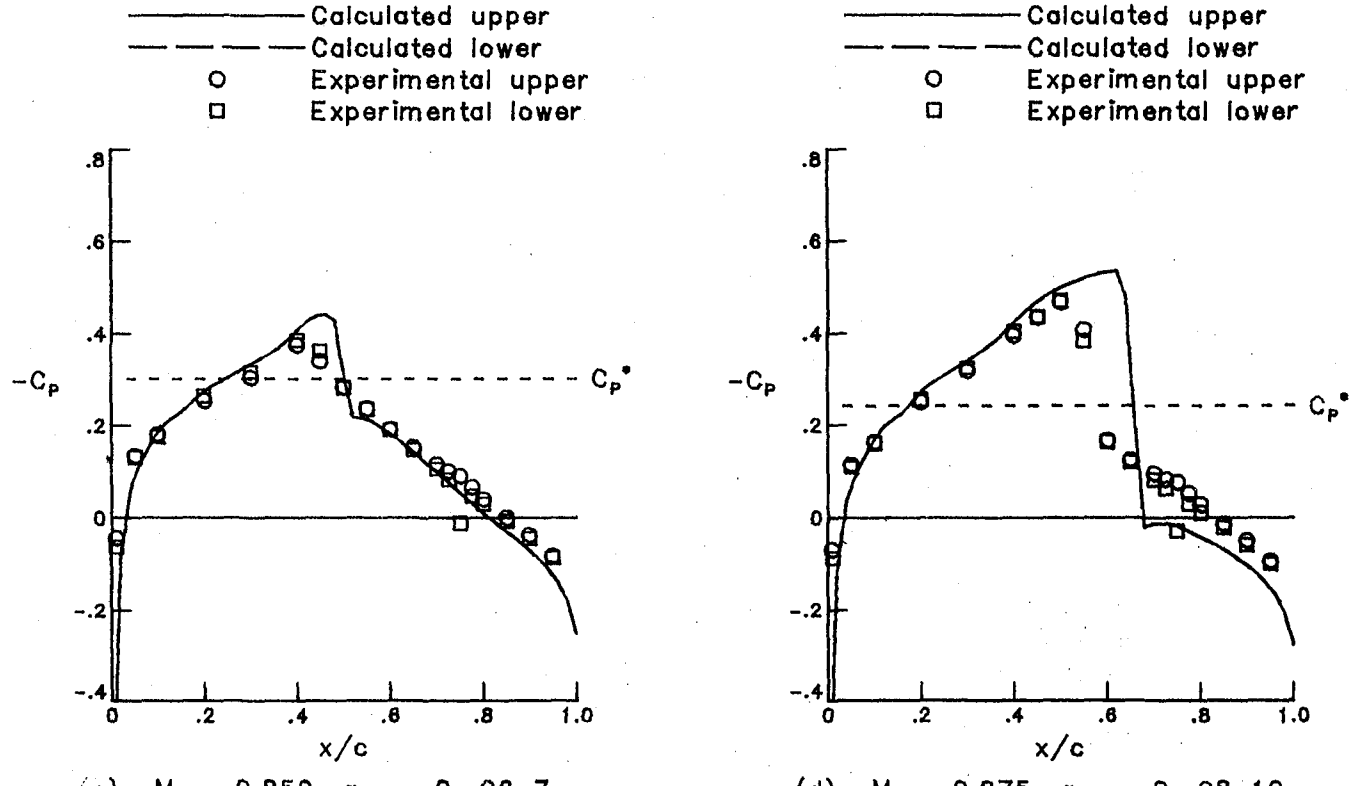

(c) M = 0.850, α_m = 0, C6-7.

(d) M = 0.875, α_m = 0, C8-10.

Figure 1.- Steady pressure distribution for NACA 64A006 Airfoil.

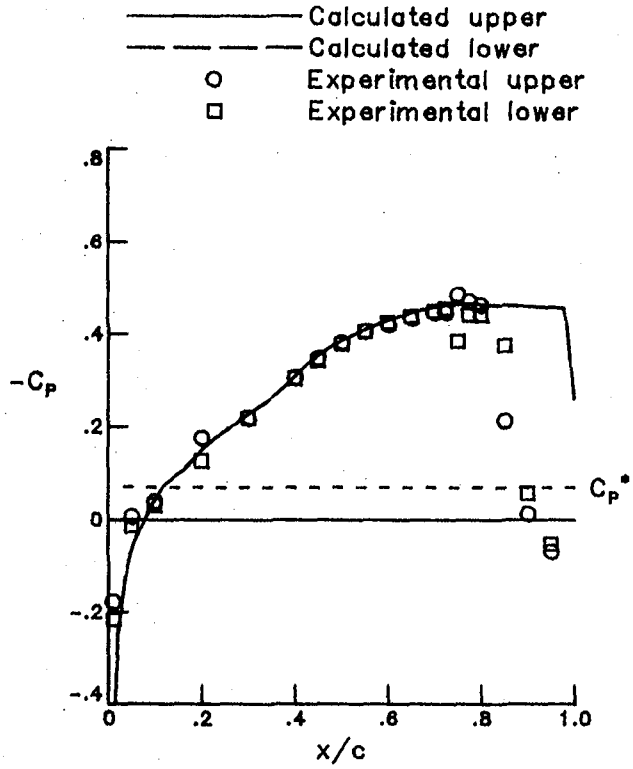

(e) M = 0.960, α_m = 0, C11-12.

Figure 1 .- Concluded.

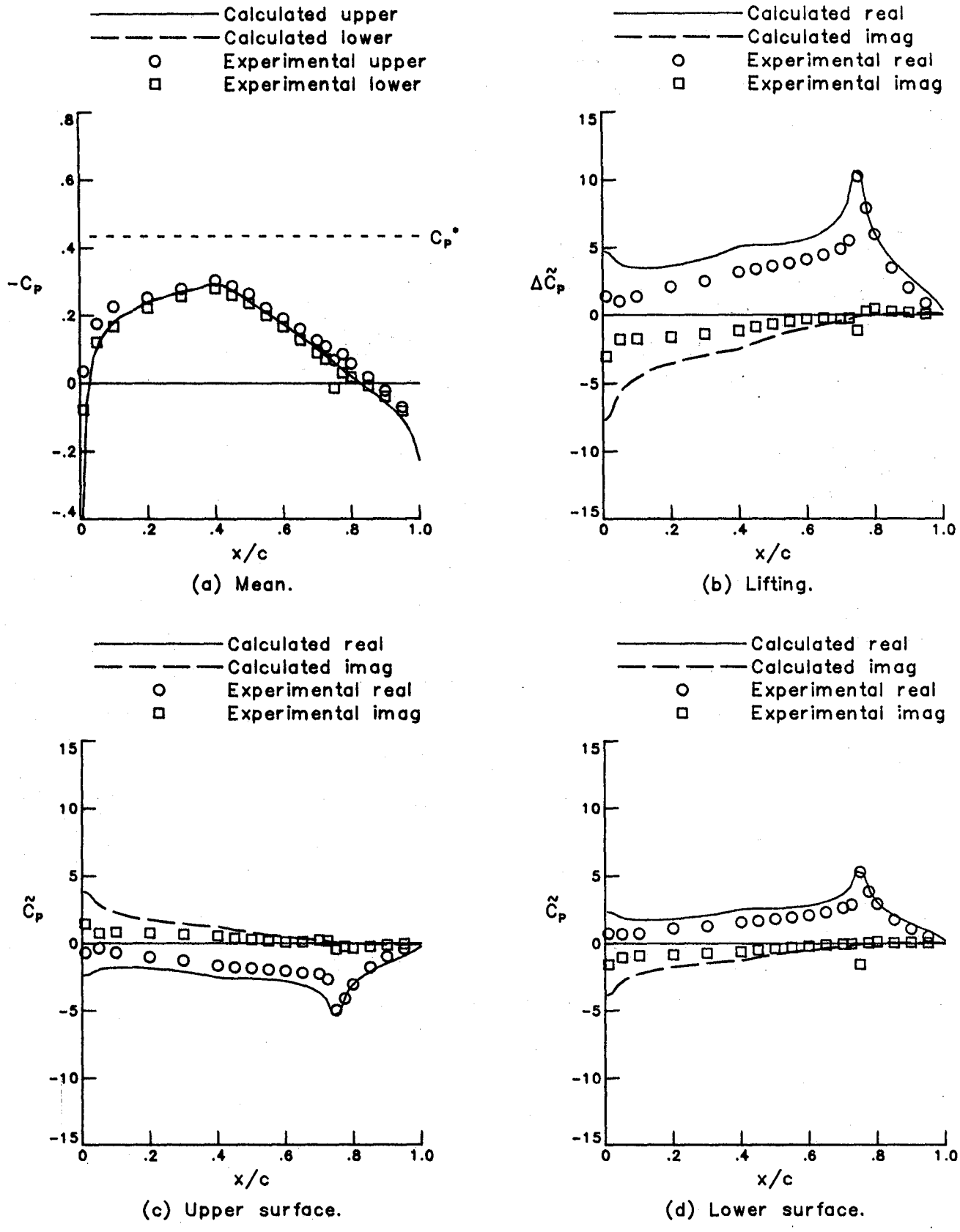

Figure 2 .- Unsteady pressure distribution for NACA 64A006 Airfoil. Case 1, M = 0.800, δ_0 = 1, k = 0.064.

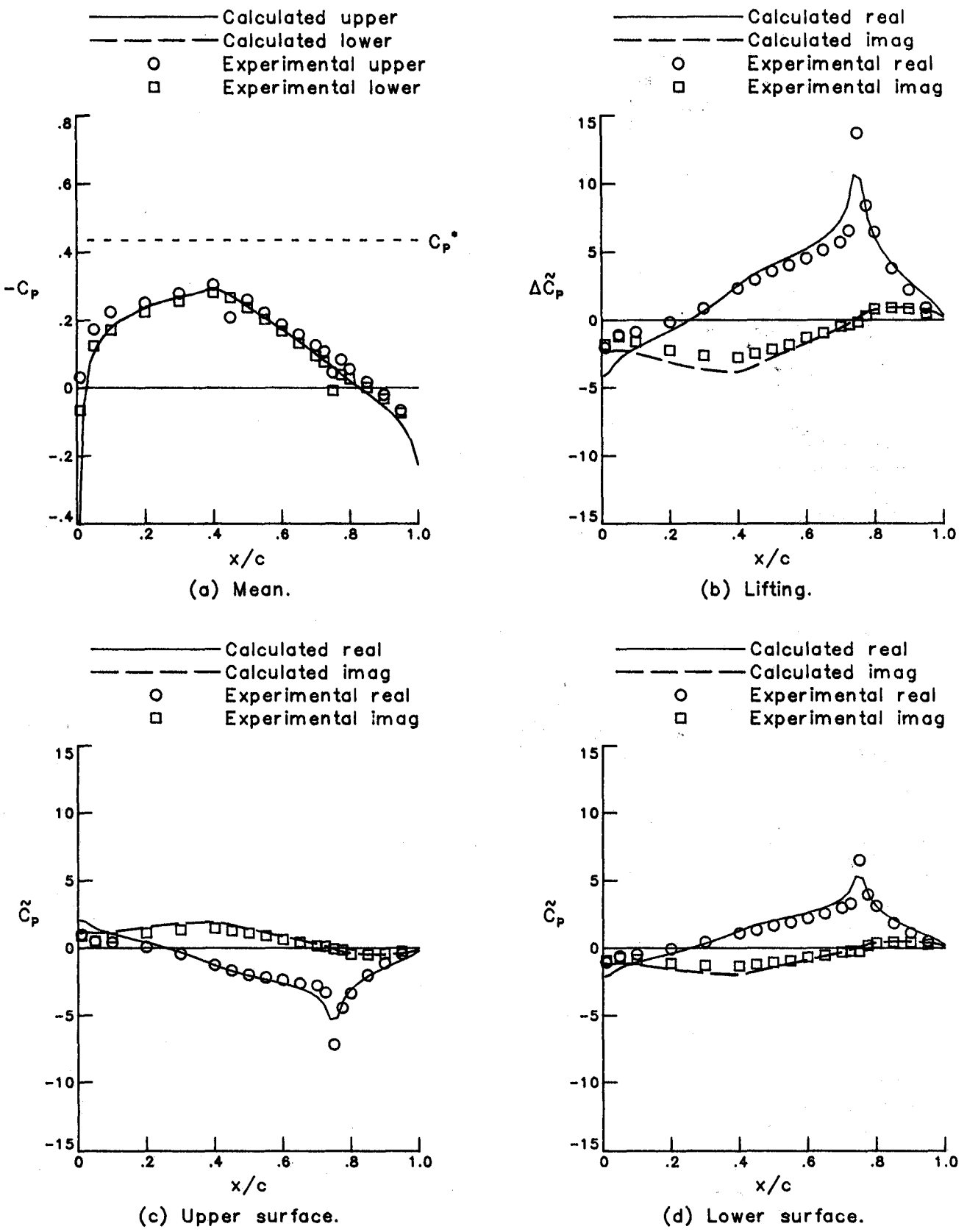

Figure 3.- Unsteady pressure distribution for NACA 64A006 Airfoil.
Case 2, M = 0.800, δ_0 = 1, k = 0.254.

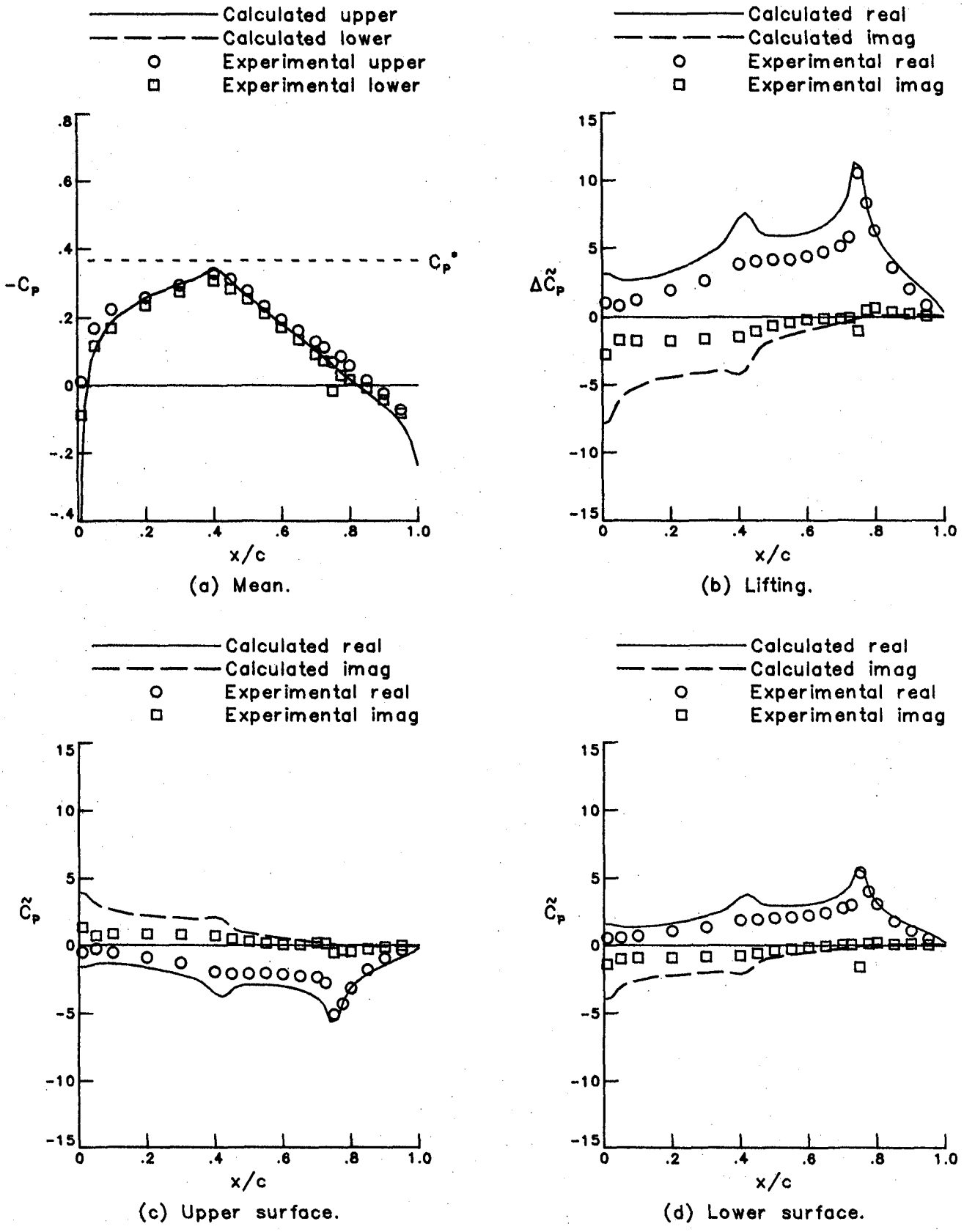

Figure 4.- Unsteady pressure distribution for NACA 64A006 Airfoil.
Case 3, M = 0.825, δ_0 = 1, k = 0.062.

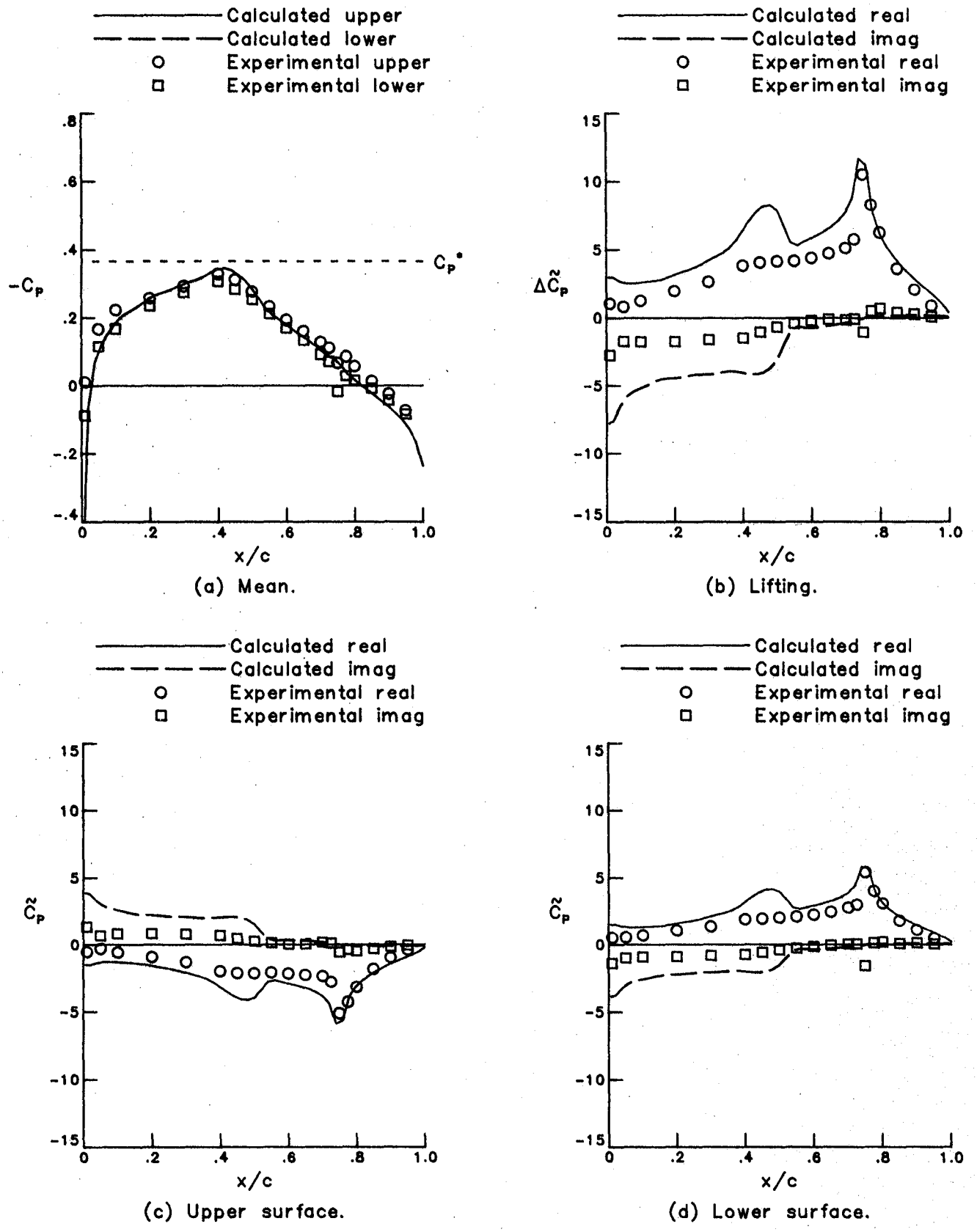

Figure 5.- Unsteady pressure distribution for NACA 64A006 Airfoil. Case 4, M = 0.825, δ_0 = 2, k = 0.062.

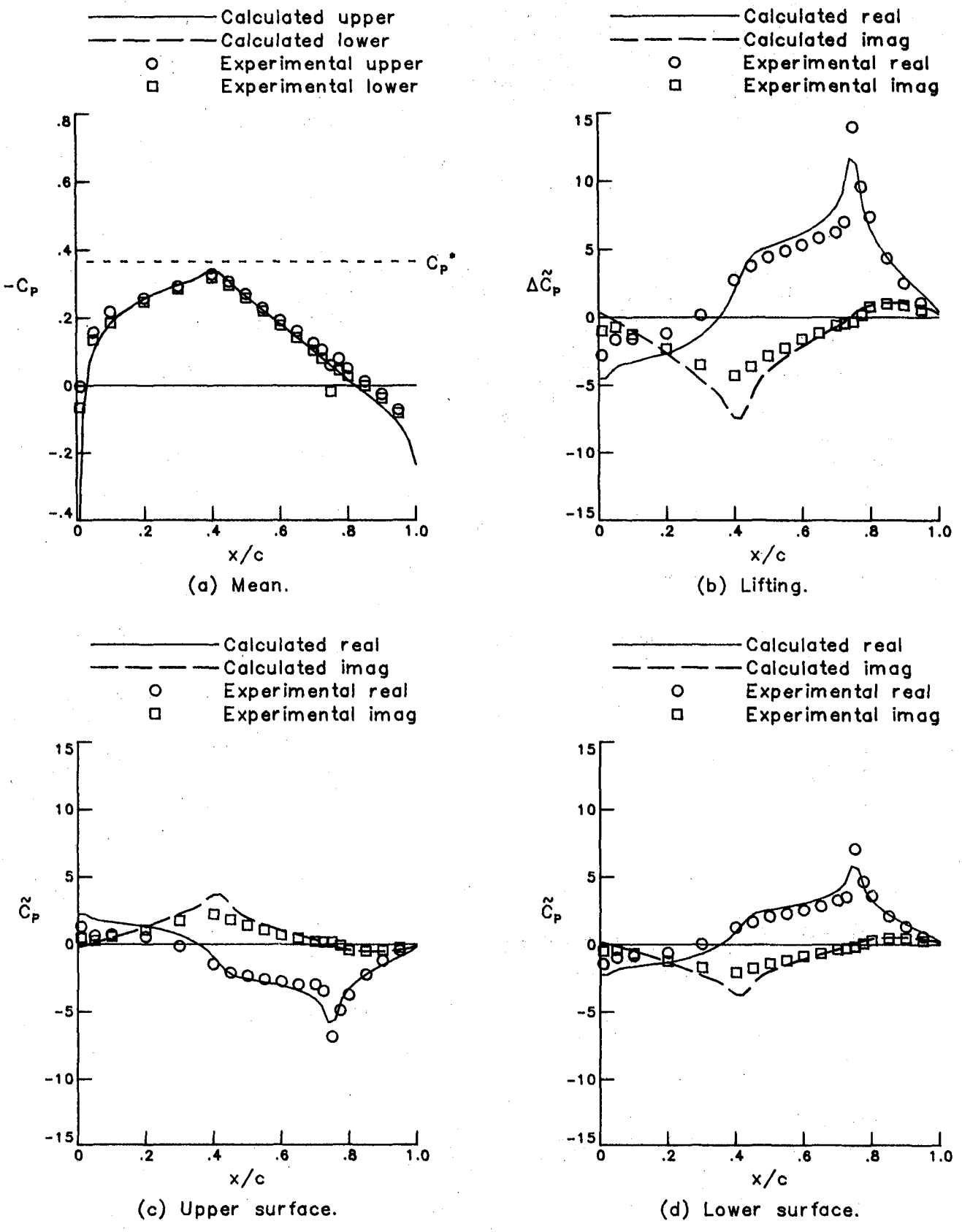

Figure 6 .- Unsteady pressure distribution for NACA 64A006 Airfoil.
Case 5, M = 0.825, δ_0 = 1, k = 0.248.

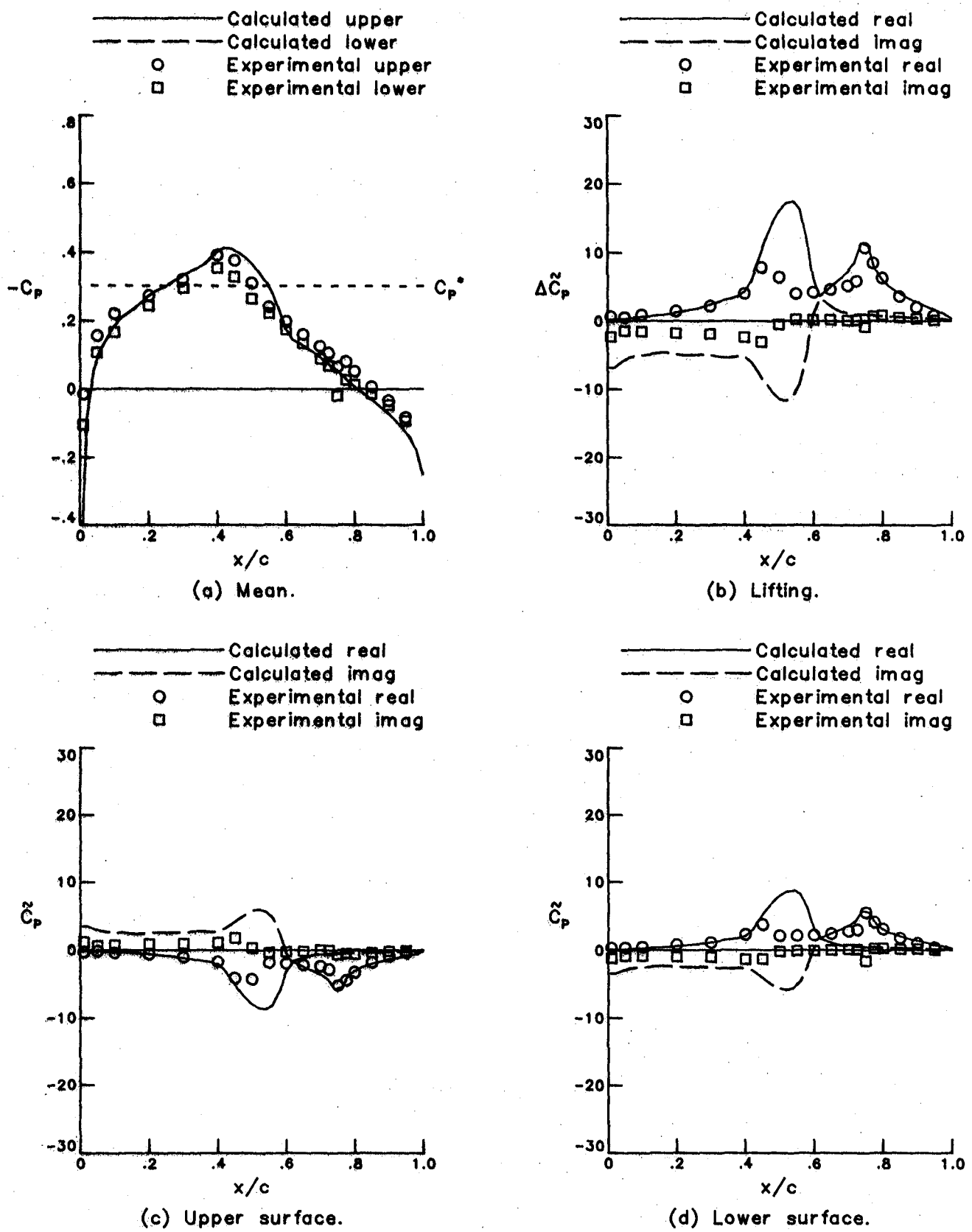

Figure 7 .- Unsteady pressure distribution for NACA 64A006 Airfoil. Case 6, M = 0.850, δ_0 = 1, k = 0.060.

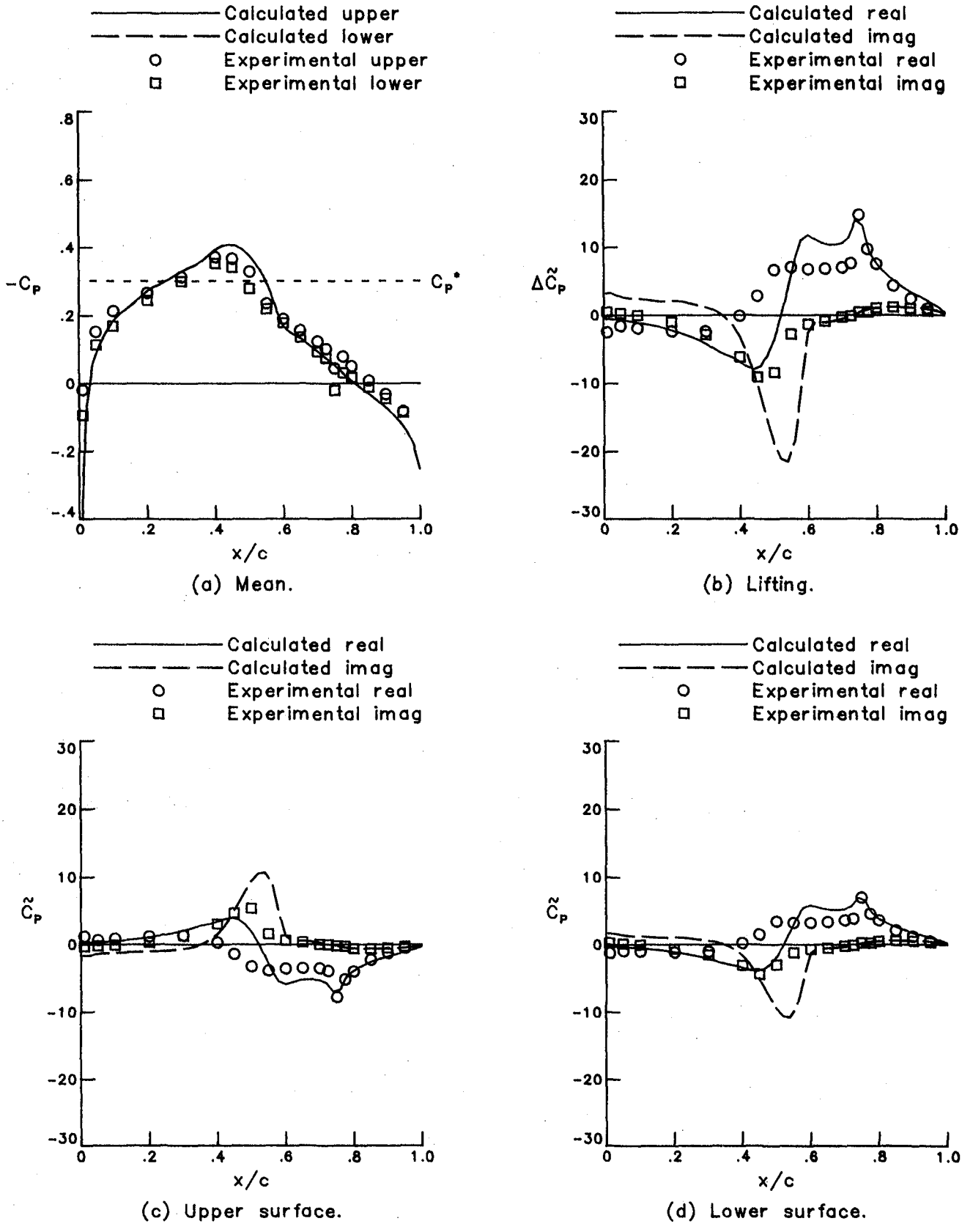

Figure 8 .- Unsteady pressure distribution for NACA 64A006 Airfoil.
Case 7, M = 0.850, δ_0 = 1, k = 0.242.

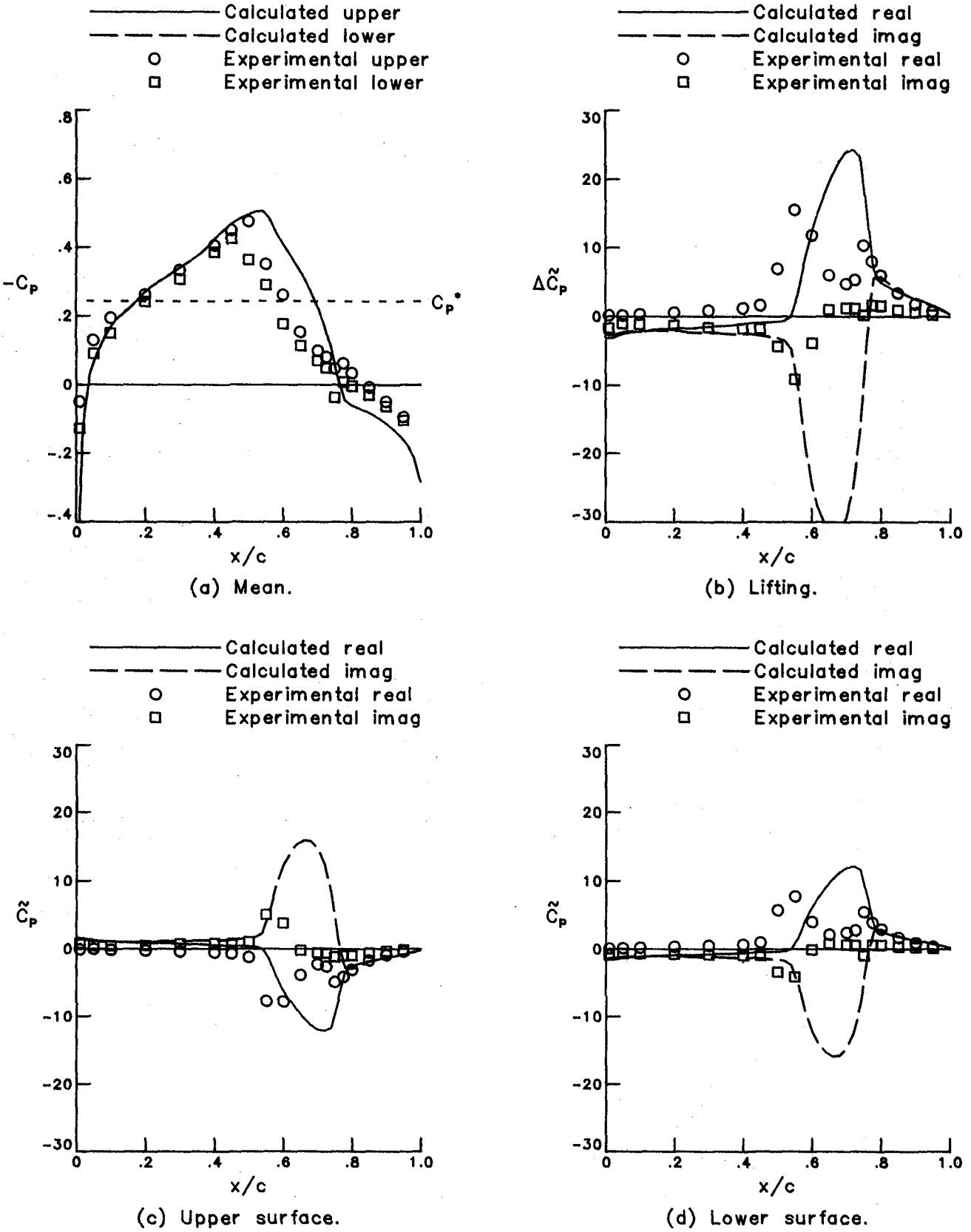

Figure 9.- Unsteady pressure distribution for NACA 64A006 Airfoil. Case 8, M = 0.875, δ_0 = 1, k = 0.059.

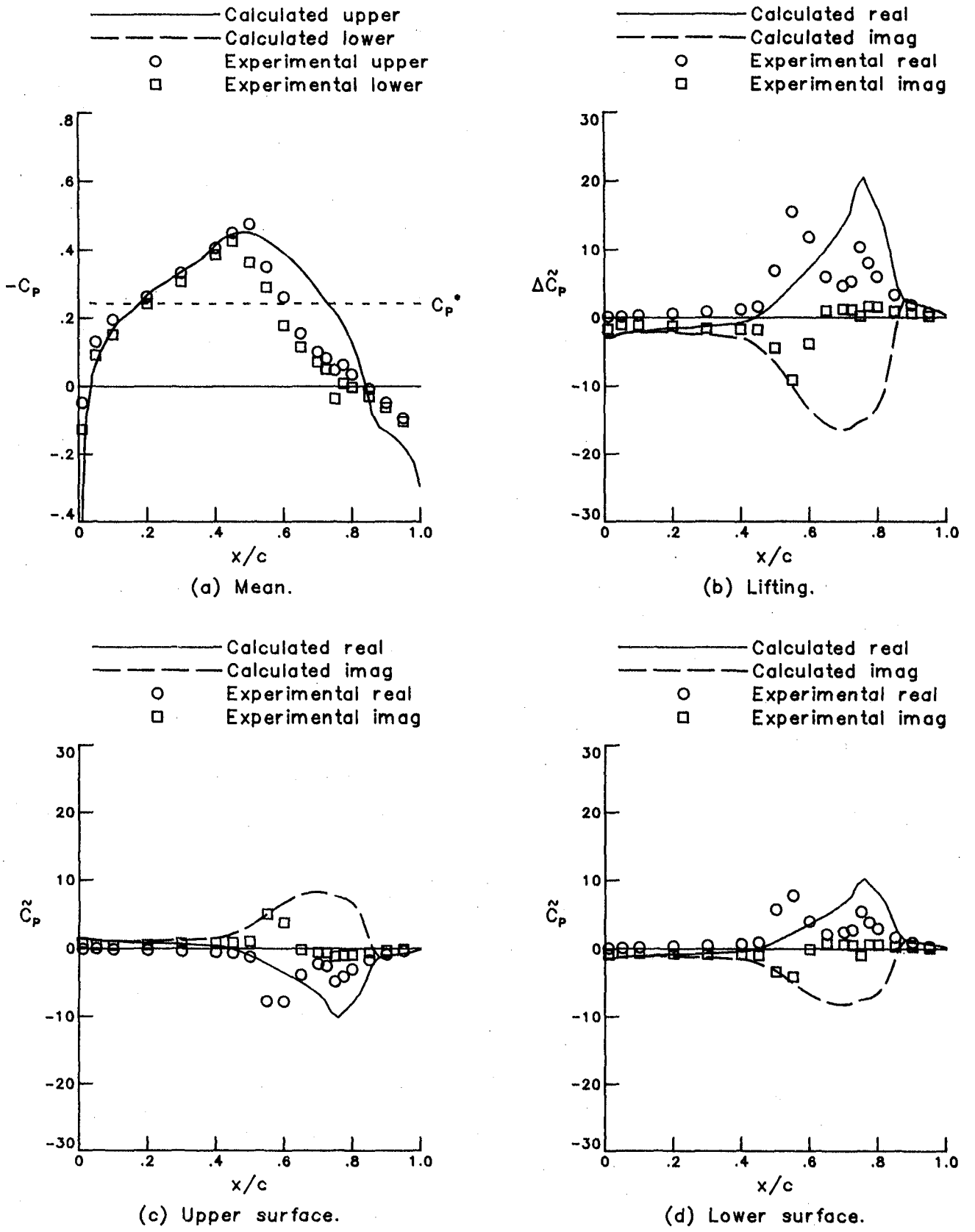

Figure 10.- Unsteady pressure distribution for NACA 64A006 Airfoil.
Case 9, M = 0.875, δ_0 = 2, k = 0.059.

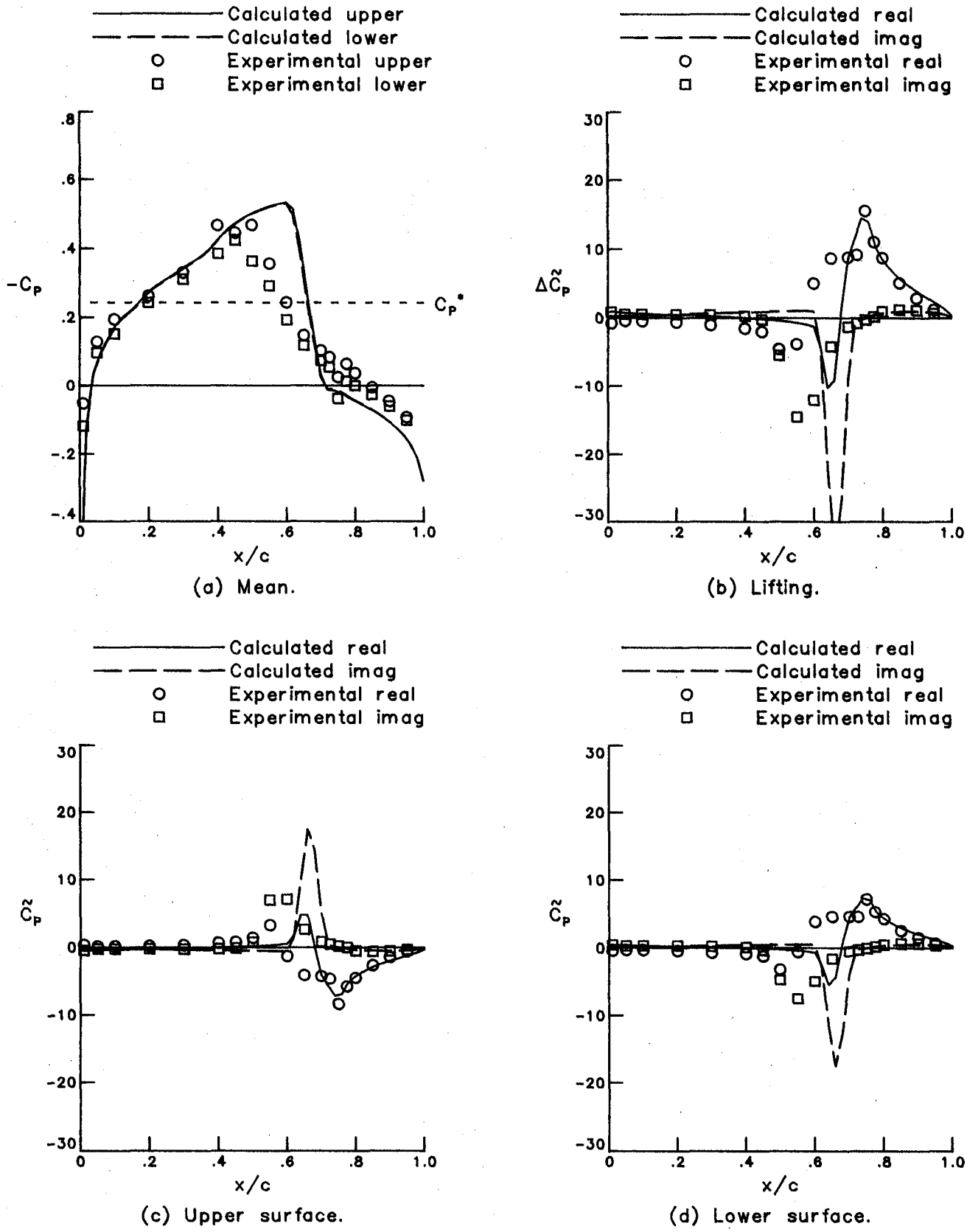

Figure 11.- Unsteady pressure distribution for NACA 64A006 Airfoil.
Case 10, M = 0.875, δ_0 = 1, k = 0.235.

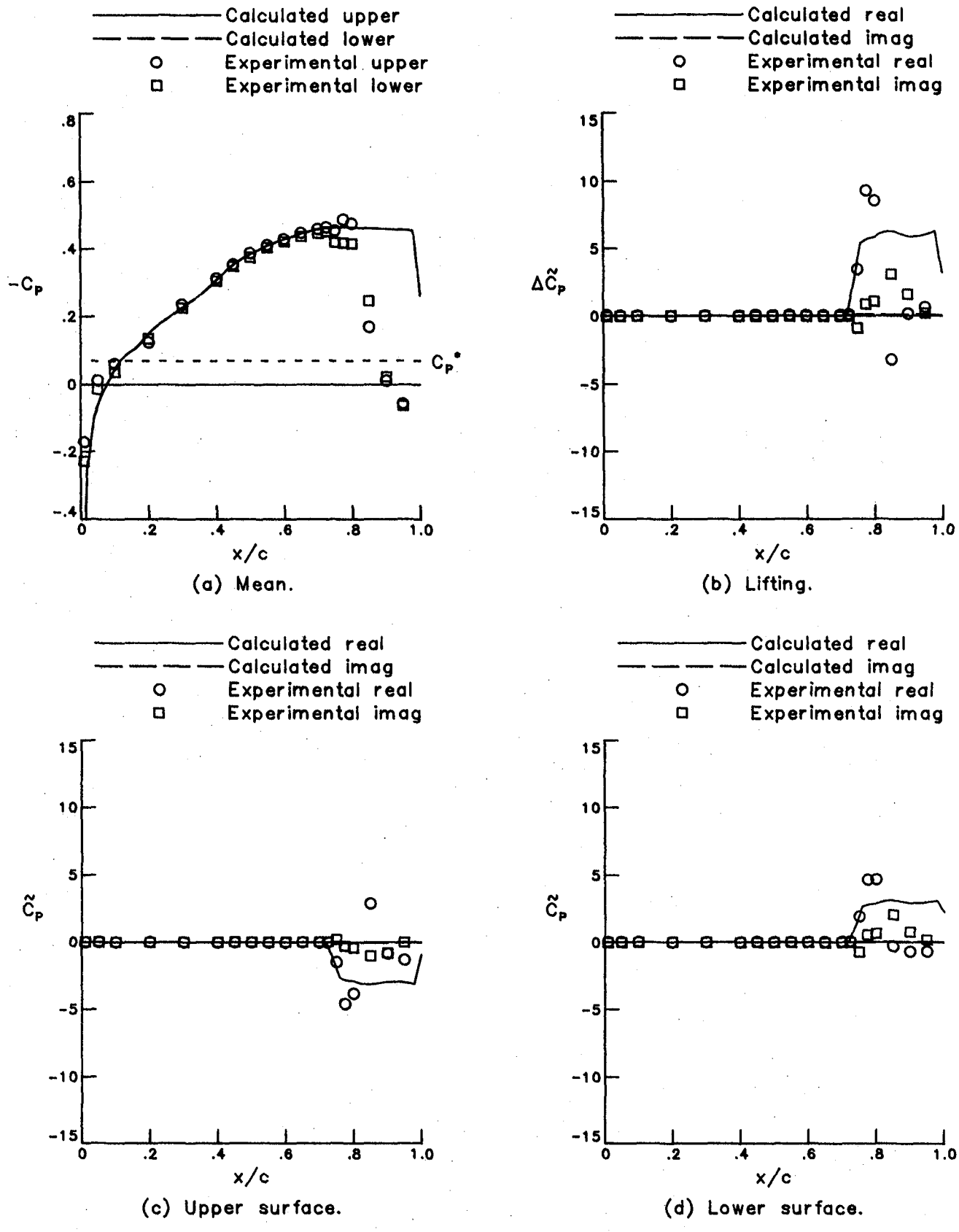

Figure 12.- Unsteady pressure distribution for NACA 64A006 Airfoil.
Case 11, M = 0.960, δ_0 = 1, k = 0.054.

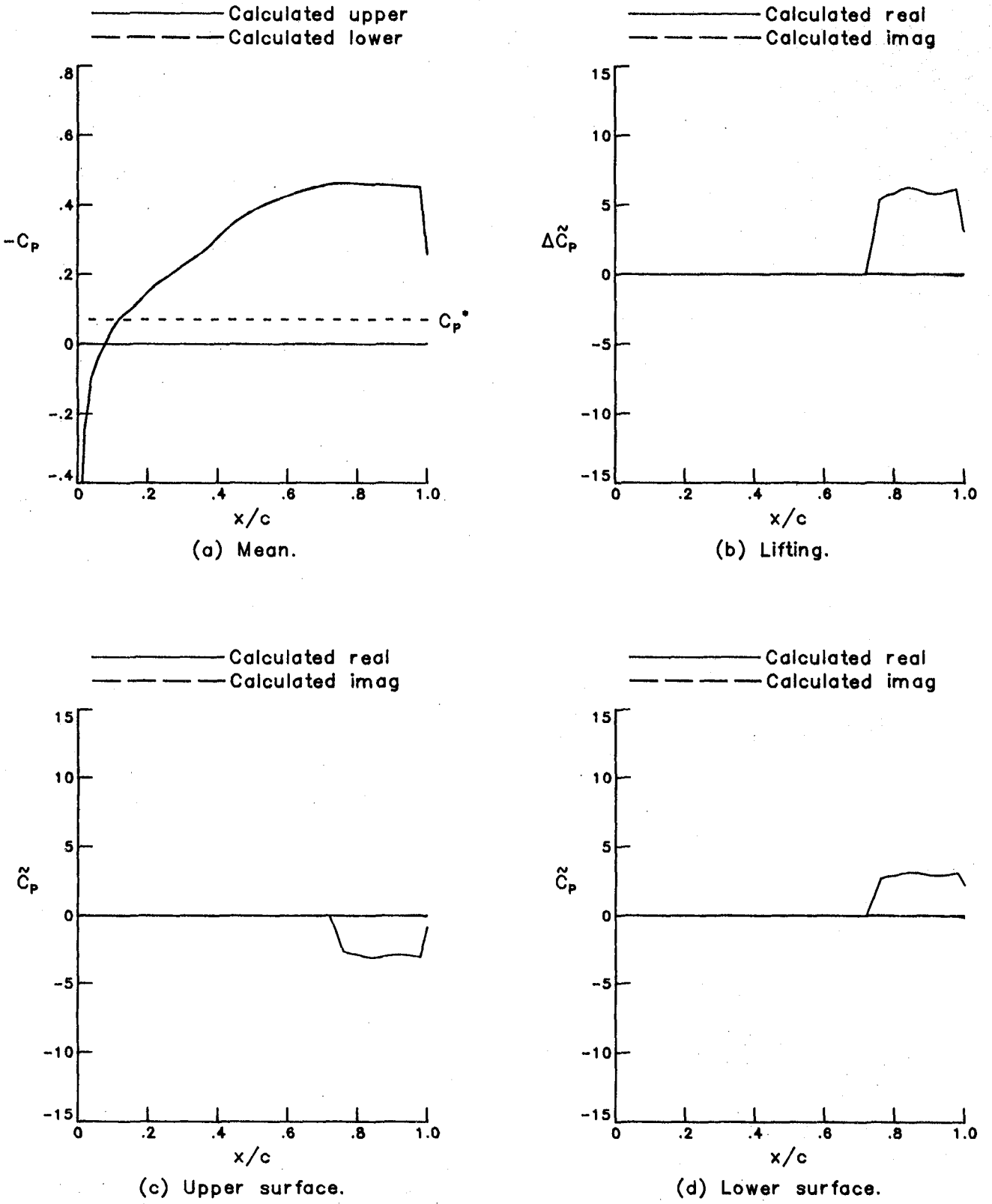

Figure 13.- Unsteady pressure distribution for NACA 64A006 Airfoil. Case 12, M = 0.960, δ_0 = 1, k = 0.217.

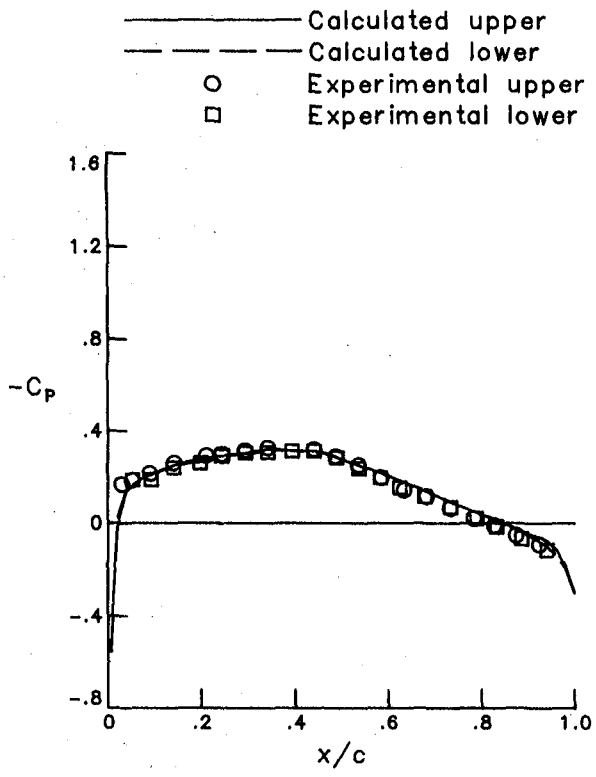

(a) M = 0.490, α_m = 0, C1.

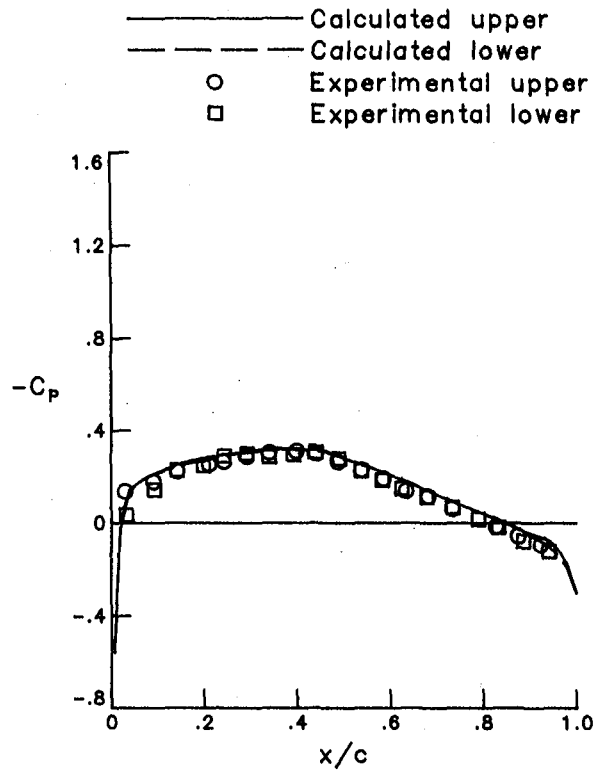

(b) M = 0.502, α_m = 0, C2.

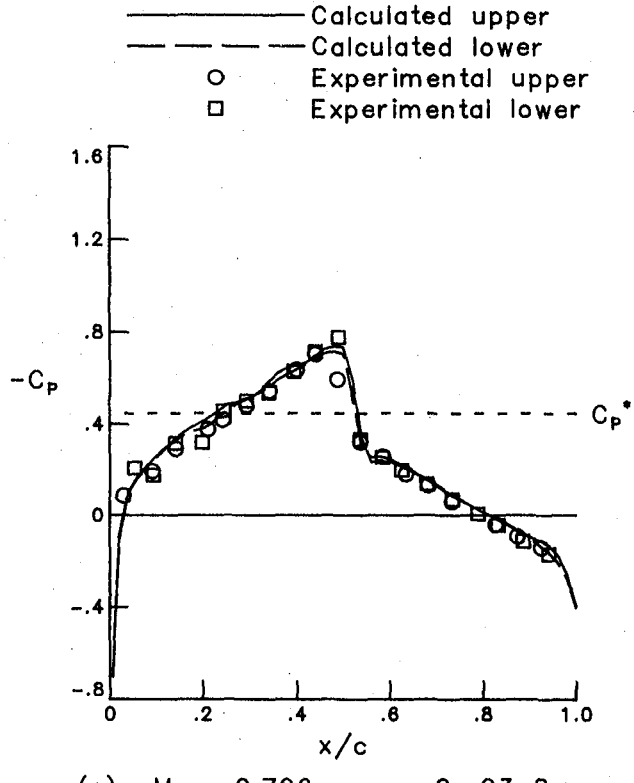

(c) M = 0.796, α_m = 0, C3-8.

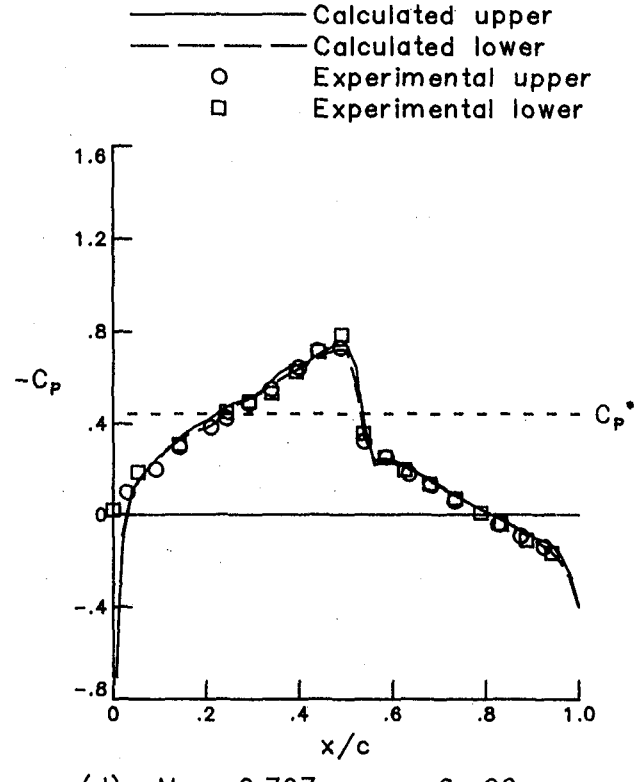

(d) M = 0.797, α_m = 0, C9.

Figure 14.- Steady pressure distribution for NACA 64A010 Airfoil.

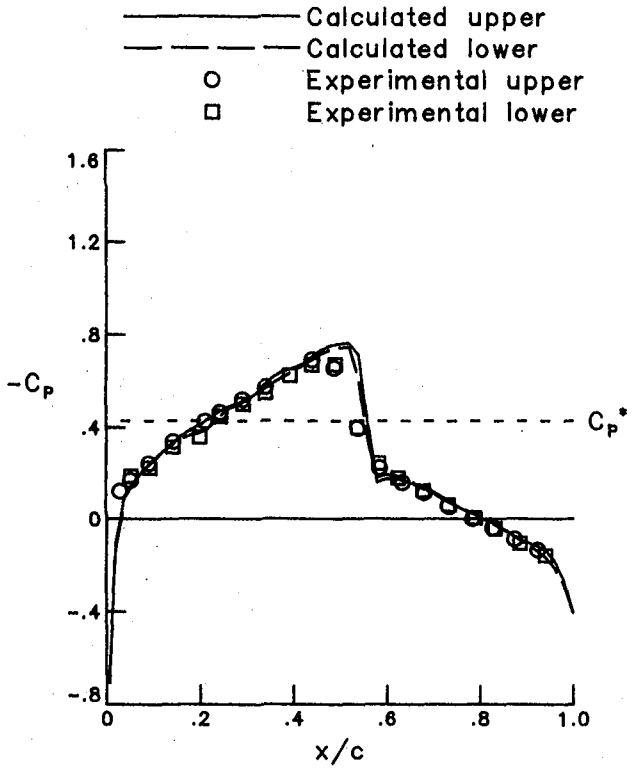

(e) M = 0.802, α_m = 0, C10.

Figure 14.- Concluded.

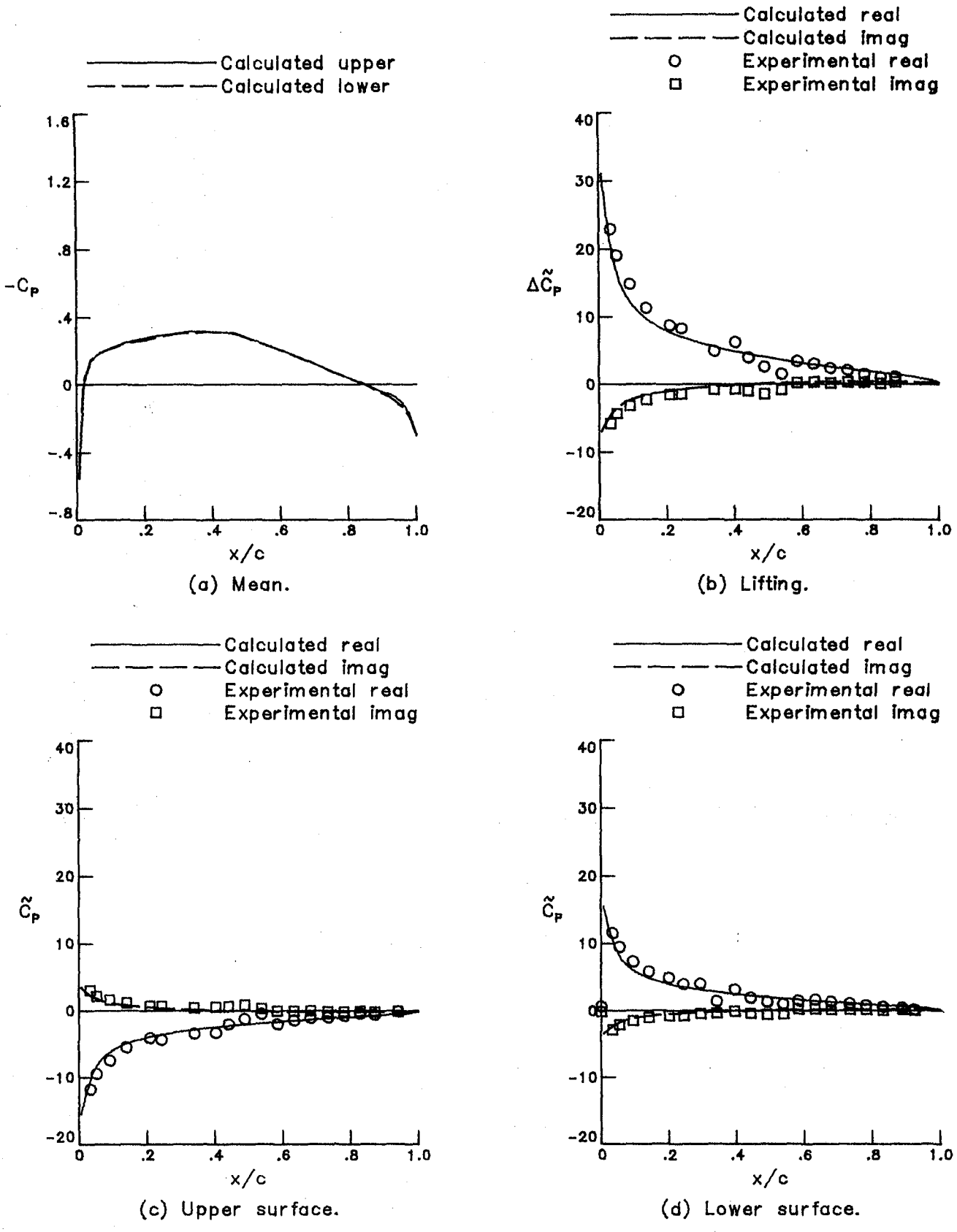

Figure 15.- Unsteady pressure distribution for NACA 64A010 Airfoil.
Case 1, M = 0.490, α_0 = 0.96, k = 0.100.

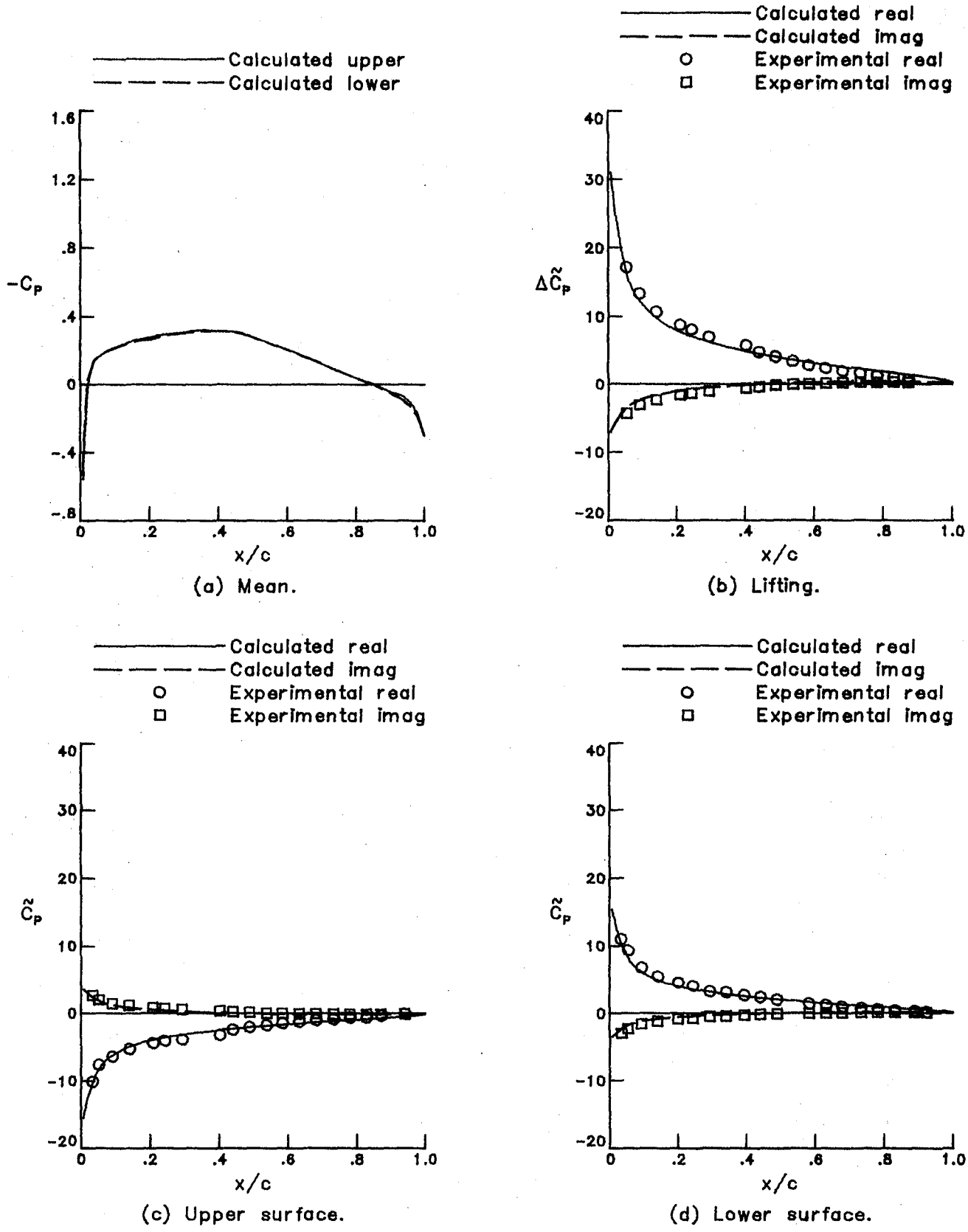

Figure 16- Unsteady pressure distribution for NACA 64A010 Airfoil.
Case 2, M = 0.502, α_0 = 1.02, k = 0.100.

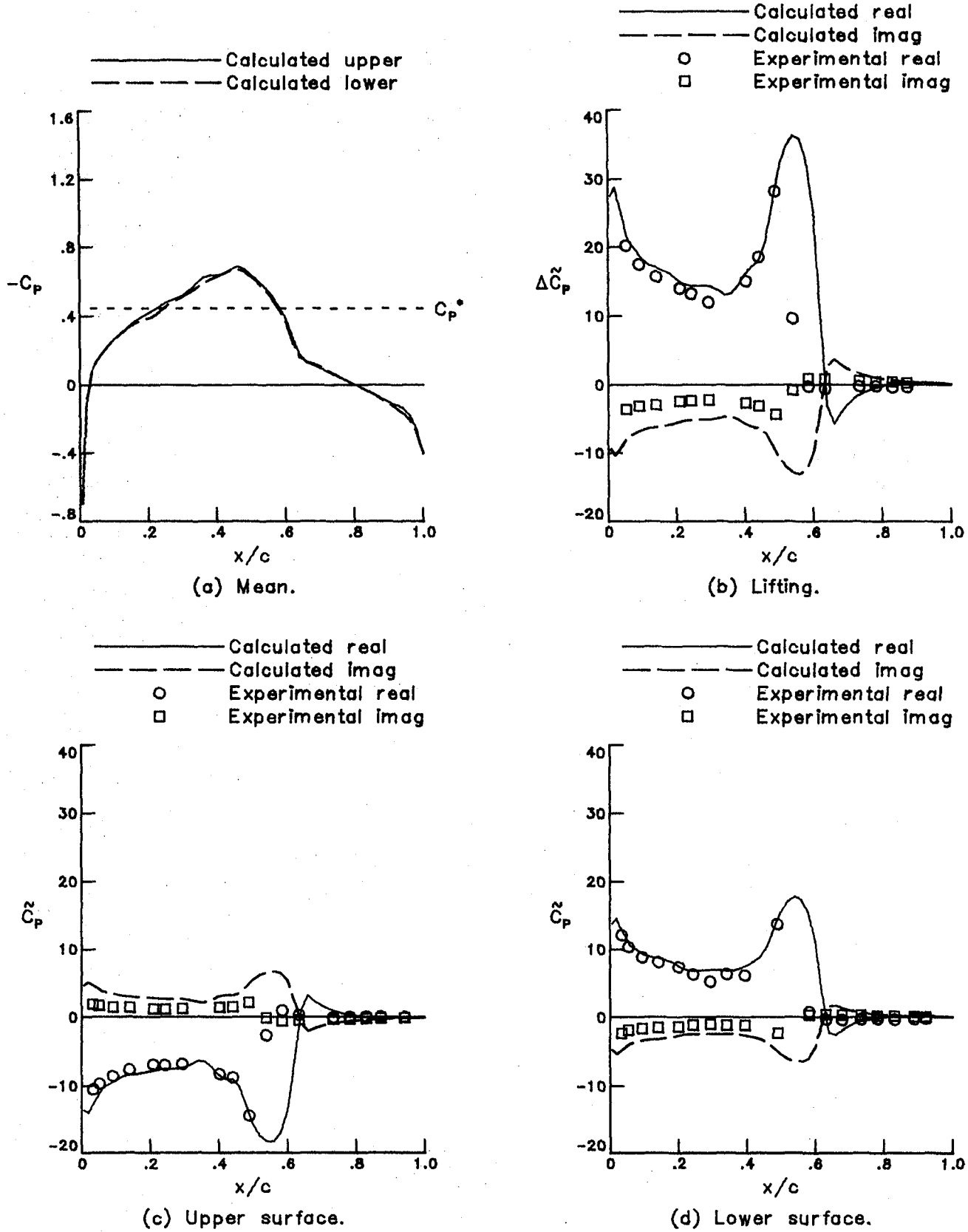

Figure 17.- Unsteady pressure distribution for NACA 64A010 Airfoil.
Case 3, M = 0.796, α_0 = 1.03, k = 0.025.

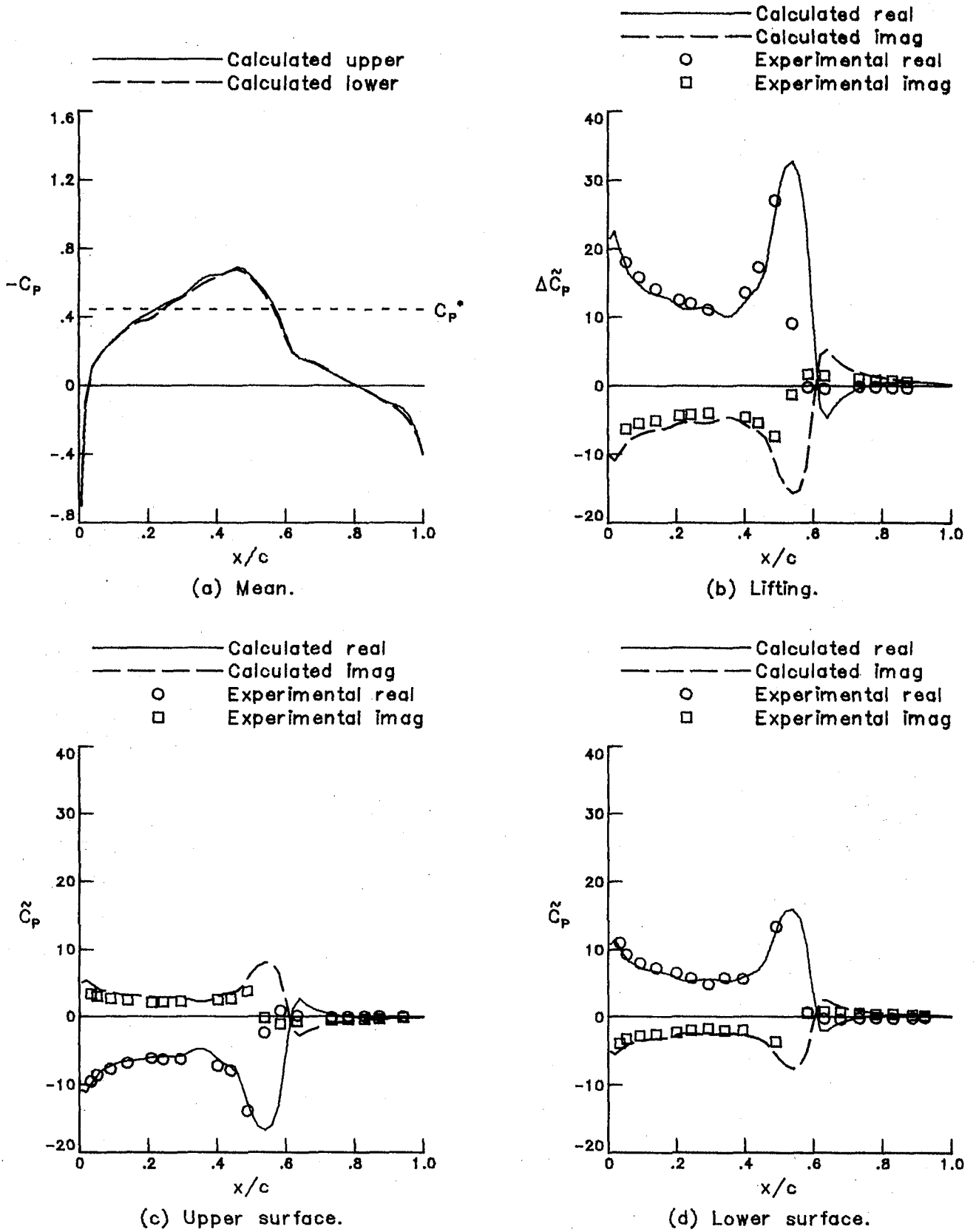

Figure 18.- Unsteady pressure distribution for NACA 64A010 Airfoil. Case 4, M = 0.796, α_0 = 1.02, k = 0.051.

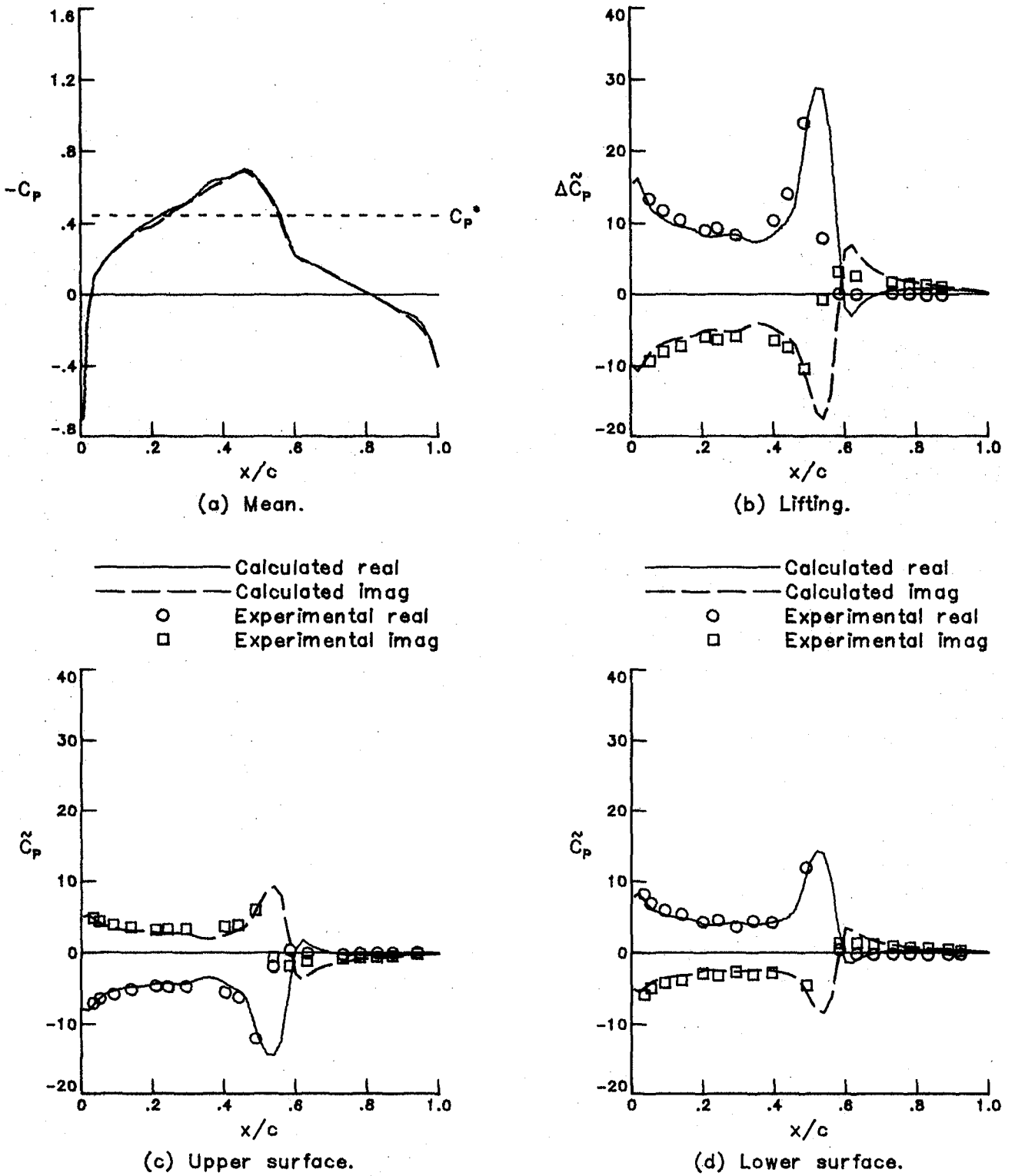

Figure 19.- Unsteady pressure distribution for NACA 64A010 Airfoil.
Case 5, M = 0.796, α_0 = 1.02, k = 0.101.

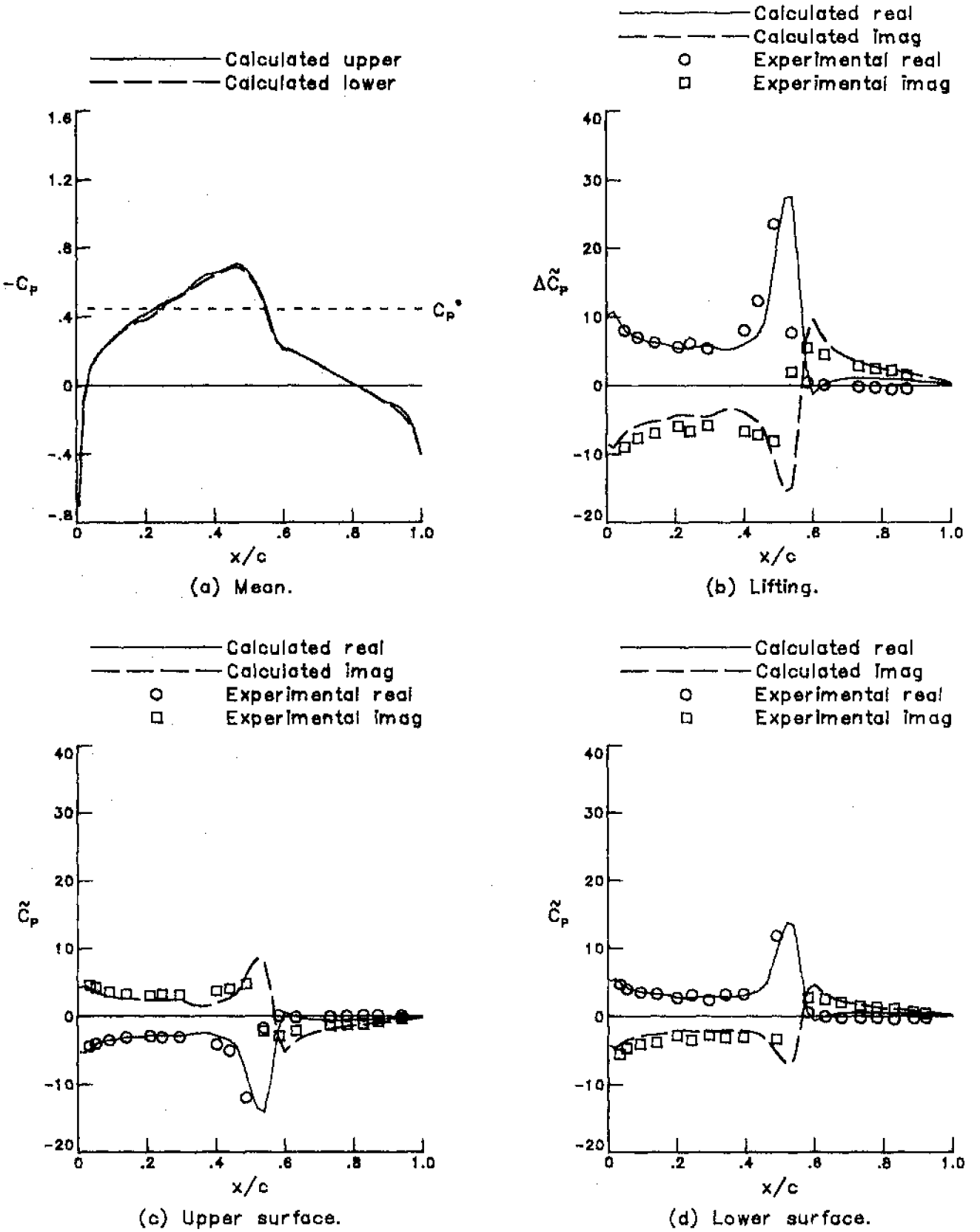

Figure 20.- Unsteady pressure distribution for NACA 64A010 Airfoil.
Case 6, M = 0.796, α_0 = 1.01, k = 0.202.

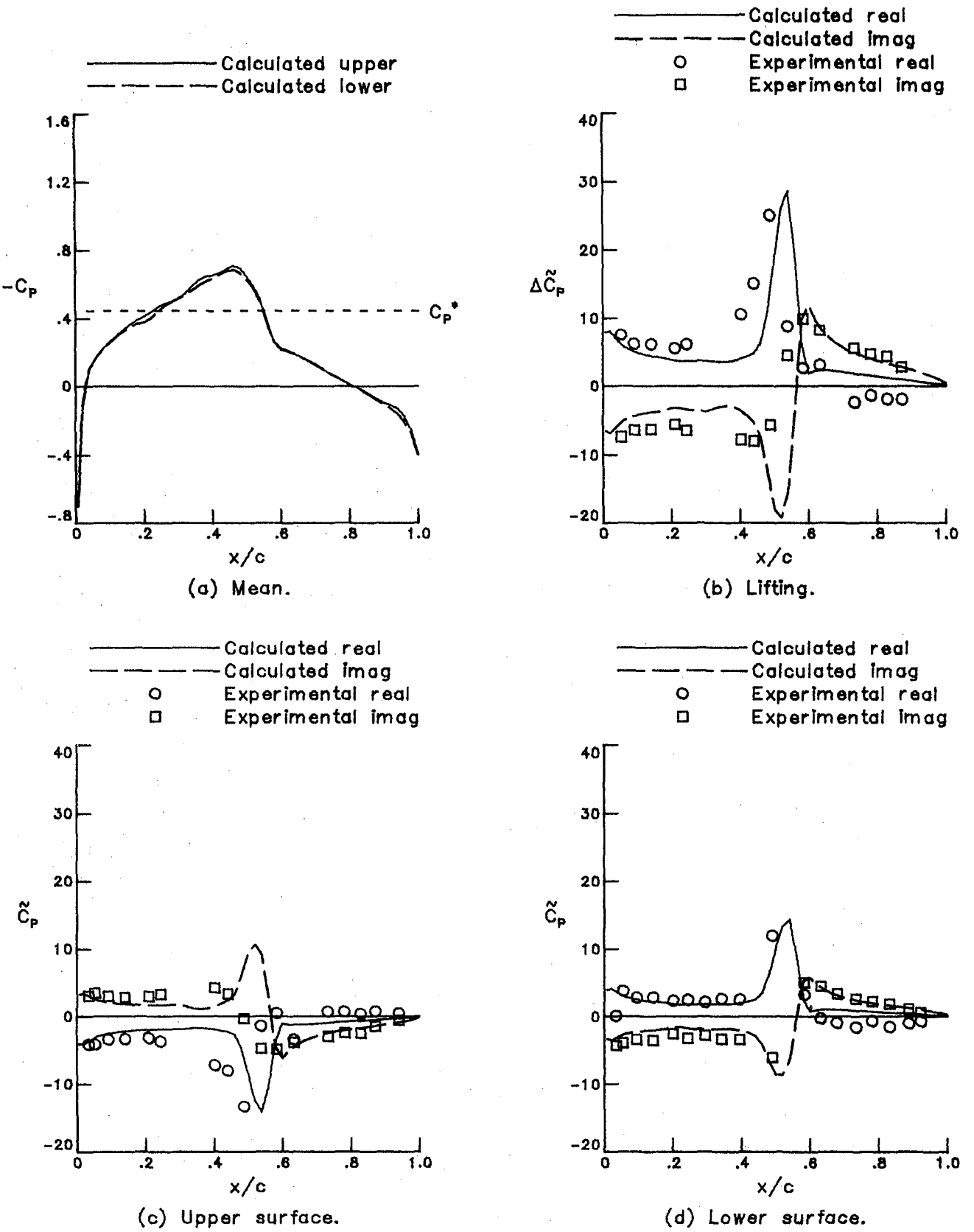

Figure 21.- Unsteady pressure distribution for NACA 64A010 Airfoil. Case 7, M = 0.796, α_0 = 0.99, k = 0.303.

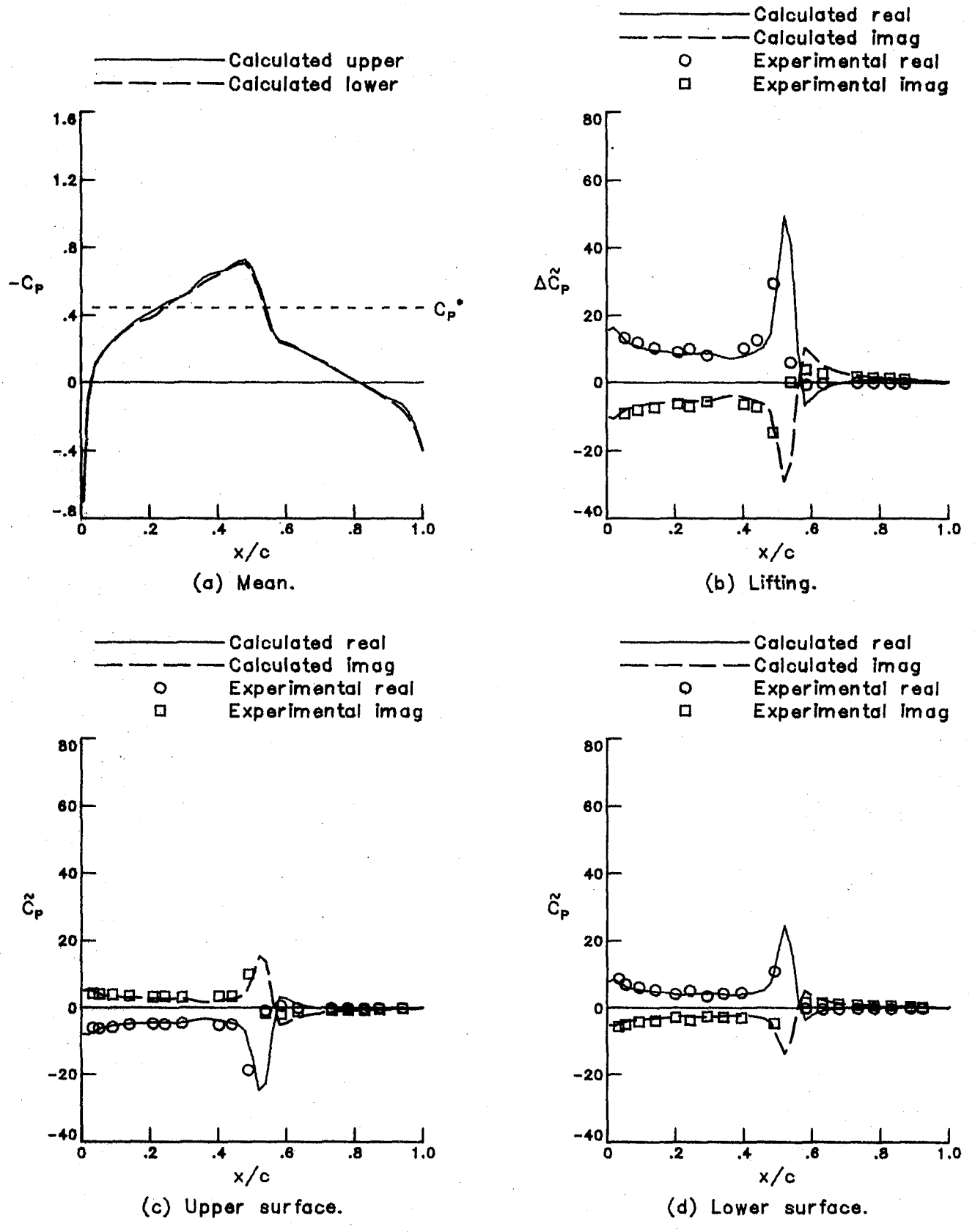

Figure 22.- Unsteady pressure distribution for NACA 64A010 Airfoil.
Case 8, M = 0.796, α_0 = 0.51, k = 0.101.

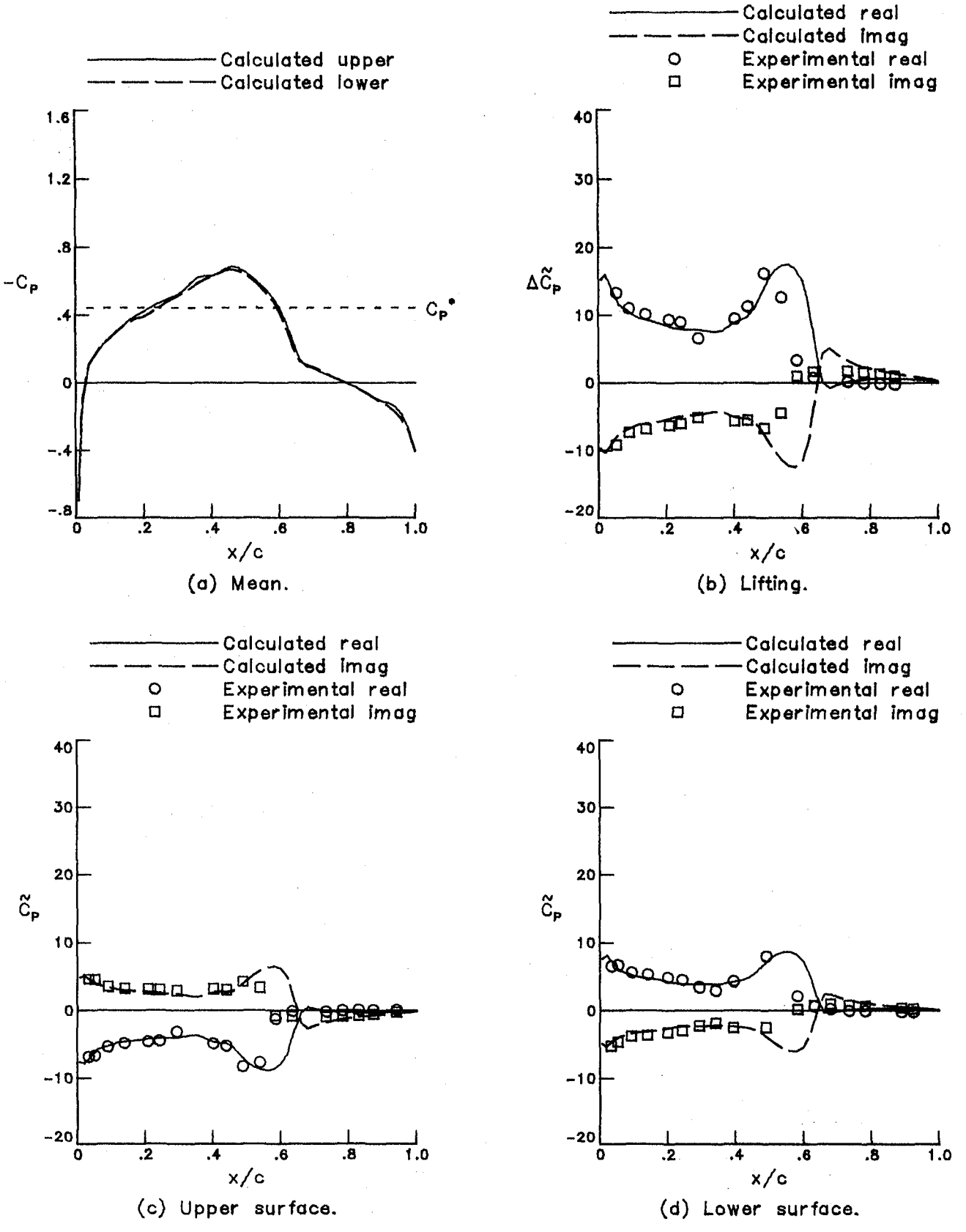

Figure 23.- Unsteady pressure distribution for NACA 64A010 Airfoil.
Case 9, M = 0.797, α_0 = 2.00, k = 0.101.

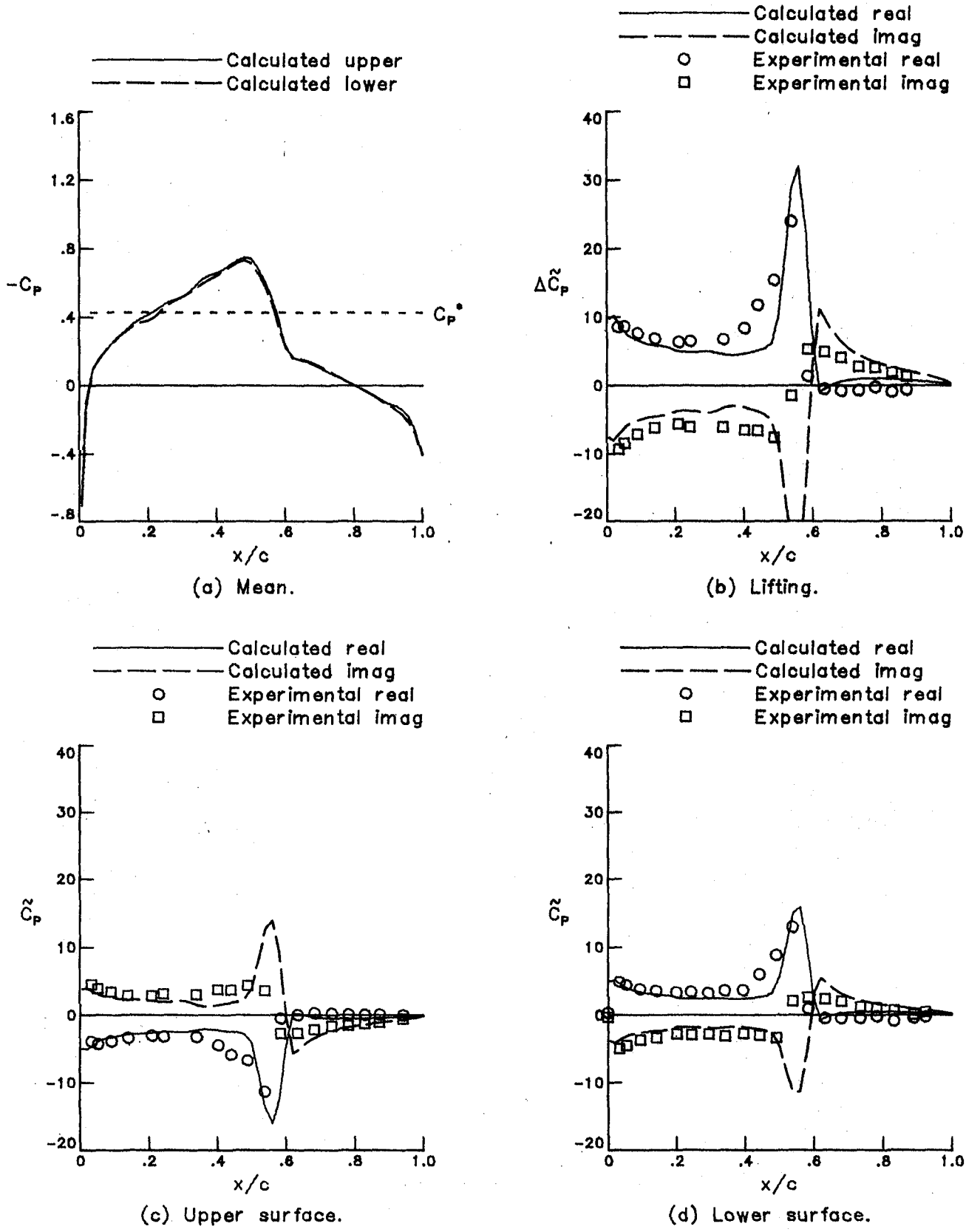

Figure 24- Unsteady pressure distribution for NACA 64A010 Airfoil.
Case 10, M = 0.802, α_0 = 0.94, k = 0.200.

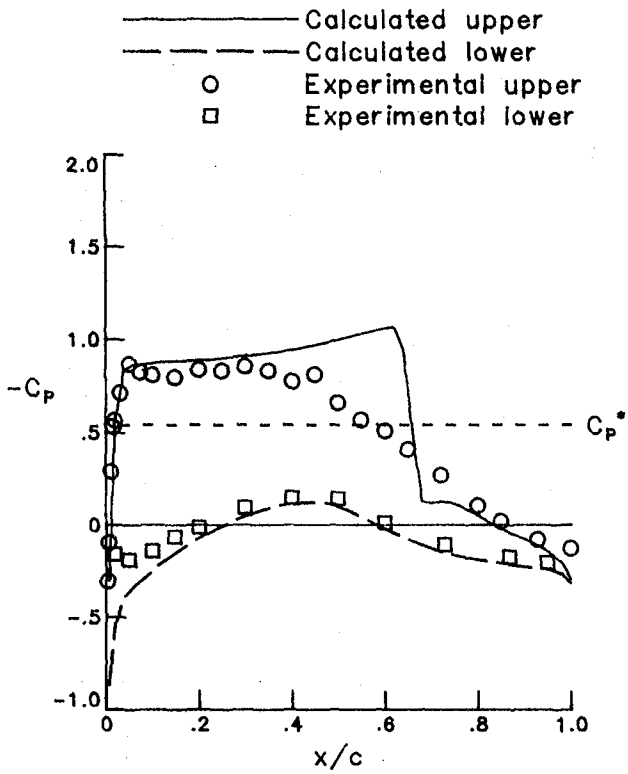

(a) M = 0.765, α_m = 1.5, C3-5,11-13.

Figure 25.- Steady pressure distribution for MBB-A3 Airfoil.

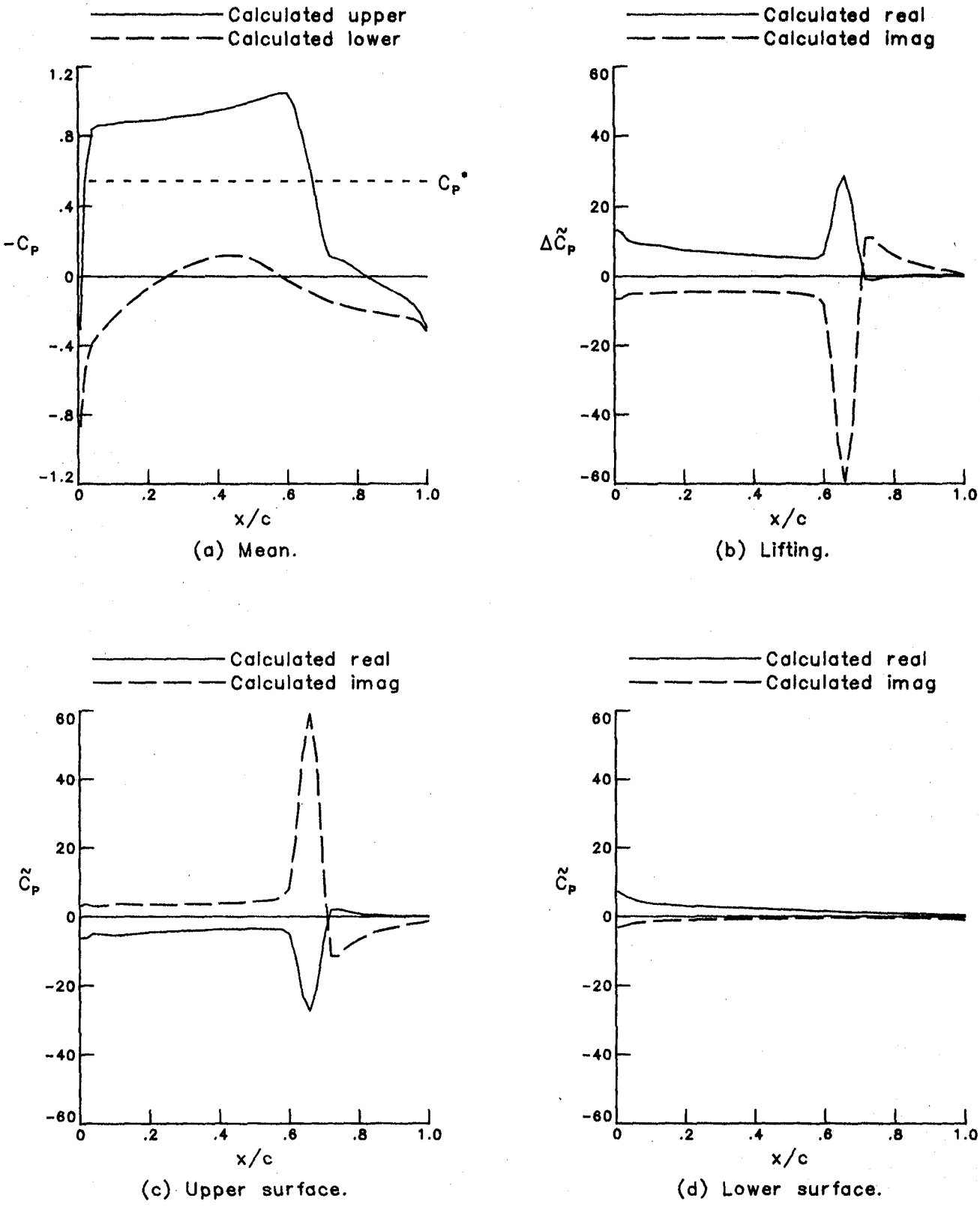

Figure 26.- Unsteady pressure distribution for MBB-A3 Airfoil.
Case 3, M = 0.765, α_m = 1.5, α_0 = 0.5, k = 0.1.

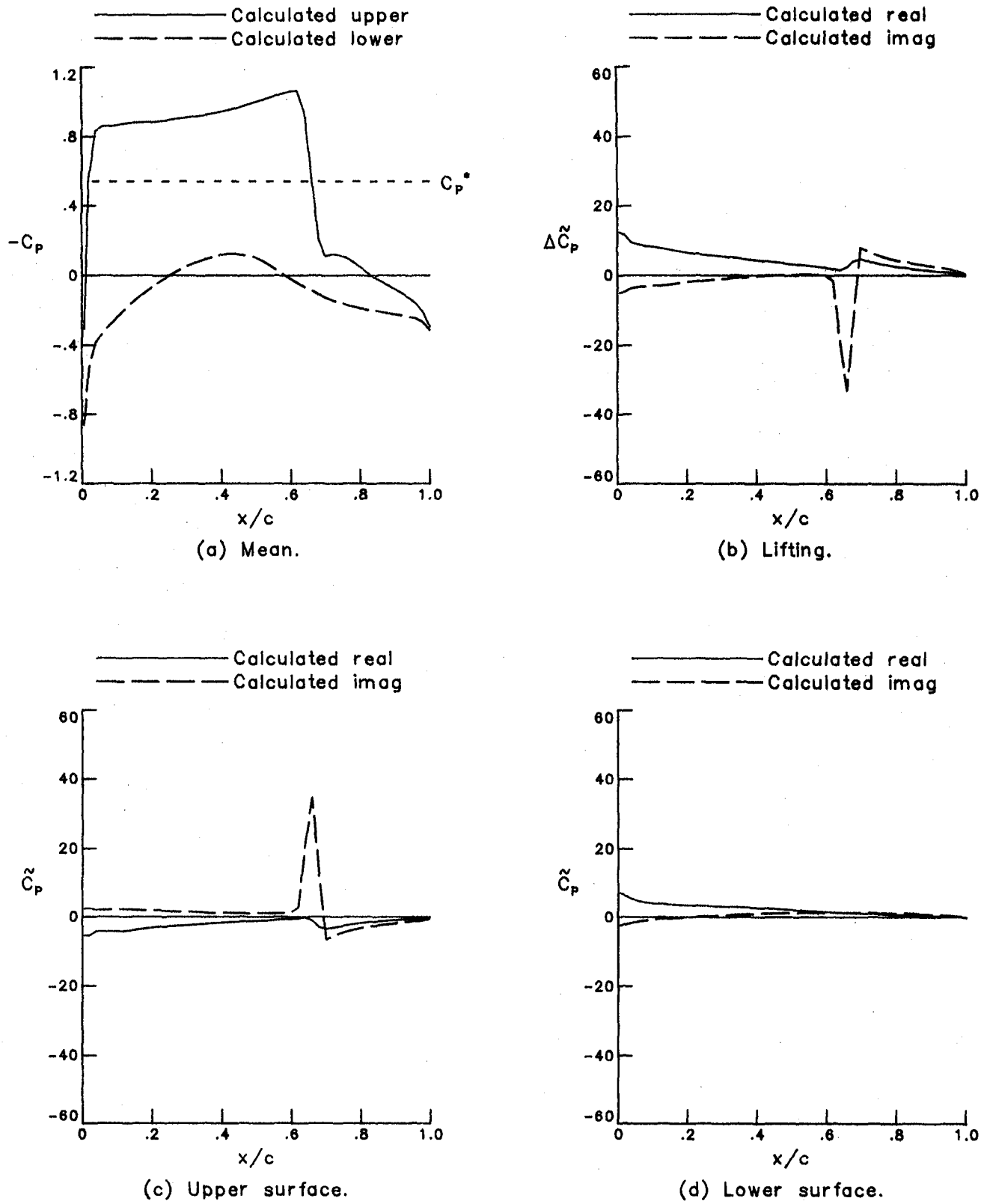

Figure 27.- Unsteady pressure distribution for MBB-A3 Airfoil.
Case 4, M = 0.765, α_m = 1.5, α_0 = 0.5, k = 0.3.

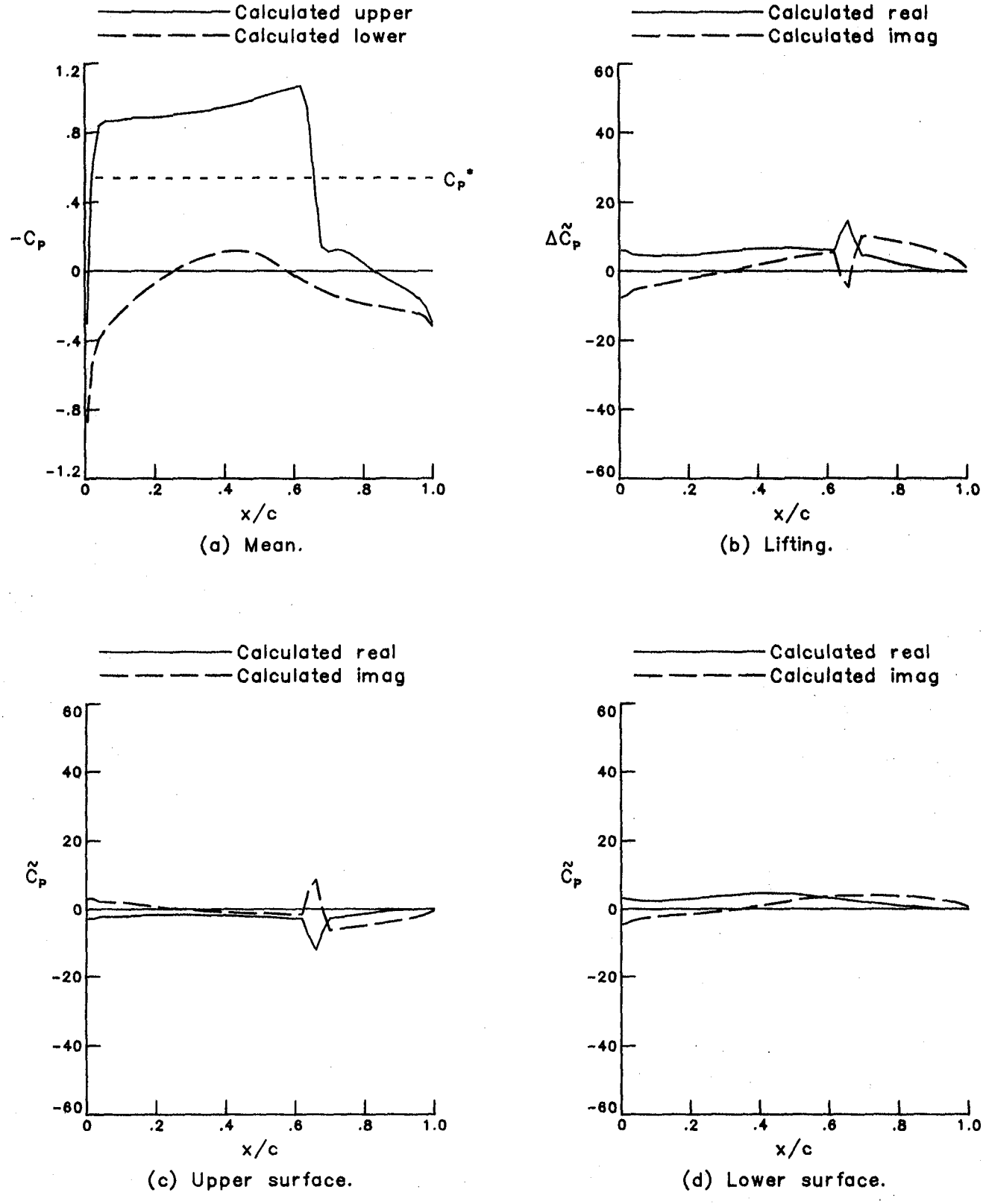

Figure 28.- Unsteady pressure distribution for MBB-A3 Airfoil.
Case 5, M = 0.765, α_m = 1.5, α_0 = 0.5, k = 0.9.

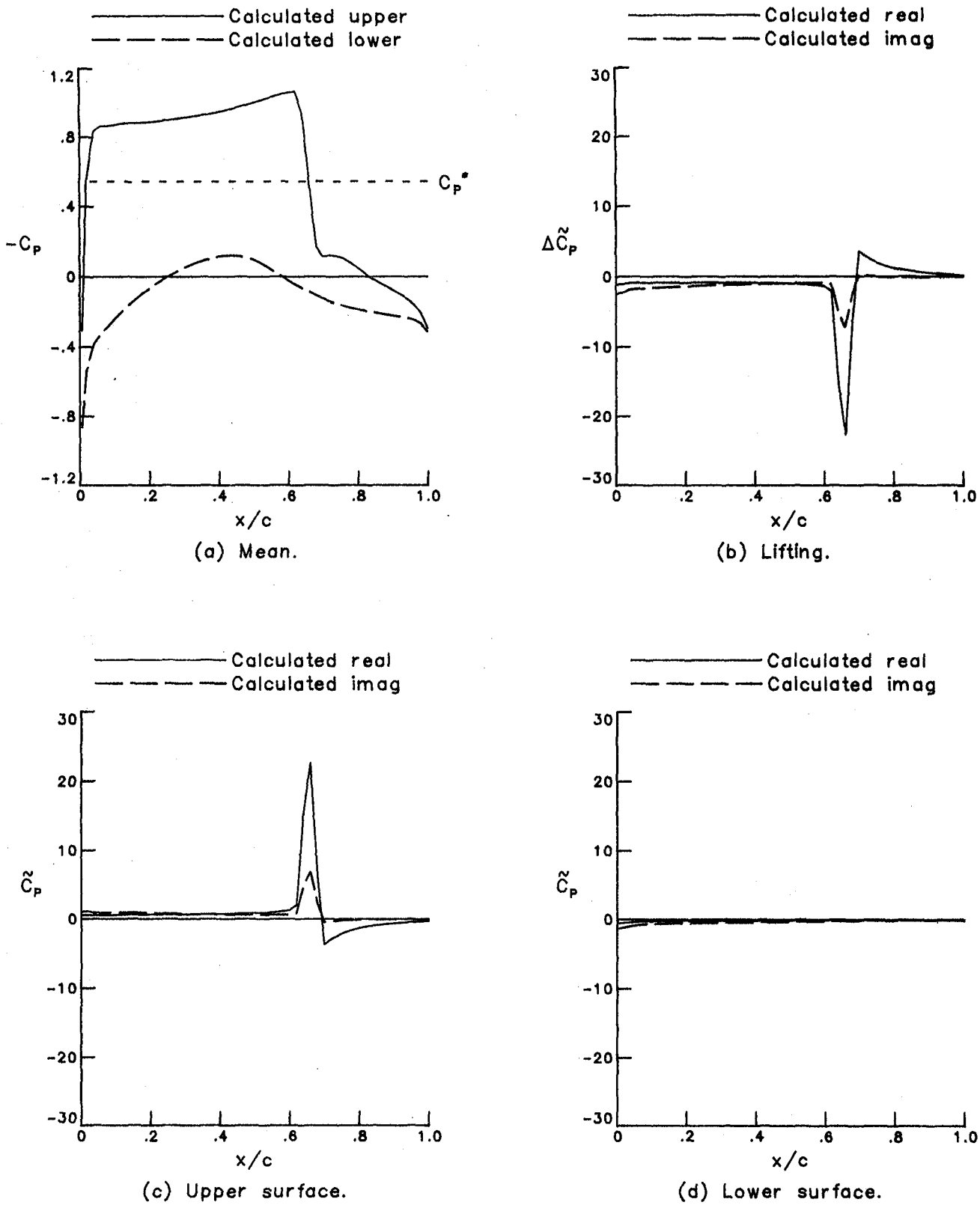

Figure 29.- Unsteady pressure distribution for MBB-A3 Airfoil.
Case 11, M = 0.765, α_m = 1.5, h_0/c = 0.01, k = 0.1.

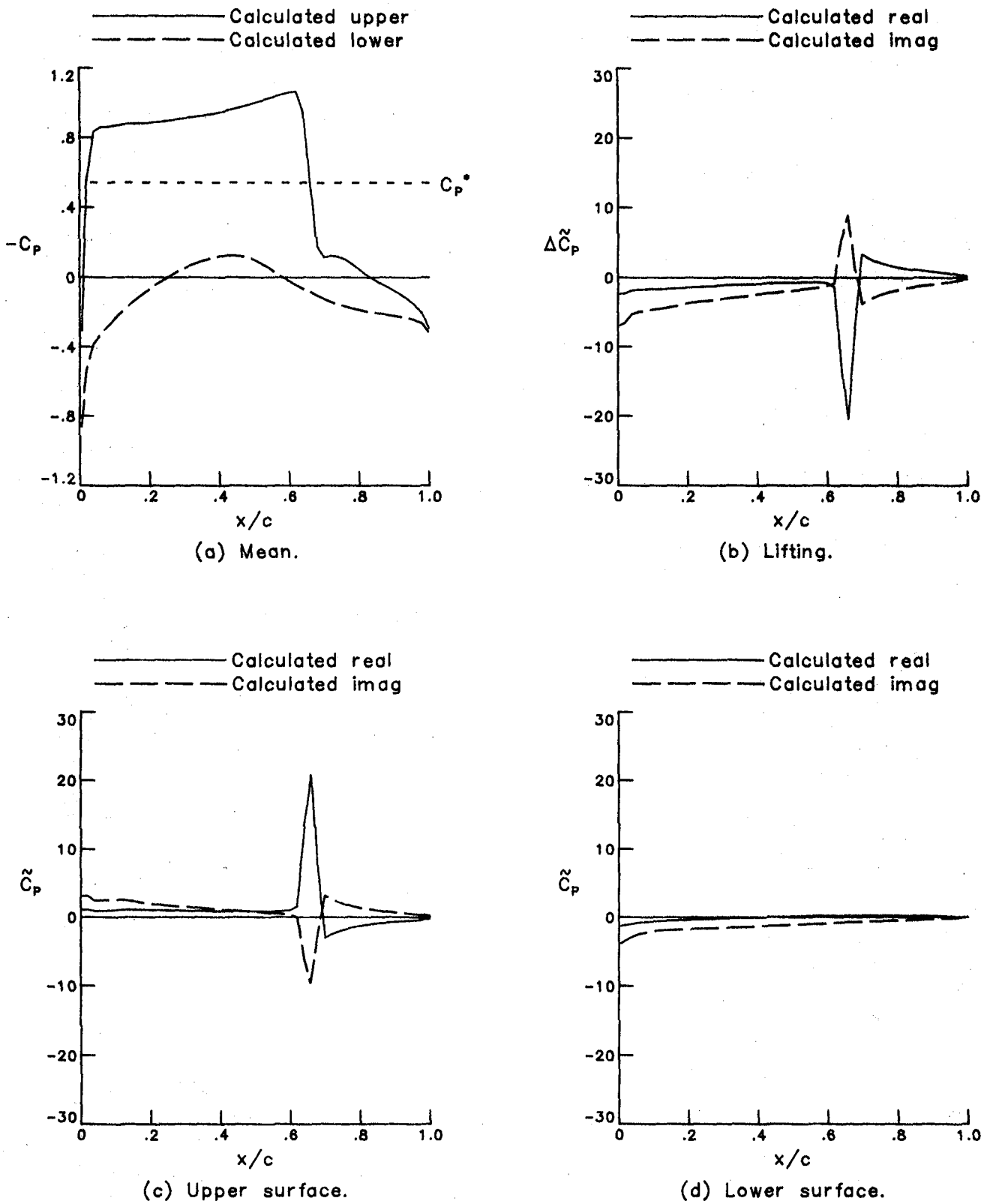

Figure 30- Unsteady pressure distribution for MBB-A3 Airfoil.
Case 12, M = 0.765, α_m = 1.5, h_0/c = 0.01, k = 0.3.

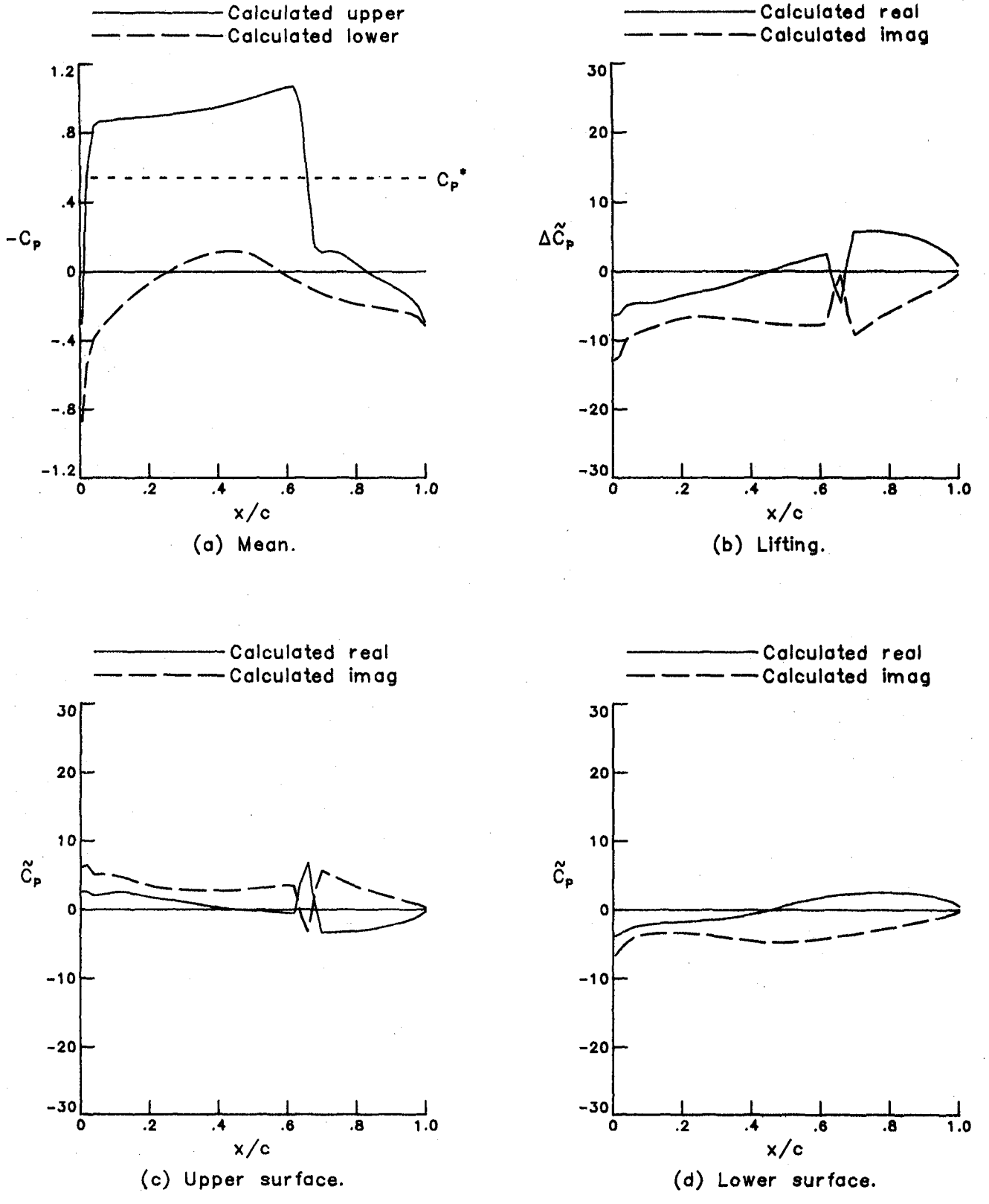

Figure 31.- Unsteady pressure distribution for MBB-A3 Airfoil.
Case 13, M = 0.765, α_m = 1.5, h_0/c = 0.01, k = 0.9.

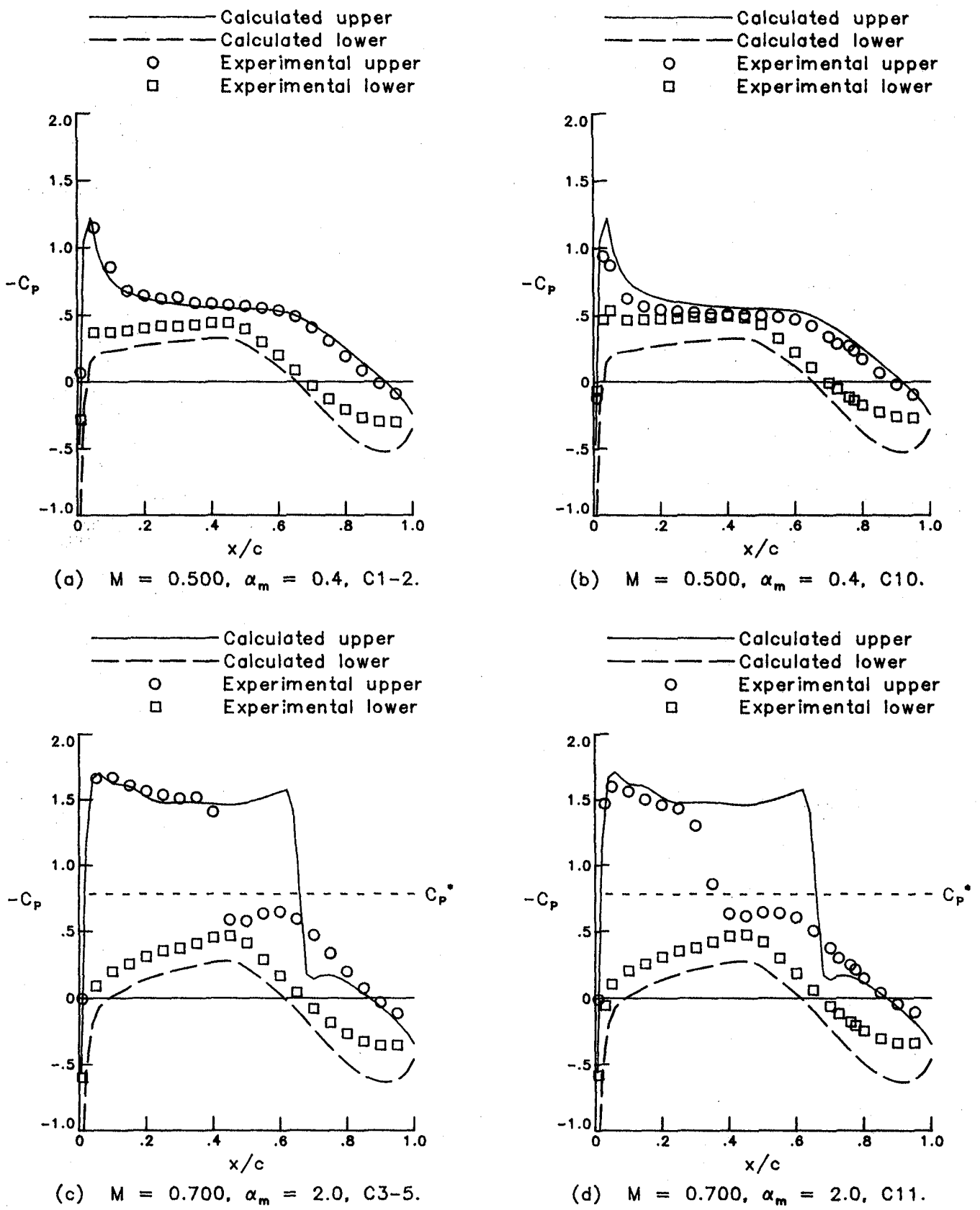

(a) M = 0.500, α_m = 0.4, C1-2.

(b) M = 0.500, α_m = 0.4, C10.

(c) M = 0.700, α_m = 2.0, C3-5.

(d) M = 0.700, α_m = 2.0, C11.

Figure 32.- Steady pressure distribution for NLR 7301 Airfoil.

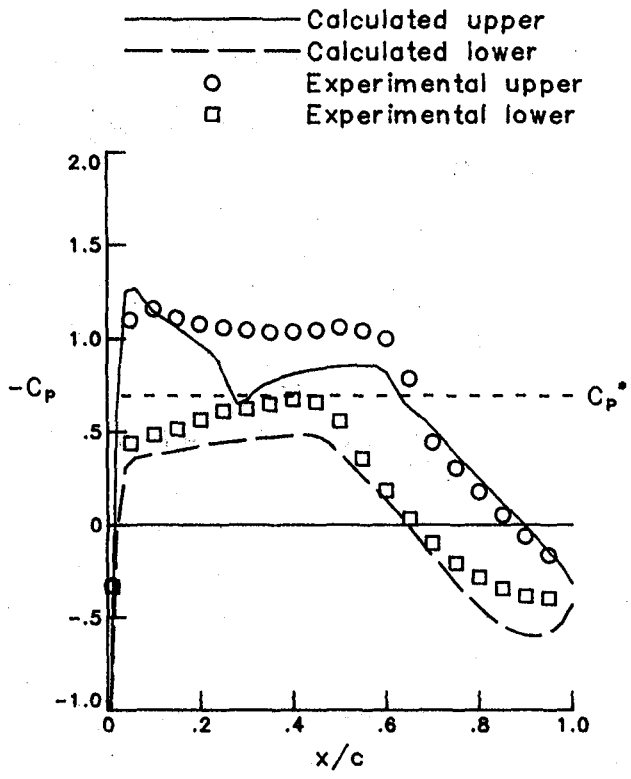

(e) M = 0.721, α_m = -0.19, C6-9.

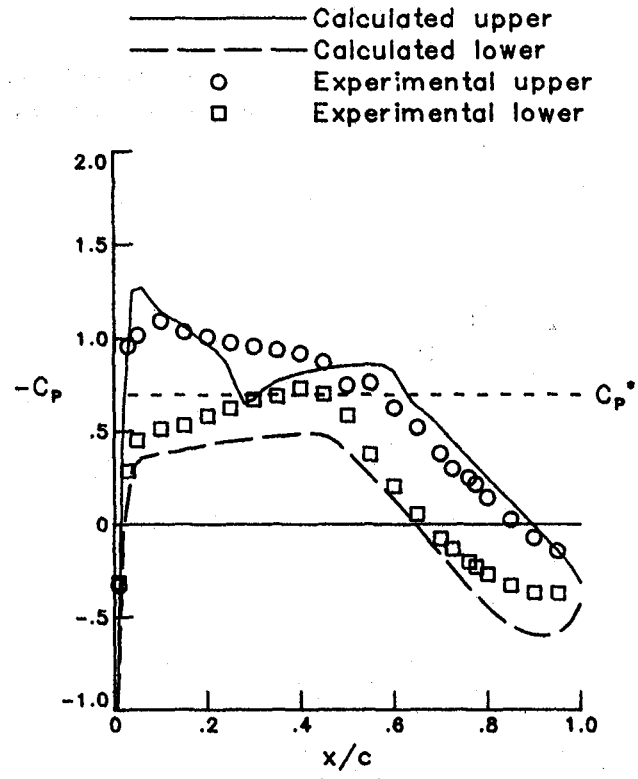

(f) M = 0.721, α_m = -0.19, C12-14.

Figure 32- Concluded.

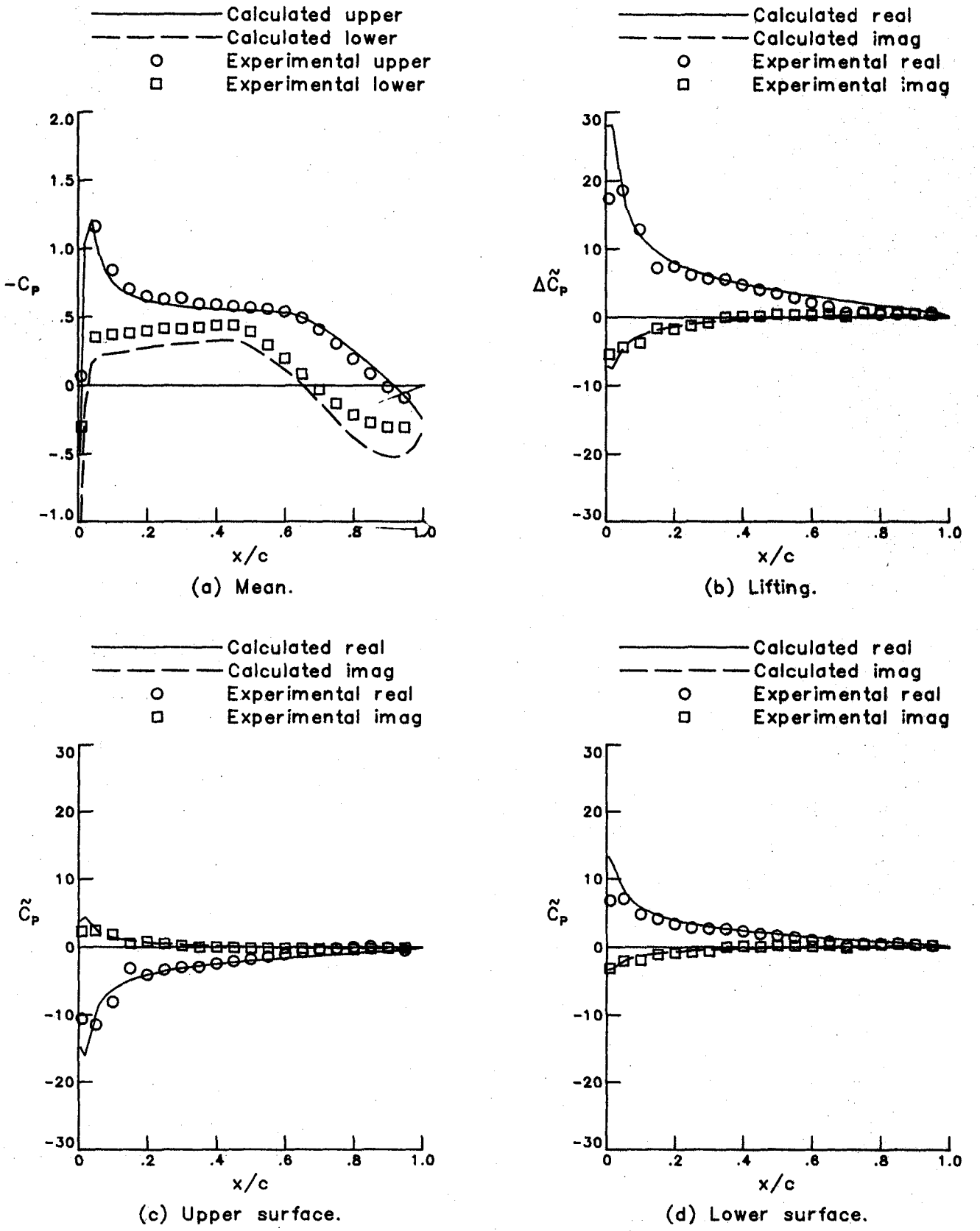

Figure 33.- Unsteady pressure distribution for NLR 7301 Airfoil.
Case 1, M = 0.500, α_m = 0.4, α_0 = 0.5, k = 0.098.

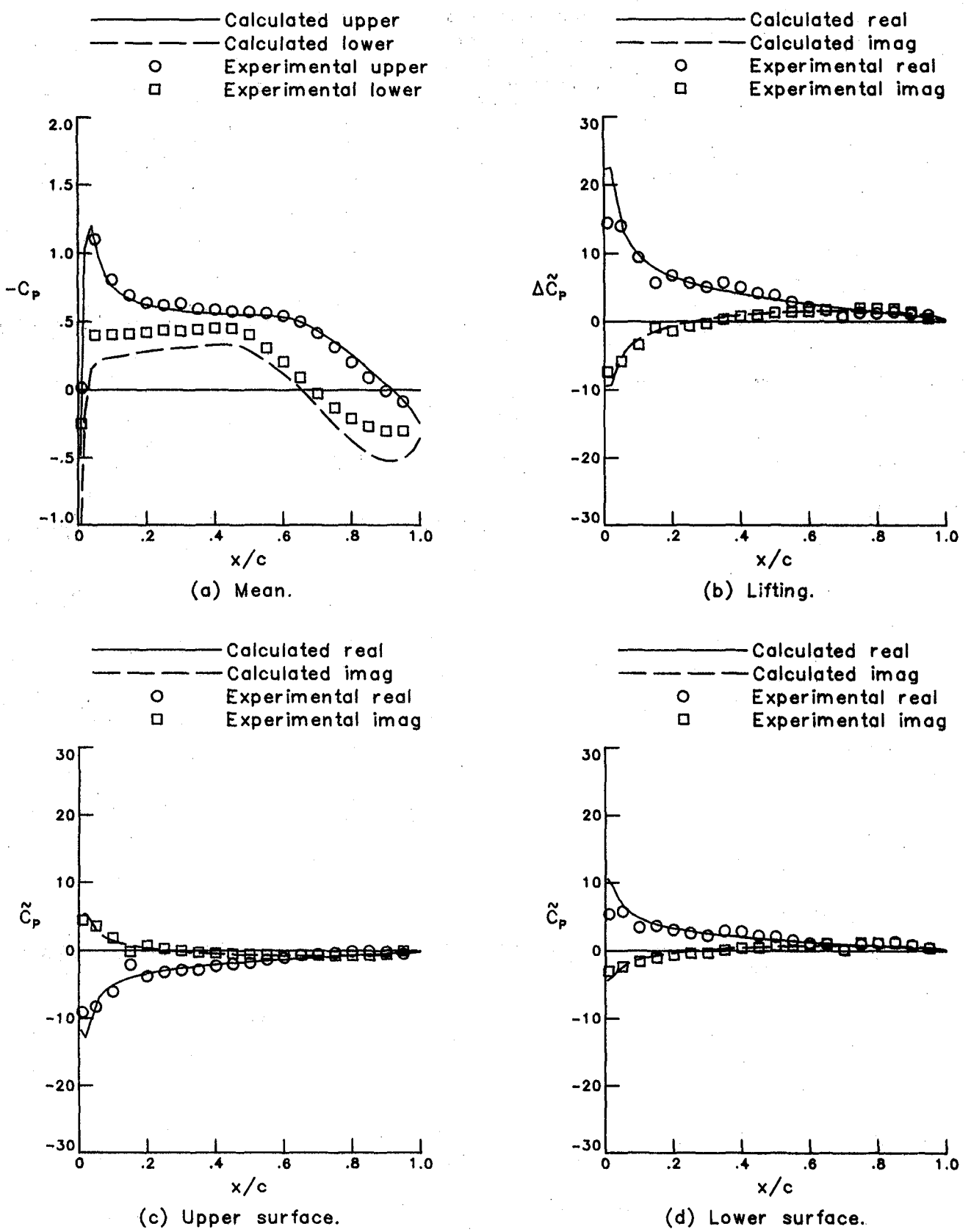

Figure 34.- Unsteady pressure distribution for NLR 7301 Airfoil.
Case 2, M = 0.500, α_m = 0.4, α_0 = 0.5, k = 0.263.

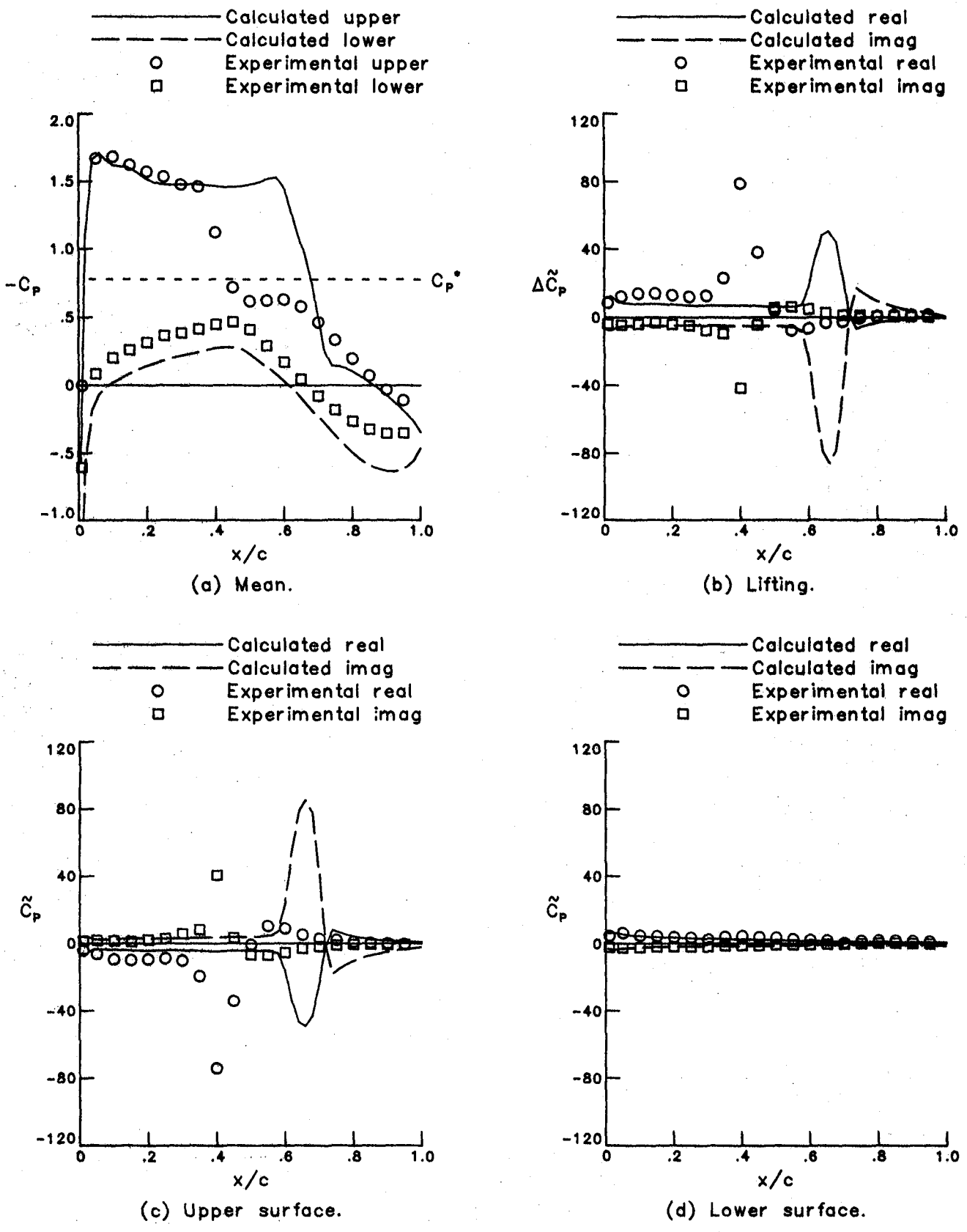

Figure 35.- Unsteady pressure distribution for NLR 7301 Airfoil.
Case 3, M = 0.700, α_m = 2.0, α_0 = 0.5, k = 0.072.

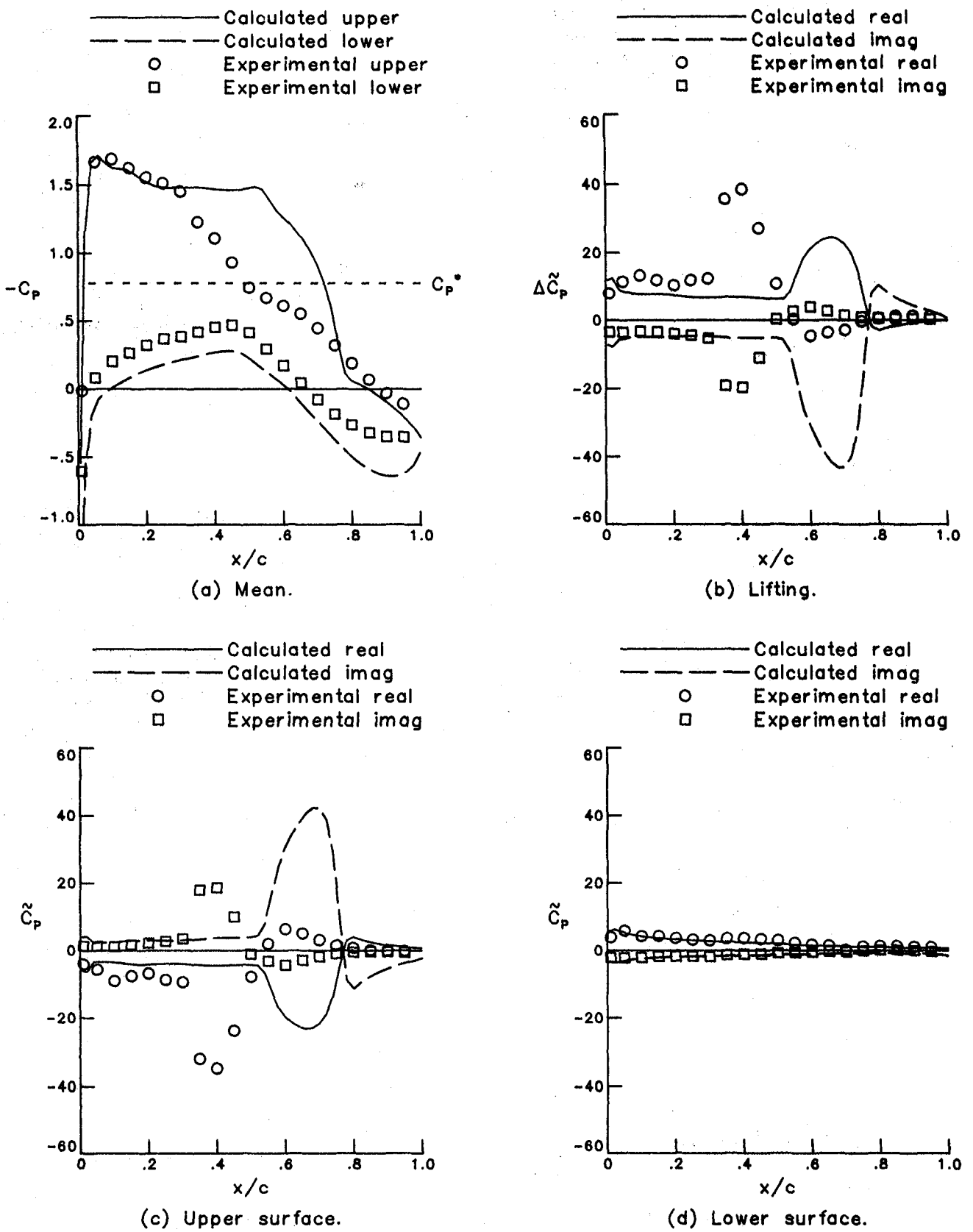

Figure 36.- Unsteady pressure distribution for NLR 7301 Airfoil.
Case 4, M = 0.700, α_m = 2.0, α_0 = 1.0, k = 0.072.

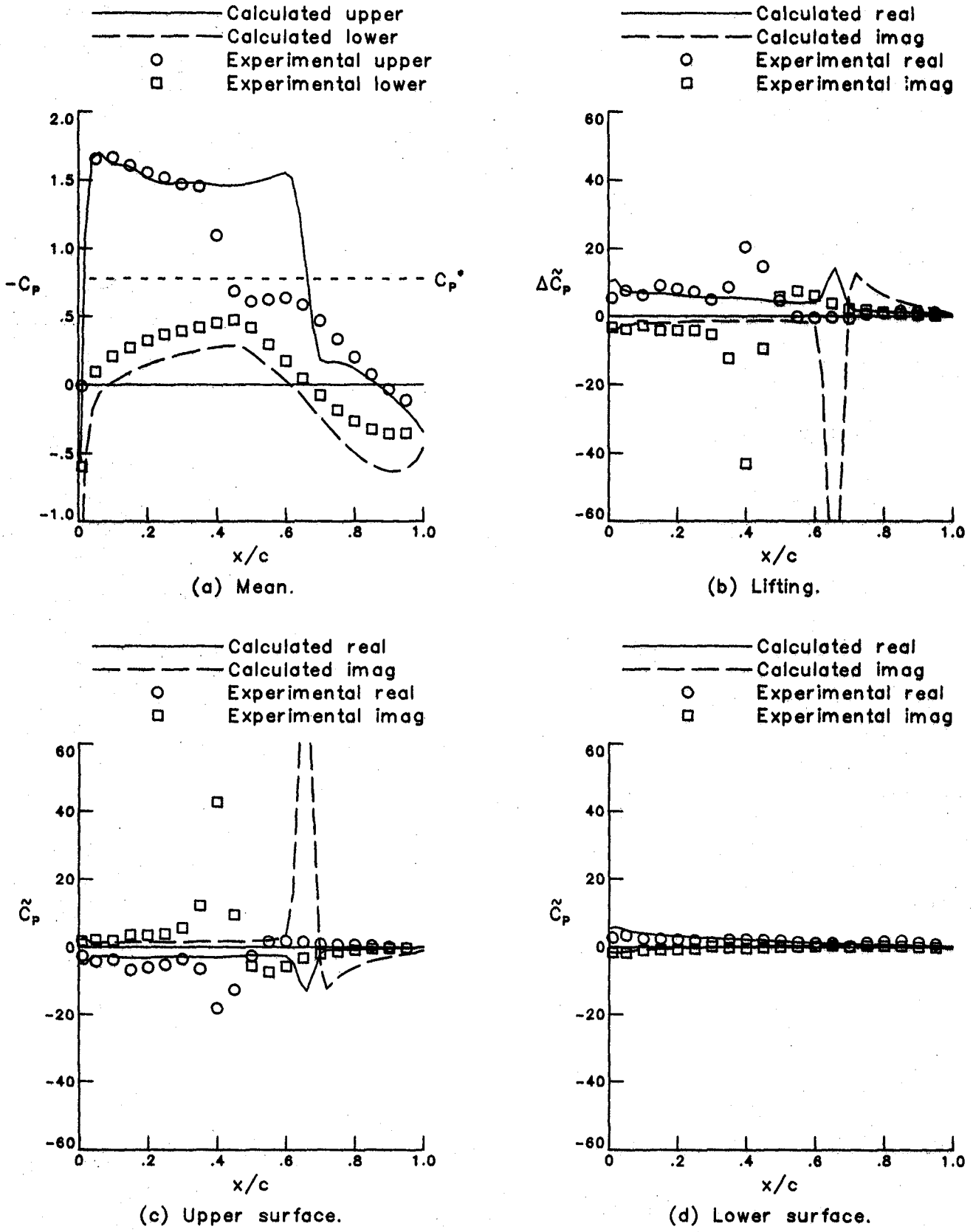

Figure 37.- Unsteady pressure distribution for NLR 7301 Airfoil.
Case 5, M = 0.700, α_m = 2.0, α_0 = 0.5, k = 0.192.

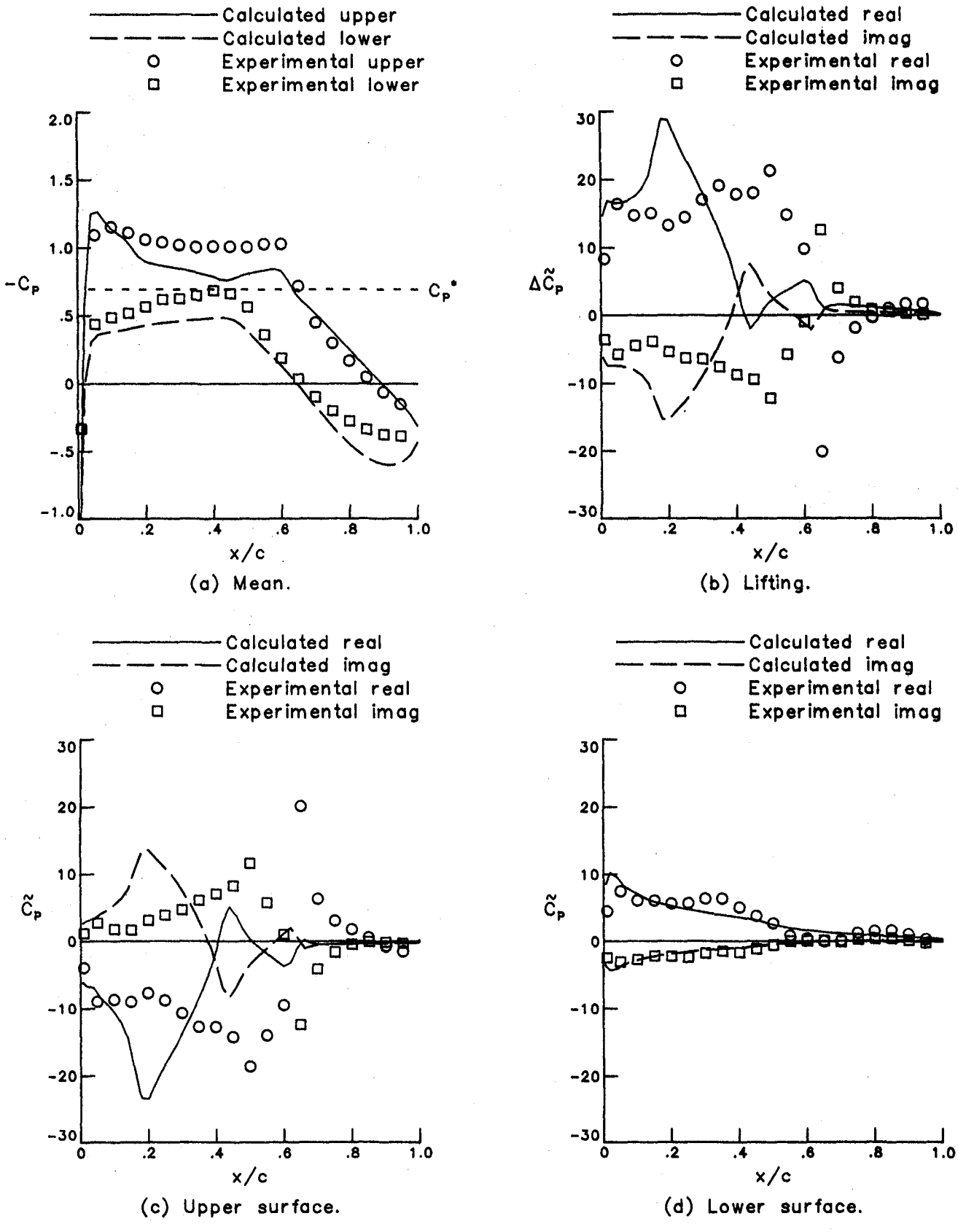

Figure 38.- Unsteady pressure distribution for NLR 7301 Airfoil.
Case 6, M = 0.721, α_m = -0.19, α_0 = 0.5, k = 0.068.

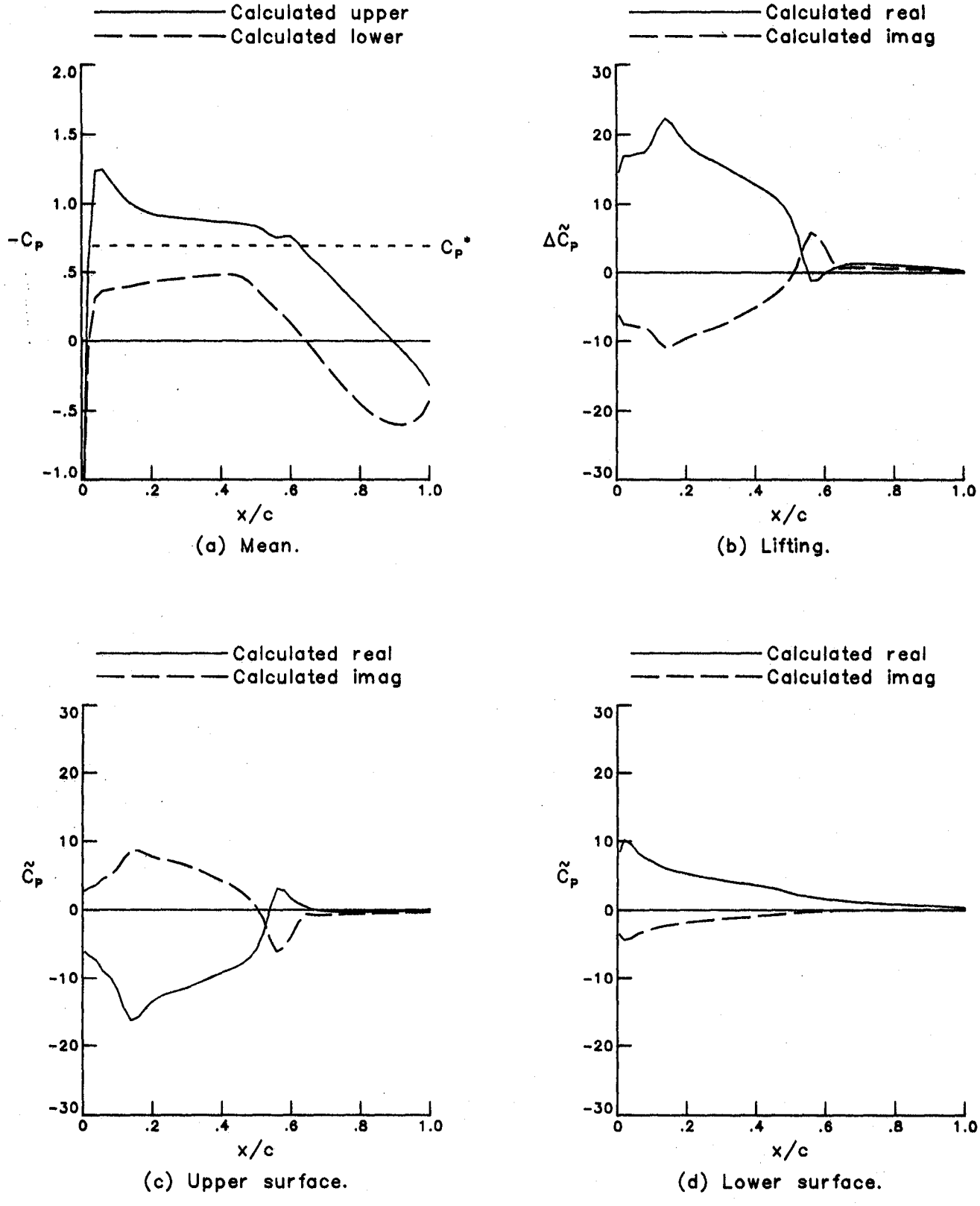

Figure 39.- Unsteady pressure distribution for NLR 7301 Airfoil.
Case 7, M = 0.721, α_m = -0.19, α_0 = 1.0, k = 0.068.

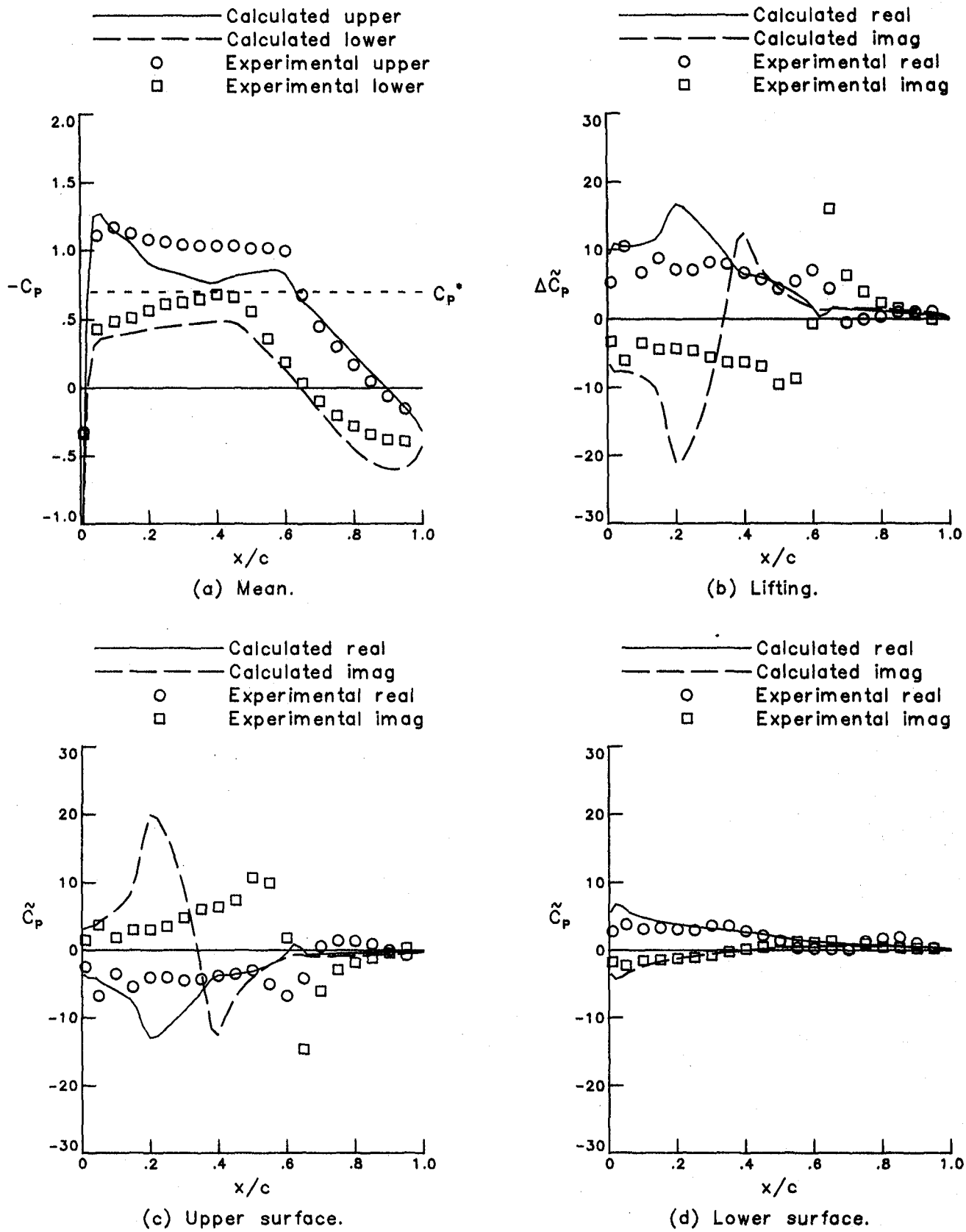

Figure 40.- Unsteady pressure distribution for NLR 7301 Airfoil.
Case 8, M = 0.721, α_m = -0.19, α_0 = 0.5, k = 0.181.

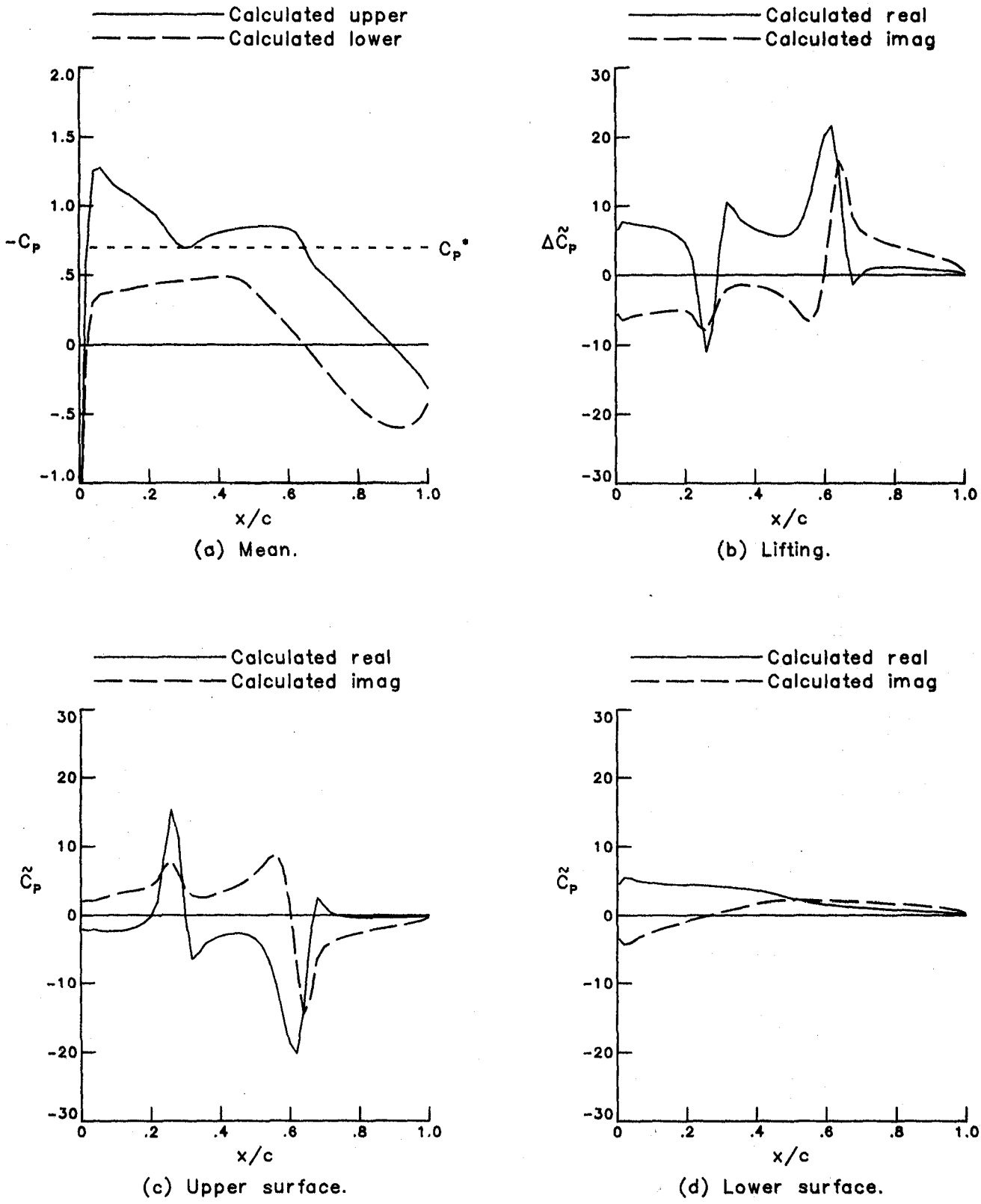

Figure 41.- Unsteady pressure distribution for NLR 7301 Airfoil.
Case 9, M = 0.721, α_m = -0.19, α_0 = 0.5, k = 0.453.

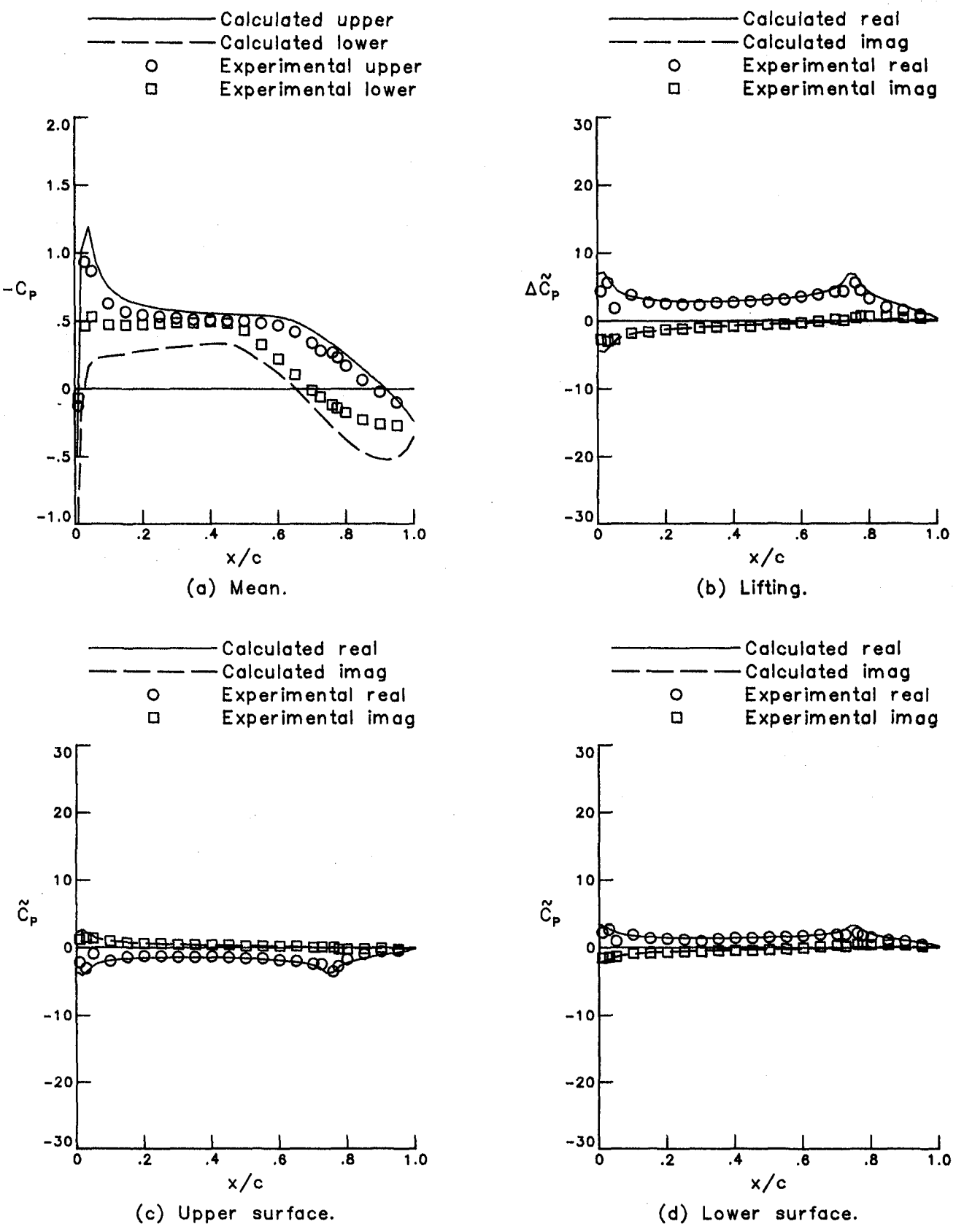

Figure 42- Unsteady pressure distribution for NLR 7301 Airfoil.
Case 10, M = 0.500, α_m = 0.4, δ_0 = 1.0, k = 0.098.

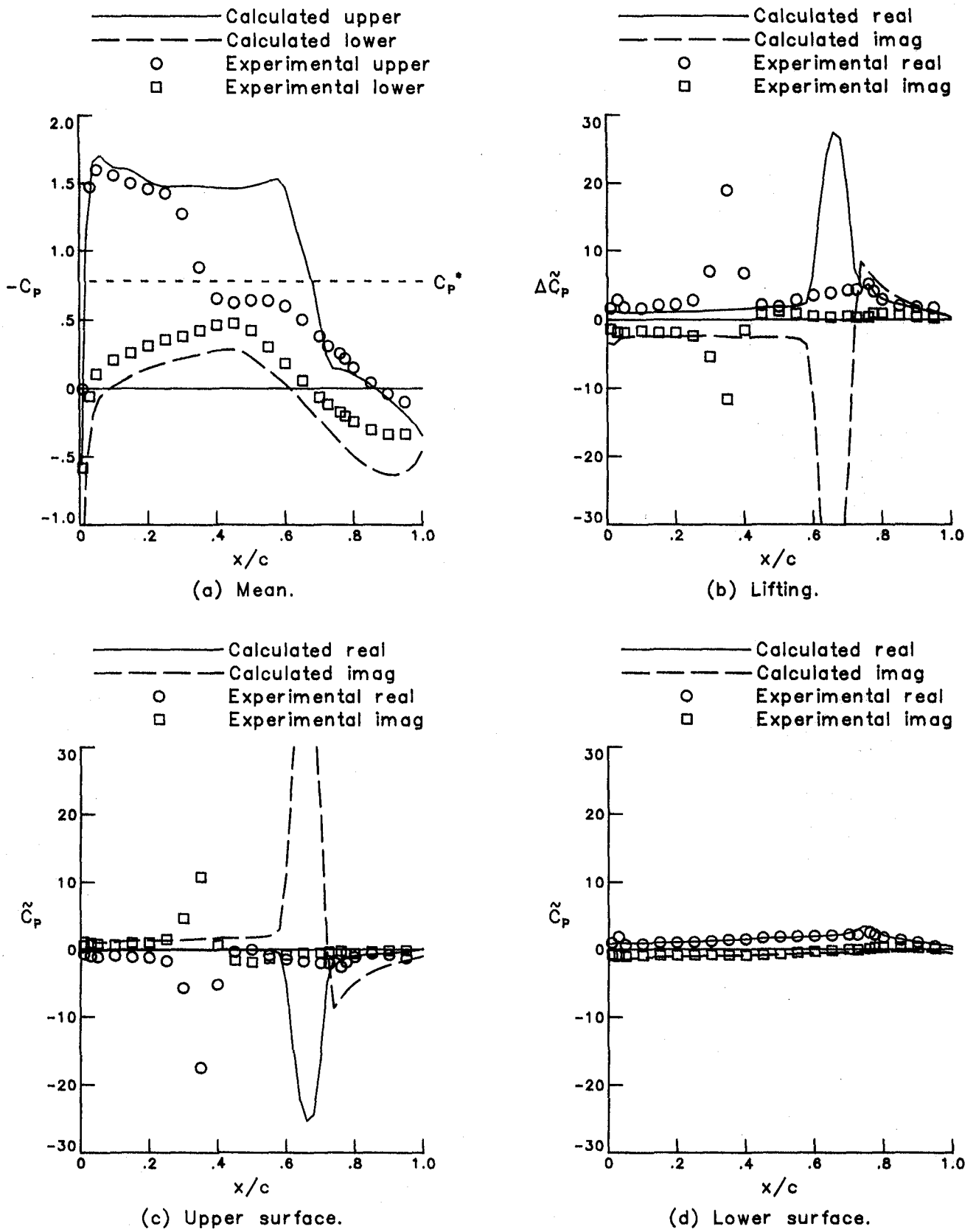

Figure 43.- Unsteady pressure distribution for NLR 7301 Airfoil.
Case 11, M = 0.700, α_m = 2.0, δ_0 = 1.0, k = 0.072.

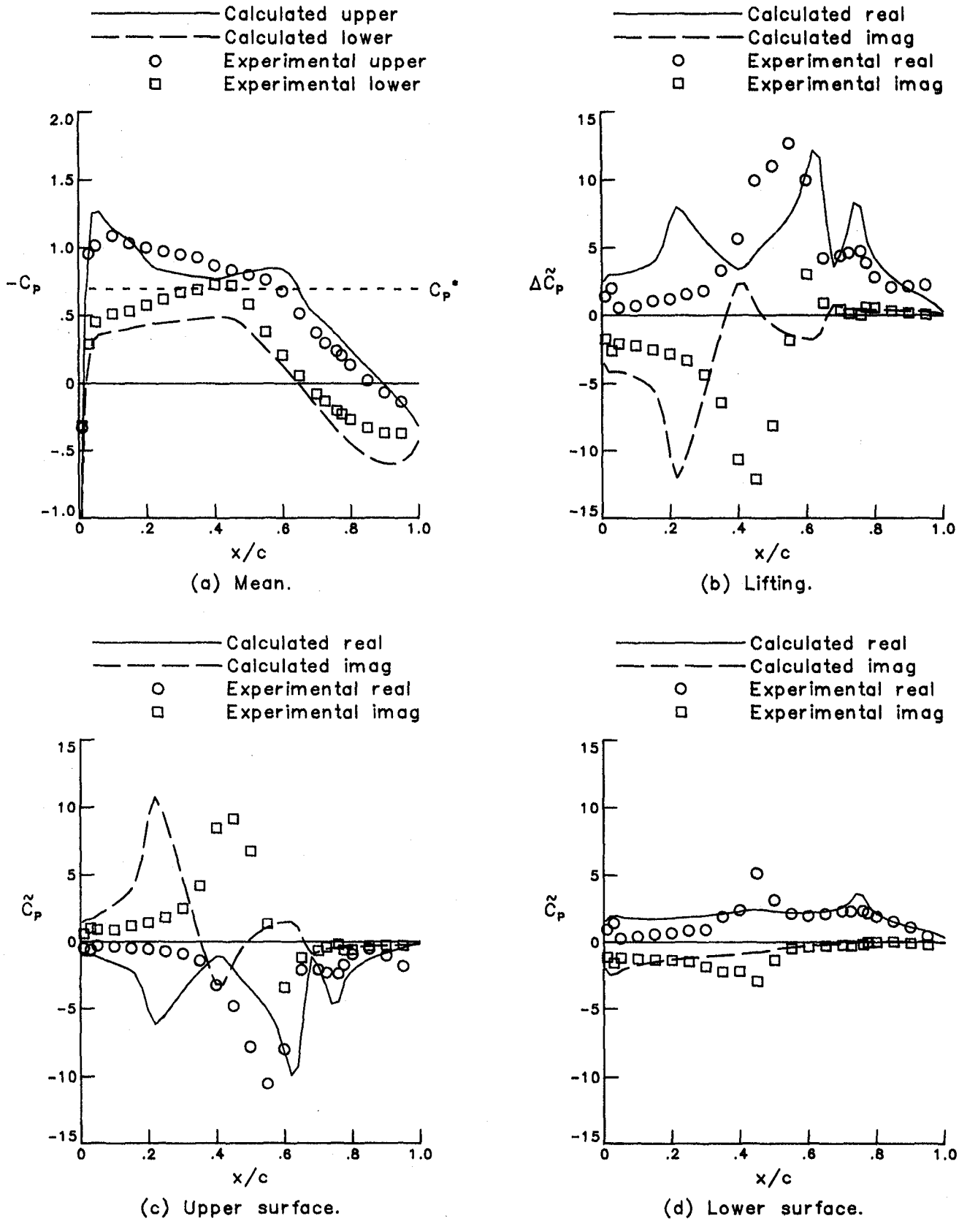

Figure 44.- Unsteady pressure distribution for NLR 7301 Airfoil.
Case 12, M = 0.721, α_m = -0.19, δ_0 = 1.0, k = 0.068.

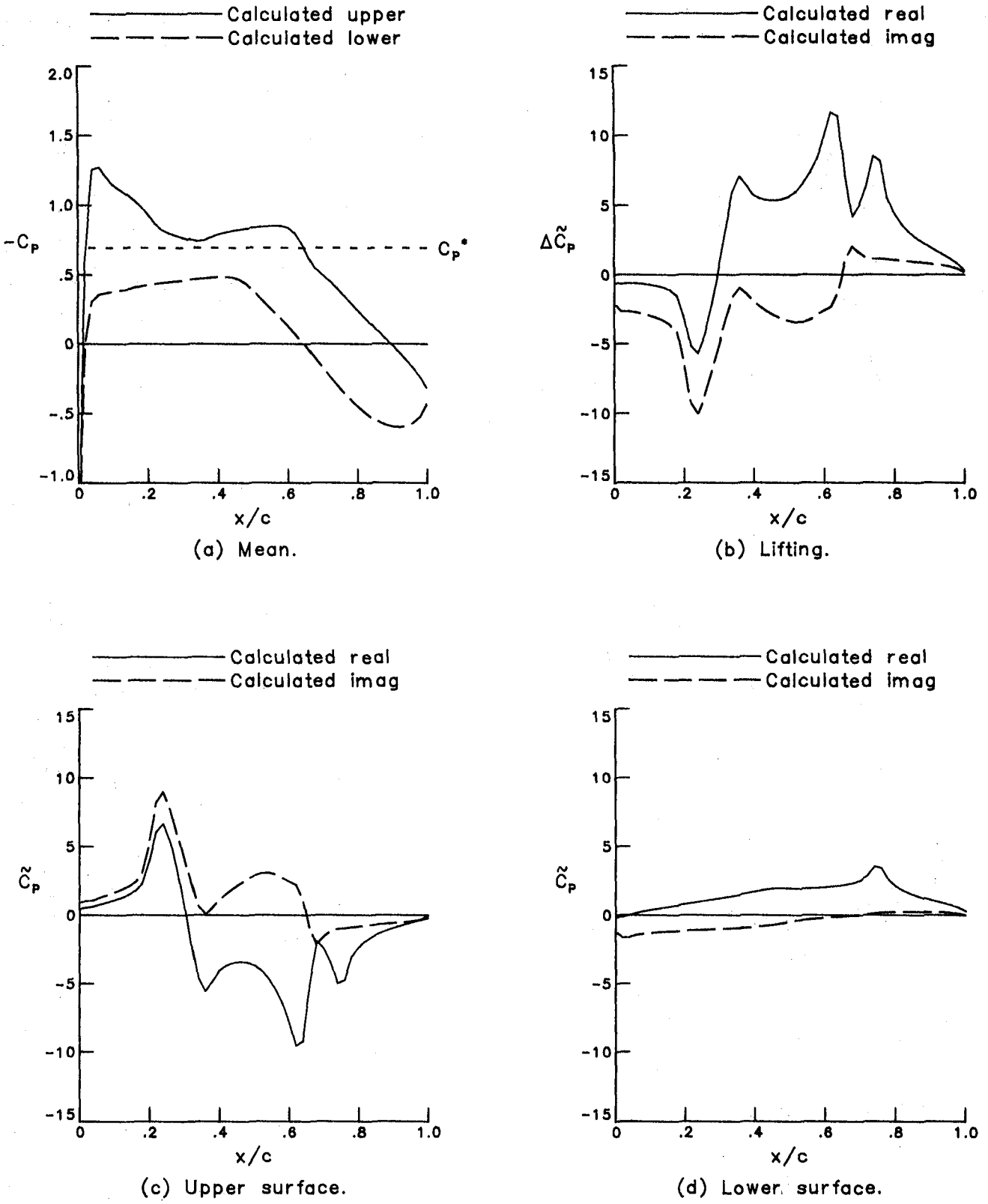

Figure 45.- Unsteady pressure distribution for NLR 7301 Airfoil.
Case 13, M = 0.721, α_m = -0.19, δ_0 = 1.0, k = 0.181.

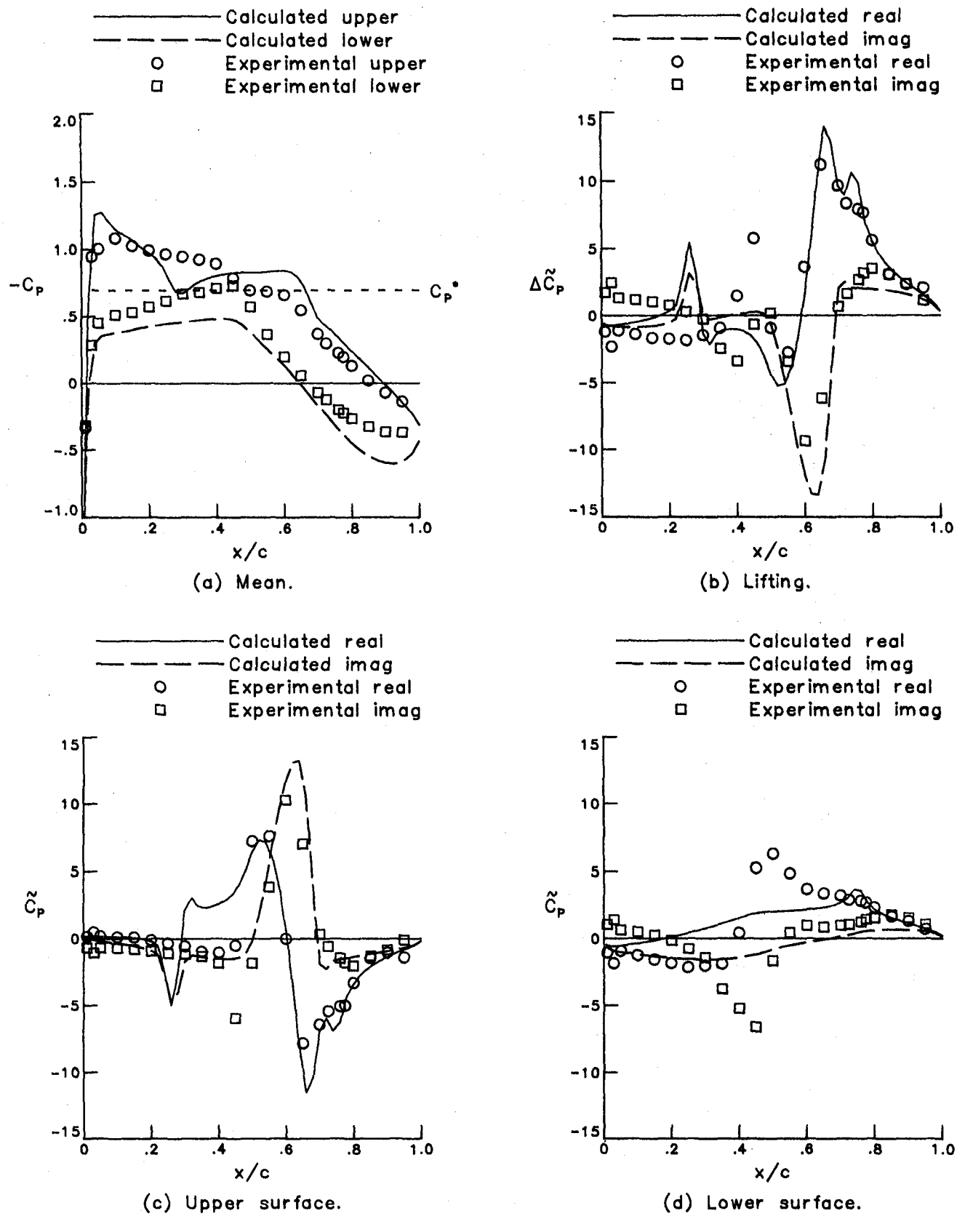

Figure 46.- Unsteady pressure distribution for NLR 7301 Airfoil.
Case 14, M = 0.721, α_m = -0.19, δ_0 = 1.0, k = 0.453.

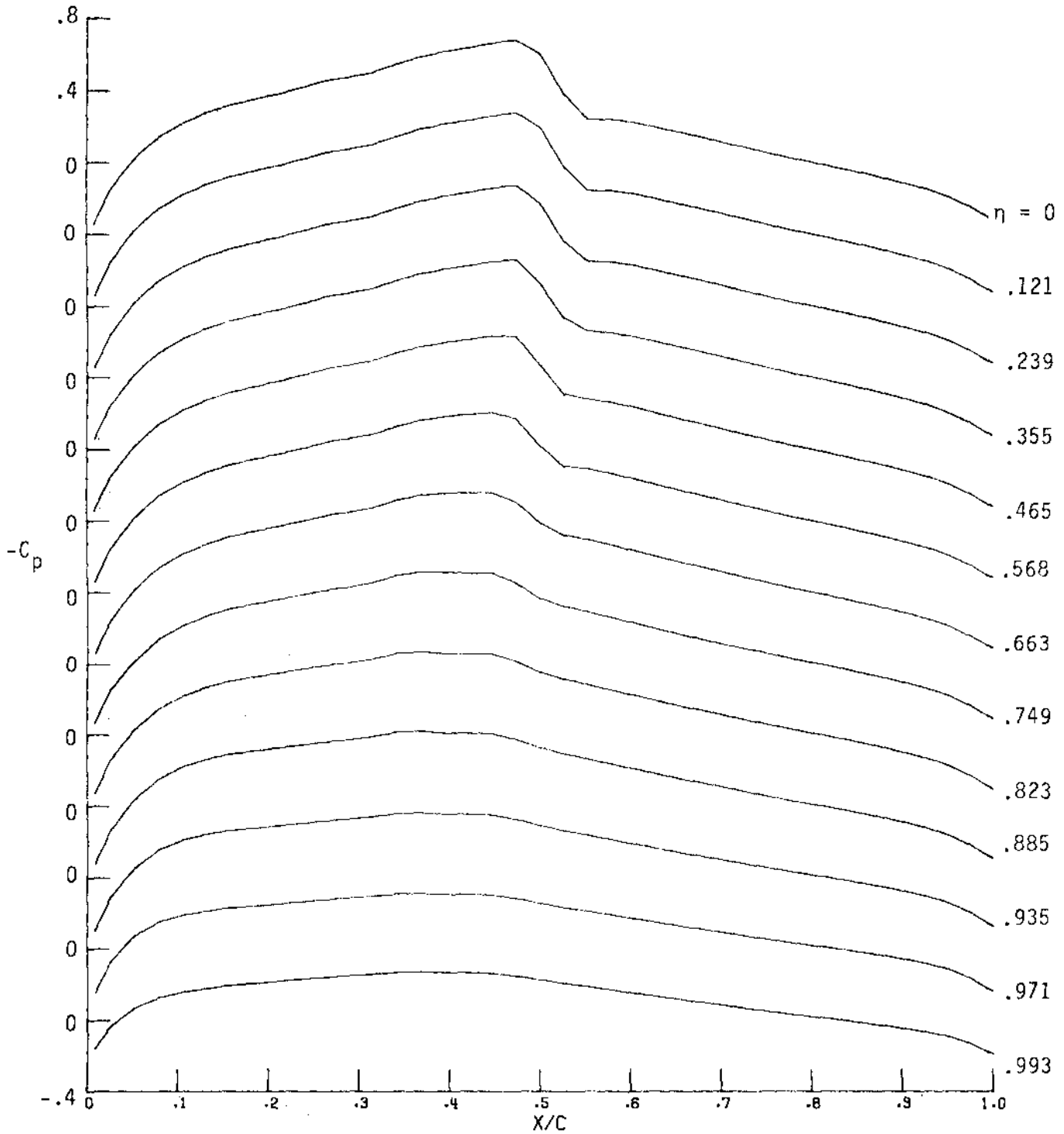

Figure 47.- Rectangular Wing, steady flow, M = 0.8.

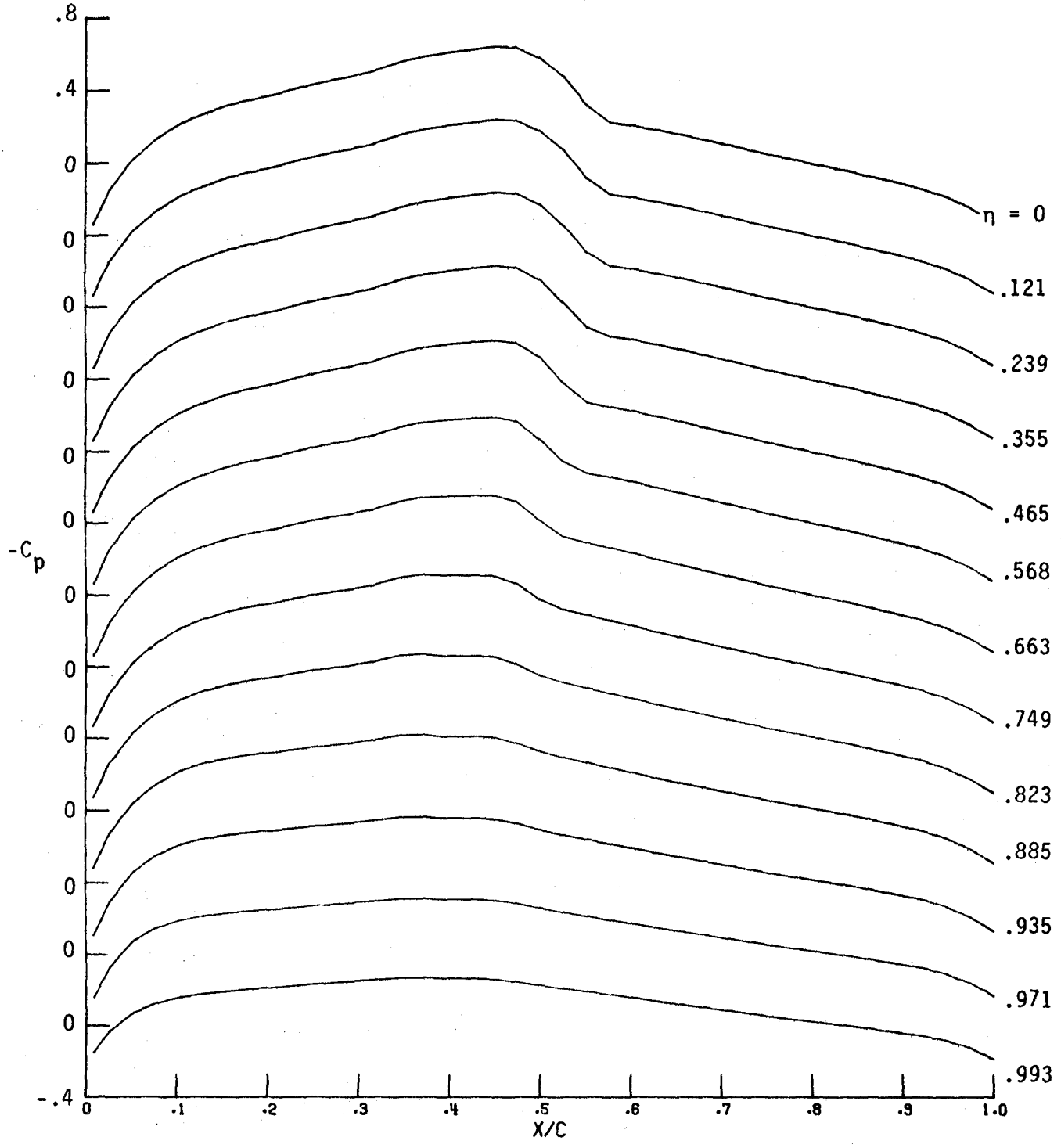

(a) Mean pressure.

Figure 48.- Rectangular Wing, C3-4, M = 0.8, k = 0.2.

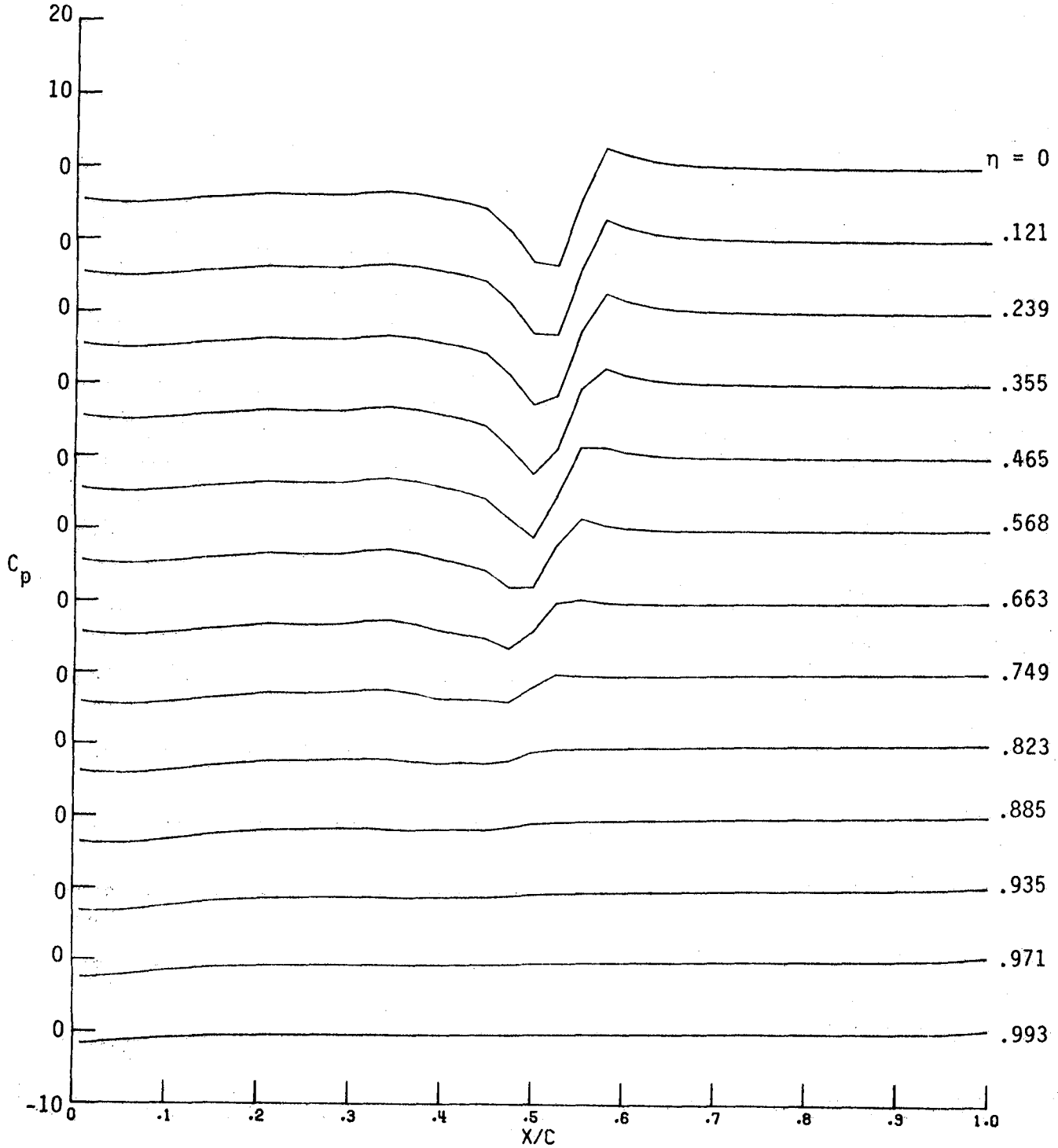

(b) Real upper pressure.

Figure 48.- Continued.

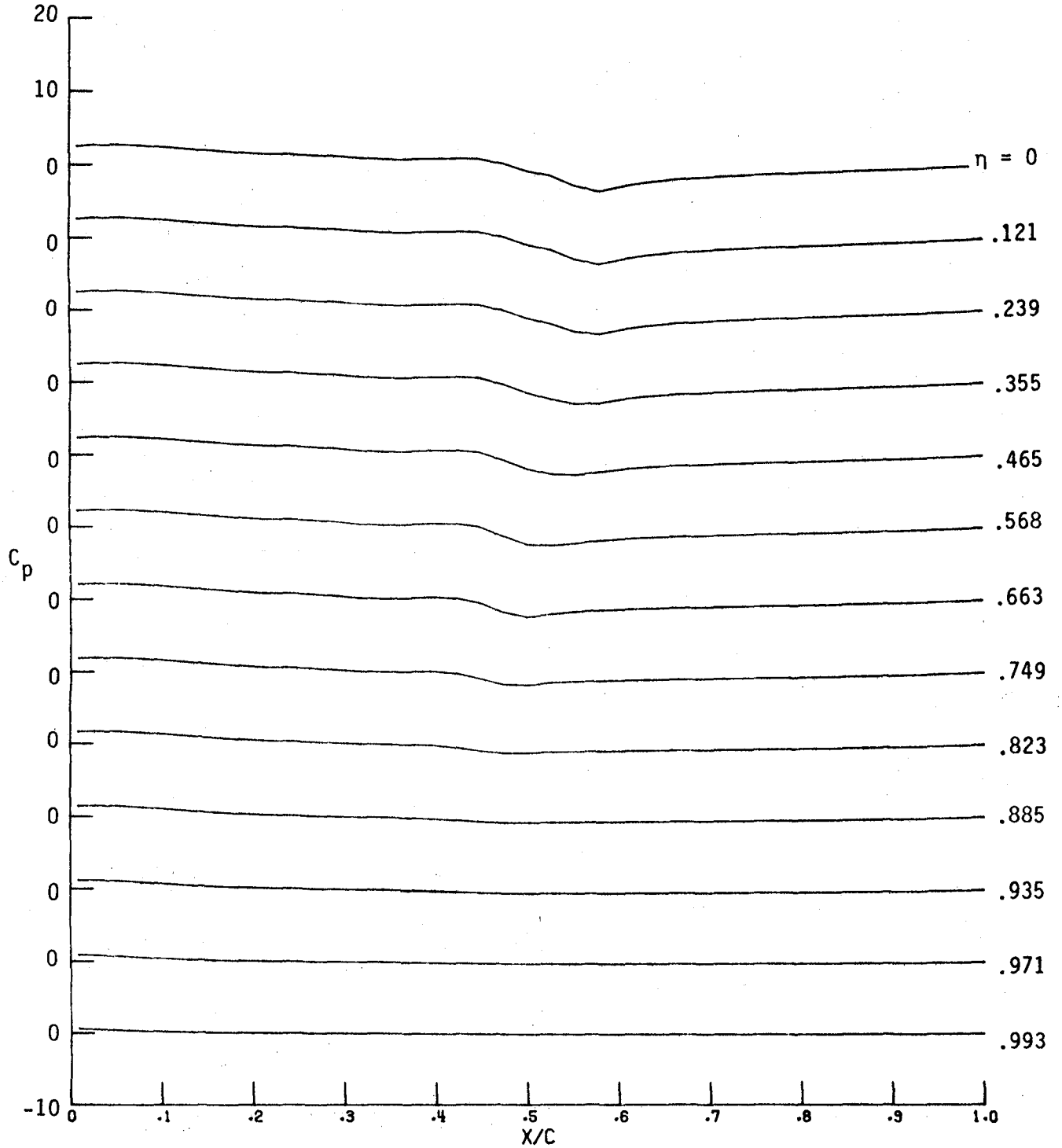

(c) Imaginary upper pressure.

Figure 48.- Concluded.

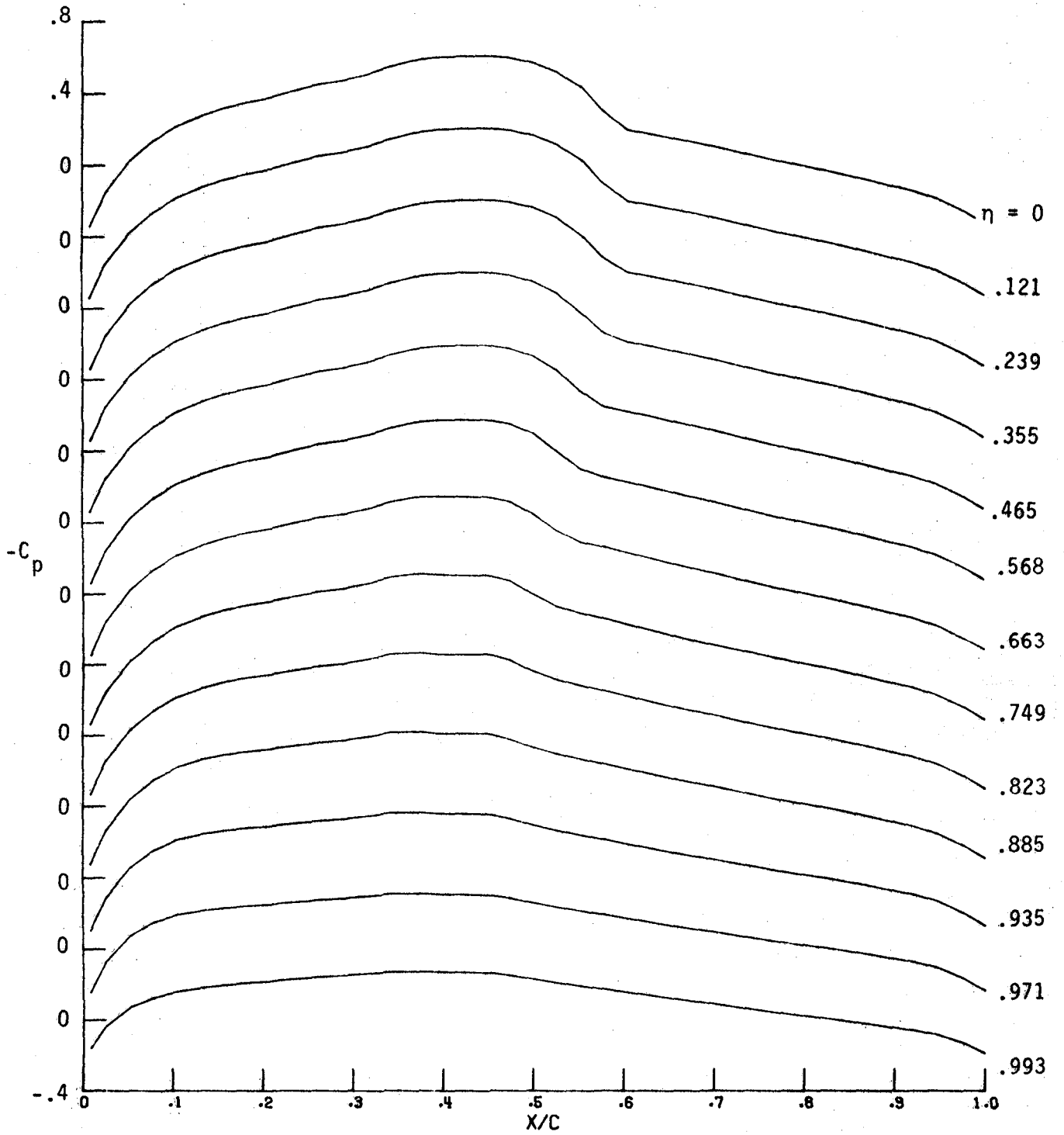

(a) Mean pressure.

Figure 49.- Rectangular Wing, C6, M = 0.8, k = 0.45.

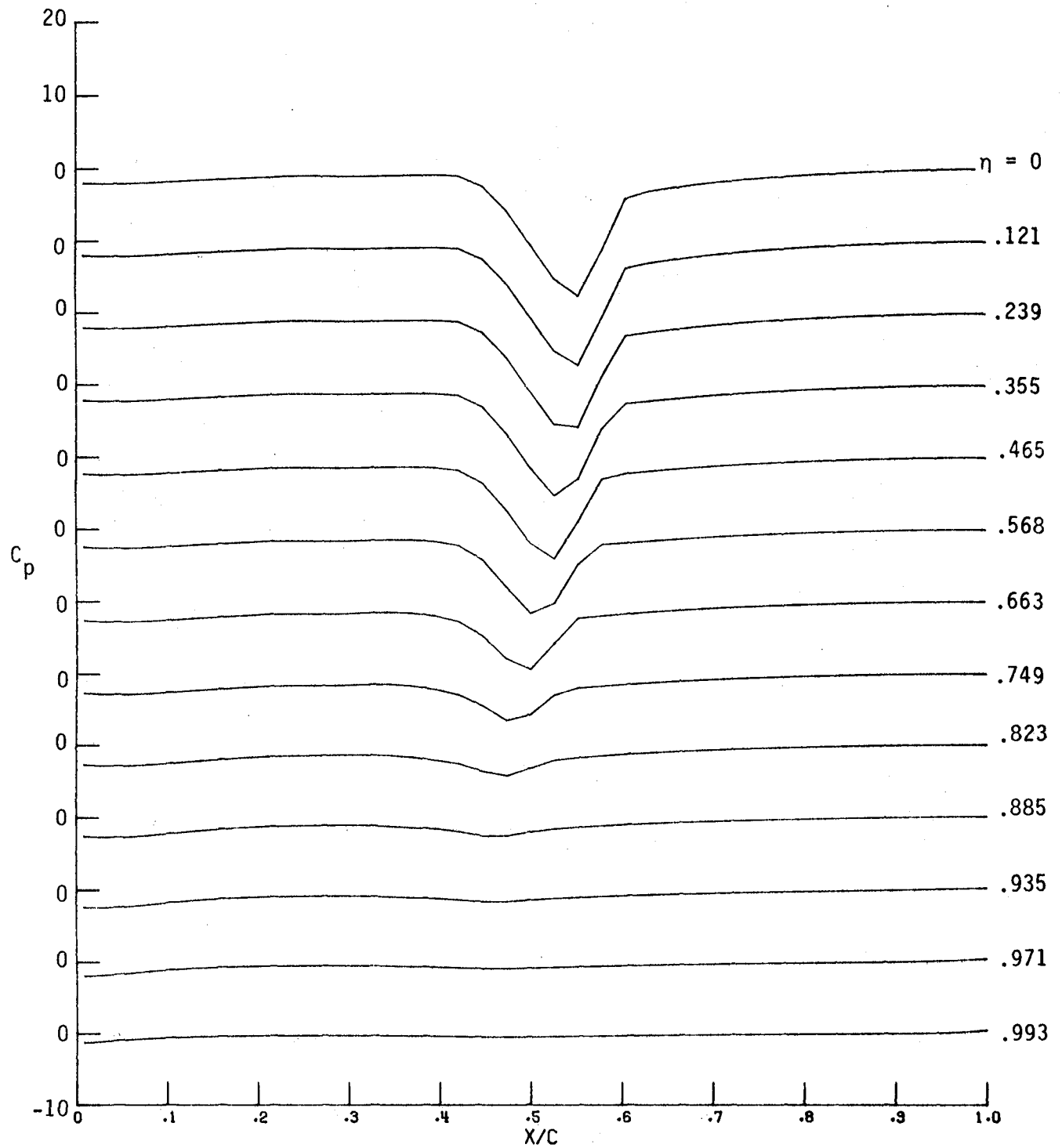

(b) Real upper pressure.

Figure 49.- Continued.

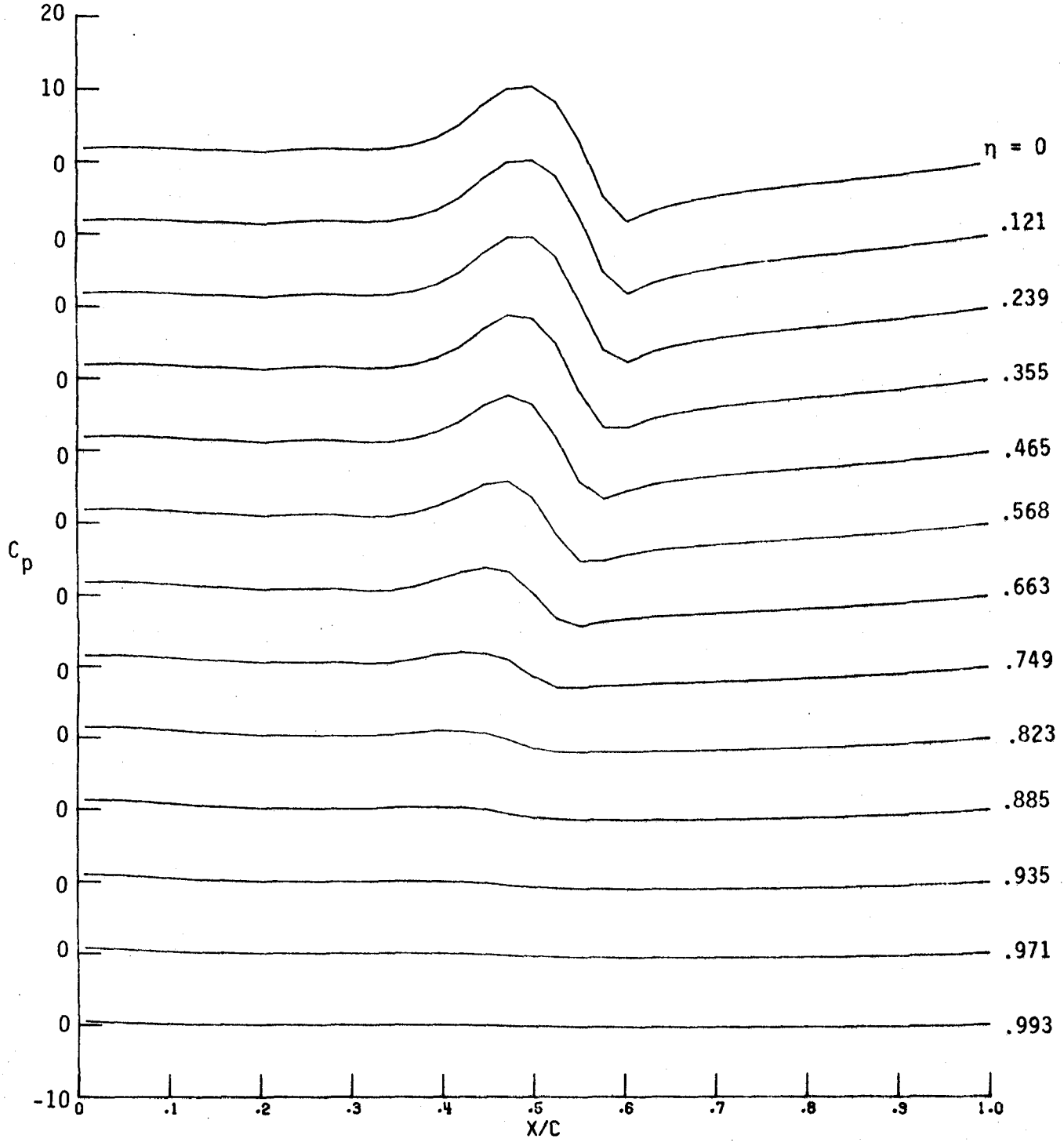

(c) Imaginary upper pressure.

Figure 49.- Concluded.

1. Report No.	2. Government Accession No.	3. Recipient's Catalog No.
NASA TM - 85817		

4. Title and Subtitle	5. Report Date
CALCULATION OF UNSTEADY AERODYNAMICS FOR FOUR AGARD STANDARD AEROELASTIC CONFIGURATIONS	May 1984
	6. Performing Organization Code 505-33-43-09
7. Author(s)	8. Performing Organization Report No.
Samuel R. Bland and David A. Seidel	
	10. Work Unit No.
9. Performing Organization Name and Address	
NASA Langley Research Center Hampton, VA 23665	11. Contract or Grant No.
	13. Type of Report and Period Covered
12. Sponsoring Agency Name and Address	Technical Memorandum
National Aeronautics and Space Administration Washington, DC 20546	14. Sponsoring Agency Code

15. Supplementary Notes

16. Abstract

Calculated unsteady aerodynamic characteristics for four AGARD standard aeroelastic two-dimensional airfoils and for one of the AGARD three-dimensional wings are reported. Calculations were made using the finite-difference codes XTRAN2L (two-dimensional flow) and XTRAN3S (three-dimensional flow) which solve the transonic small disturbance potential equations. Results are given for the 36 AGARD cases for the NACA 64A006, NACA 64A010, and NLR 7301 airfoils with experimental comparisons for most of these cases. Additionally, six of the MBB-A3 airfoil cases are included. Finally, results are given for three of the cases for the rectangular wing.

17. Key Words (Suggested by Author(s))	18. Distribution Statement
Transonic Unsteady Aerodynamics AGARD Configurations	Unclassified - Unlimited Subject Category - 02

19. Security Classif. (of this report)	20. Security Classif. (of this page)	21. No. of Pages	22. Price
Unclassified	Unclassified	79	A05

N-305

For sale by the National Technical Information Service, Springfield, Virginia 22161